Evaporated organic films of tetrathiafulvalene and related materials

Maria Kilitziraki

EVAPORATED ORGANIC FILMS OF TETRATHIAFULVALENE AND RELATED MATERIALS

M. KILITZIRAKI

EVAPORATED ORGANIC FILMS OF TETRATHIAFULVALENE AND RELATED MATERIALS

by

MARIA KILITZIRAKI, B. Sc.

Graduate Society

A Thesis submitted in partial fulfilment

of the requirements for the degree of

Doctor of Philosophy

School of Engineering

University of Durham

September 1996

DECLARATION

I hereby declare that the work reported in this thesis has not previously been sumbitted for any degree, and is not being currently submitted in candidature for any other degree.

Signed .....

The work reported in this thesis was carried out by the candidate

Signed .....

Director of Studies

.....

Candidate

STATEMENT OF COPYRIGHT

ACKNOWLEDGEMENTS

Several people have had an important input to the completion of this thesis. Primarily, I must thank my supervisor Prof. Mike Petty for his guidance and innovative ideas and mainly for giving my English style. My second supervisor Prof. Martin Bryce kindly refined my chemistry knowledge. I am for ever grateful to Harry Kelly for building the vacuum system and finding the leaks. From the ME group, I would like to thank especially Chris Pearson for helping me with my lab techniques and for the productive discussions through which solutions to important problems arose. The constant encouragement of my parents Αννα και Γεωργιο Κιλιτζιρακη is highly appreciated. I must thank Dr. Kulesza for introducing me to the experimental world of physics and also for his precious advice about life. Finally, I would like to thank Greece for joining the EU so that I could get my grant.

ABSTRACT

This thesis describes the design, construction and application of a novel vacuum system for the preparation of thin films of organic charge-transfer compounds. The method of thermal evaporation was used for four materials: tetrathiafulvalene (TTF) and three of its derivatives, dimethyltetrathiafulvalene (DiMe-TTF), trimethyltetrathiafulvalene (TriMe-TTF) and bis(ethylenedithio)tetrathiafulvalene (BEDT-TTF). The resulting thin layers were characterised using optical and electron microscopy, infrared/visible spectroscopy and dc conductivity measurements down to 77K.

Thin films of tetrathiafulvalene, after doping with iodine, exhibited a maximum value of dc, in-plane room temperature conductivity σ of 8.0±2.4 S cm^{-1}. Semiconducting behaviour was exhibited over the range 77-300 K with ΔE = 0.09±0.02 eV. The effect of the deposition rate on film morphology is reported. TTF iodide layers were also prepared by co-evaporating the two components. These films exhibited a maximum conductivity of 2.9±0.4 S cm^{-1} at room temperature. Again, semiconducting behaviour was noted over the range 77-300 K with ΔE = 0.2±0.02 eV. A comparison of the optical, structural and electrical properties of the two types of films is made.

DiMe-TTF and TriMe-TTF thin films were also successfully prepared. Doping with iodine resulted in in-plane, dc room temperature conductivities of 10^{-6} and 10^{-7} S cm^{-1}, respectively. These values, together with data from optical spectroscopy, suggested that both salts were in the full charge-transfer state.

(BEDT-TTF) iodide thin films were deposited by evaporating the organic compound and subsequent doping. Doped films possessed a dc, in-plane room temperature conductivity of 10^{-3} S cm^{-1}. Annealing these layers at 60°C resulted in an increase in conductivity with a

final value of 1.6 S cm^{-1}. Semiconducting behaviour over the range 77-300 K was exhibited by the annealed films (ΔE = 0.028 eV).

Finally, thin film transistors, incorporating TTF and BEDT-TTF doped layers, were fabricated and their electrical characteristics measured.

CONTENTS

CHAPTER ONE

INTRODUCTION

'Organic metals' is a relatively new and very promising area of materials research. Though organic compounds are usually electrically insulating, certain materials can be as conductive as ordinary metals. They may even exhibit superconductivity. This phenomenon was originally observed in 1980 for compounds under applied pressure. Currently, the highest critical temperature for an organic material (excluding fullerenes) is 11.5K at ambient pressure (for κ-(BEDT-TTF)$_2$Cu[N(CN)$_2$] Br) and at 12.5K for applied pressure (for κ-(BEDT-TTF)$_2$Cu[N(CN)$_2$] Cl at 0.3 kbar).

Most conductive organic compounds exist in the form of a powder or as single crystals. Their unique electrical properties can therefore be difficult to exploit. In contrast, thin films are easily incorporated in microelectronic devices. Different methods can be used for film formation; the most common techniques are spin-coating, electrochemical deposition, Langmuir-Blodgett deposition and thermal evaporation. In this thesis, we examine thin films fabricated by thermal evaporation. The technique has been extensively used for inorganic materials to prepare a variety of coatings. However, it is only relatively recently that the method has been used to form organic thin films.

This thesis is concerned with thermally evaporated thin films of materials based on the electron donor tetrathiafulvalene (TTF). Chapter 2 introduces the background to organic metals and provides a chronological review of the most important developments in this area. Work on single crystals of the materials studied is also reported. Chapter 3 describes the

method used for film formation. It also includes reviews of previous work and discusses the incorporation of charge-transfer layers in a thin film transistor structure. In chapter 4 the various experimental techniques used are described, while chapter 5 gives a detailed description of a purpose-built vacuum system designed and built for this project. Chapter 6 reports on the properties of thin films of tetrathiafulvalene prepared using the single source and co-evaporation methods. The effect of the deposition rate and substrate temperature on film formation is discussed. In chapter 7, thin films of three more related materials are given. These are dimethyl-TTF, trimethyl-TTF and BEDT-TTF. The two first were synthesised in the Chemistry Department at Durham while the third was purchased commercially. Finally, in chapter 8, layers of TTF and BEDT-TTF are incorporated in thin film transistor structures. Chapter 9 summarises all the results and makes suggestions for future work.

CHAPTER TWO

ORGANIC CHARGE-TRANSFER MATERIALS

2.0 Introduction

In this chapter, an introduction to 'organic metals' is given. This is followed by the history of the development of these materials. Work that has been reported on the compounds studied in this thesis is discussed in detail.

2.1 Organic Metals

2.1.1 Physical Concepts

Most organic solids are electrical insulators with values of electrical room temperature conductivity in the range 10^{-9}-10^{-14} S cm^{-1}. Organic metals are charge-transfer and ion-radical salts that can exhibit conductivities σ as high as 10^{5} S cm^{-1}. The magnitude of σ for most of these materials is generally much less than that of a metal. Some of these organic metals also become superconducting at low temperatures. Examining the temperature dependence of conductivity, several different behaviours can be seen. These are summarised in Figure 2.1. The temperature dependence of the conductivity of a metal, copper in this case, is also shown for comparison. Metallic behaviour (increasing σ with decreasing temperature T) is seen for $(TMTSF)_2ClO_4$. Below a temperature called the

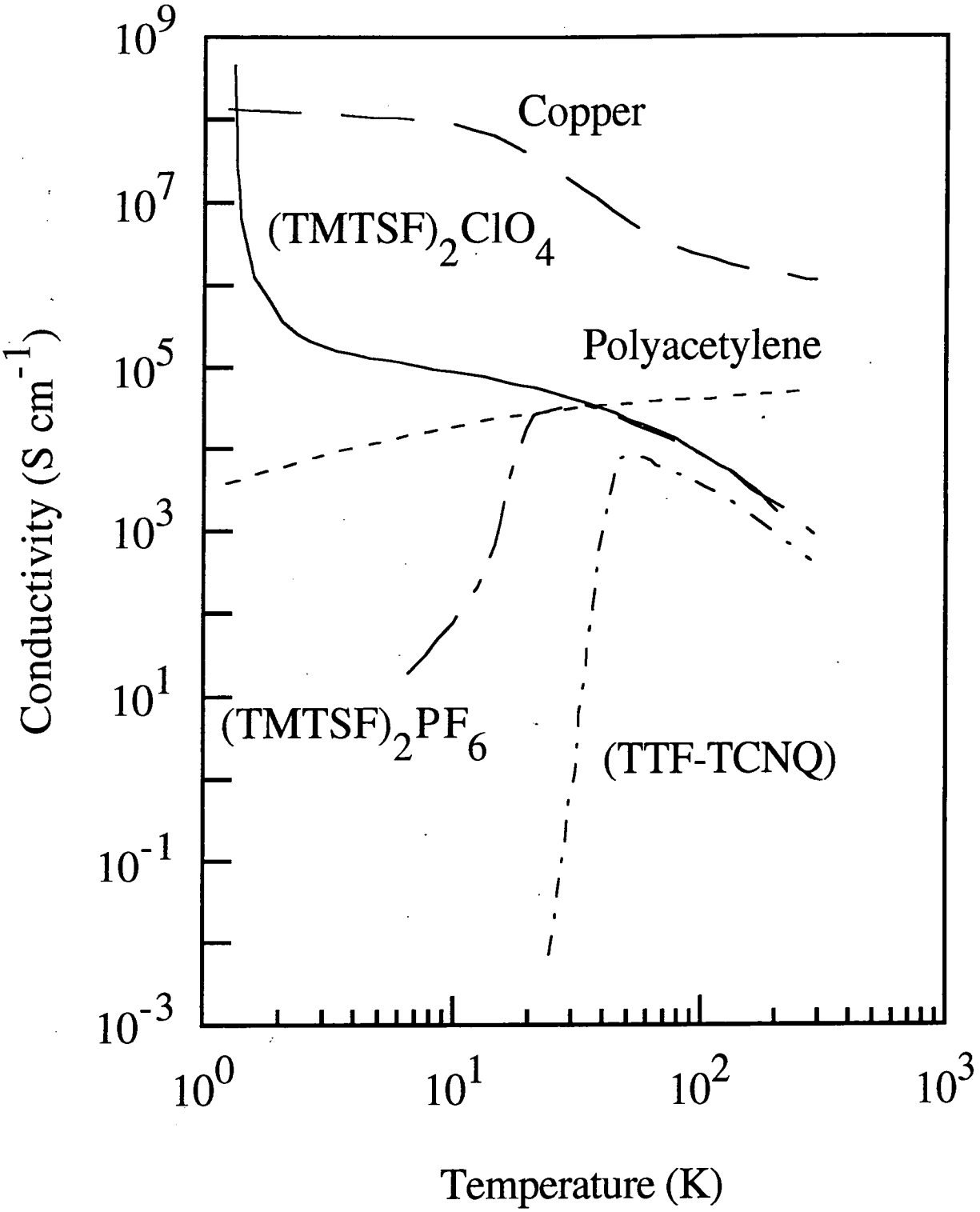

Figure 2.1: Variable temperature conductivity values at ambient pressure for a range of highly conducting materials.

critical temperature T_c, a transition to a superconducting state is evident. Another salt of the TMTSF family, $(TMTSF)_2PF_6$ is also metallic down to a temperature (transition temperature) at which a metal-semiconductor transition occurs. The same behaviour is observed for TTF-TCNQ (Figure 2.1). Semiconducting behaviour is often observed for organic charge-transfer compounds. In this case, conductivity decreases with temperature in the following manner

$$\sigma = \sigma_0 \exp\left(-\frac{\Delta E}{KT}\right) \qquad (2.1)$$

where ΔE is called the activation energy. For an intrinsic semiconductor ΔE represents half the band gap, while for an extrinsic material ΔE may be equal to half the energy between a donor or acceptor level and the corresponding band edge.

Organic metals consist of donor and acceptor molecules between which a reaction of the following sort takes place

$$DA \leftrightarrow [D^{+\bullet}]\,[A^{-\bullet}]$$

where D and A stand for the donor and acceptor species, respectively and $D^{+\bullet}$ represents the presence of a radical ion. In Figures 2.2 & 2.3, the most widely investigated organic donors and acceptors are shown. Organic metals can be either single-chain, ion-radical salts, e.g., $(TMTSF)_2^{+\bullet}X^-$ salts, where the anion is a closed shell species or two-chain conductors, e.g. $TTF^{+\bullet}$-$TCNQ^{-\bullet}$ charge-transfer complexes, in which both components are open shell molecules. The donor and acceptor molecules often stack face-to-face within the crystal lattice. Two alternative structures are possible, the mixed and segregated stacks, Figure 2.4.

DONORS

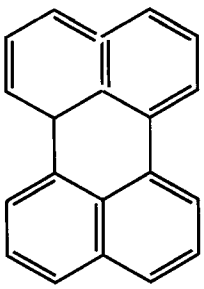

Perylene

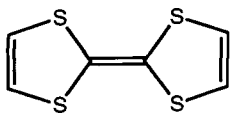

TTF

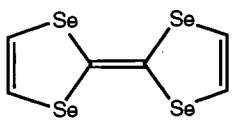

TSF

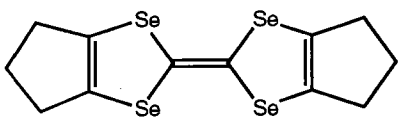

HMTSF

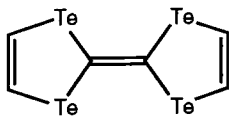

TTeF

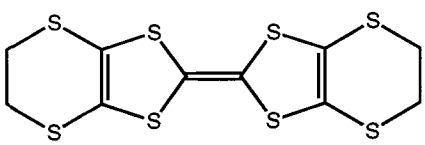

BEDT-TTF

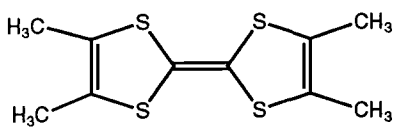

TMTTF

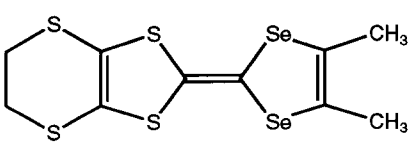

DMET

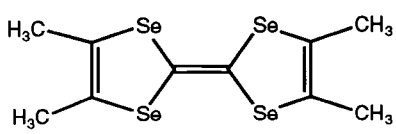

TMTSF

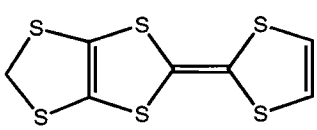

MDT-TTF

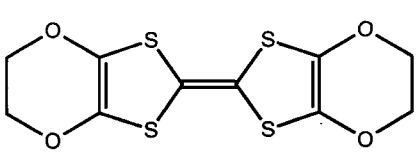

BEDO-TTF

Figure 2.2: Some organic donor molecules.

ACCEPTORS

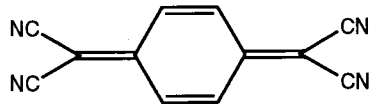

TCNQ

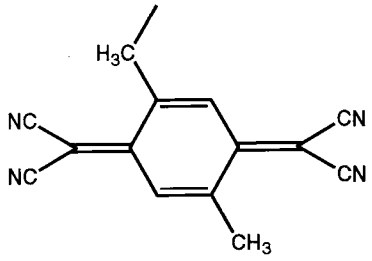

2,5-DMTCNQ

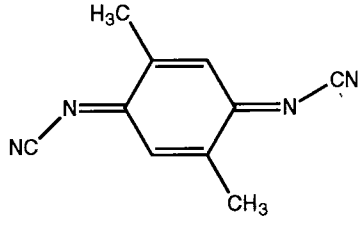

2,5- DMDCNQI

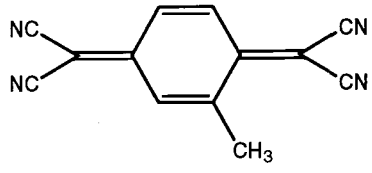

MTCNQ

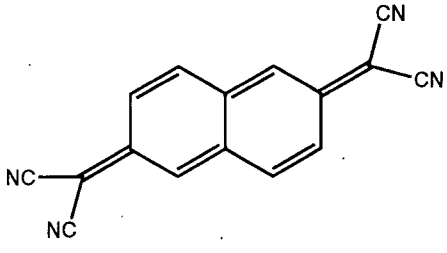

TNAP

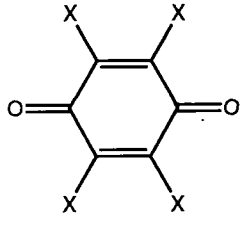

X_4BQ

X = F, Cl, Br, I

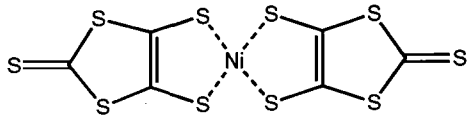

$Ni(dmit)_2$

Figure 2.3: Some organic acceptor molecules.

Figure 2.4: (a) Mixed and (b) Segregated donor-acceptor stacks.

Molecular compounds with mixed stacks are not highly conductive due to electron localisation on the stacks. High conductivity is associated with crystal structures in which the donor and acceptor molecules are relatively planar and form segregated stacks with considerable π-electron overlap and delocalisation along these stacks. Conduction is therefore highly anisotropic, with the width of the conduction band dependent upon interactions between the molecular orbitals of neighbouring molecules. As a consequence, organic metals are termed quasi-one-dimensional. Two-dimensionality has also been exhibited, where the inter and intrastack distances are similar and conduction can occur in two-dimensional sheets.

The degree of charge-transfer ρ represents the average number of electrons transferred from the donor to the acceptor molecule. This is a very important factor in a charge-transfer compound and depends principally upon the ionisation potential of the donor and the electron affinity of the acceptor on average. The ionisation potential is the energy required to remove an electron from a donor while the electron affinity represents the tendency of the acceptor to accept an electron and form an anion. For ρ=1, charge transfer is complete (all donor molecules are ionised) and only conduction of the following sort is possible

$$D^{+\bullet} + D^{+\bullet} \rightarrow D^{2+} + D^{0}$$

where for simplicity only the donor stack is considered. In this case, conduction can only occur down the stack at the cost of a large Coulombic energy U_0, where U_0 is the

Coulombic repulsion energy between two charge carriers on the same molecule. The activation energy in this case will be given by $\Delta E=U_0-V_1$ where V_1 is the Coulombic repulsion between electrons on adjacent molecules. For $\rho<1$, neutral molecules and ions are present and the stack is of a mixed valence. The unpaired carrier can move along the stack, as shown below, without having to overcome large Coulombic interactions and the system is a conductor.

$$TTF^0 + TTF^{+\bullet} \rightarrow TTF^{+\bullet} + TTF^0$$

2.1.2 Historical Review

The first experimental indication that molecular compounds could exhibit significant electrical conductivity was from Akamatu *et al.*, who reported a room temperature conductivity σ_{RT} of around 10^{-1} S cm^{-1} for a bromine salt of perylene [1]. Perylene itself is an insulator with $\sigma_{RT} = 10^{-15}$ - 10^{-17} S cm^{-1}. This was a verification of the prediction made in 1911 that certain organic solids might exhibit an electrical conductivity comparable to that of metals [2].

The first stable, conducting organic molecule was synthesised by Melby *et al.* [3]. The compound was 7,7,8,8-tetracyano-*p*-quinodimethane (TCNQ), an electron acceptor; its structure is depicted in Figure 3.2. Many salts of TCNQ were found to be electrically conductive, for example $Cs_2(TCNQ)_3$ was conductive but became insulating when the temperature was lowered [4]. Most of the $M(TCNQ)_2$ salts, in which M is a monovalent cation (alkali metal or organic) were found to be semiconductors (i.e. having thermally activated electrical conduction) with activation energies of 0.05-0.2 eV.

In 1970, Wudl *et al.* [5] synthesised the organic donor tetrathiafulvalene (TTF) and observed that highly conducting materials could be prepared when it reacted with halogens and pseudo-halogens. The first salt to be prepared was the chloride with $\sigma_{RT} \approx 3$ S cm^{-1}. Combining TTF with TCNQ resulted in a 1:1 salt that was the first molecular crystal to exhibit metallic behaviour. Between the temperatures of 298K and 60K, the salt possesses the characteristics of a metal (increasing σ with decreasing T) [6]. Below 60K metal-semiconductor transition prevented the appearance of superconductivity. The conductivity was 500 S cm^{-1} at room temperature, with a maximum of 10^4 S cm^{-1} at 60K.

After the discovery of TTF-TCNQ, one of the most obvious modifications was the replacement of sulphur in TTF with a heavier chalcogen. Such a substitution could result in increased dimensionality of the system due to the spatial increase of the chalcogen orbitals in the interstack directions, reduce the Coulombic repulsion via the more polarizable substituting atoms and change the band filling by changing the ionisation potentials of the new donors. In 1974, tetraselenofulvalene (TSF) was synthesised and its 1:1 salt with TCNQ was prepared [7]. This proved to be another organic metal with a metal-semiconductor transition at *ca.* 40K. The room temperature conductivity was 800 S cm^{-1}, greater than that of TTF-TCNQ.

A decrease in the transition temperature was exhibited by the 1:1 salt of TCNQ with another donor, hexamethylenetetraselenafulvalene (HMTSF) [8]. In this salt, the phase transition was suppressed to 1.1K. The close Se...N contacts provided increased dimensionality.

In 1978, Jacobsen *et al.* prepared the charge-transfer salt (tetramethylselenafulvalene) -dimethyltetracyano-*p*-quinodimethane (TMTSF-DMTCNQ) [9]. In this 1:1 salt, the effect

of pressure in suppressing the metal-semiconductor transition was seen. The maximum conductivity observed was 10^5 S cm^{-1} at 1K and 10 kbar.

The first highly conductive organic salts that did not contain TCNQ or one of its derivatives were found by combining tetramethyl-TTF (TMTTF) and tetrahalo-*p*-benzoquinones (X_4BQ, where X= F, Cl, Br, I) [10]. The maximum conductivity was observed by the pressed powder of the chlorine salt (σ_{RT} = 20 S cm^{-1}). Single crystals were only obtained for the bromine salt. These exhibited a thermally activated conductivity (σ_{RT} = 5 S cm^{-1}).

Superconductivity was first discovered in organic metals in the TMTSF family in 1980 [11]. The $(TMTSF)_2X$ salts, where X is a monovalent anion, known as the Bechgaard salts, were all highly conductive (σ_{RT} = 430-780 S cm^{-1}). Most of these compounds underwent a phase transition below 20K; an exception was seen for the PF_6^- salt where superconductivity was observed at 0.9K when applying the pressure of 12 kbar. The $(TMTSF)_2ClO_4$ complex was the first superconducting material ($T_c \approx$ 1.3K) at ambient pressure, but only when slowly cooled. The structure of the $(TMTSF)_2X$ salts was found to be two-dimensional. The TMTSF molecules formed stacks along the α crystallographic axis, which was also the direction of the highest electrical conductivity. These stacks also resulted in the formation of infinite two-dimensional molecular sheets, with the TMTSF molecules connected through interstack Se...Se interactions. These interactions added dimensionality beyond that provided solely by the one-dimensional stacking of the TMTSF molecules. A three-dimensional network was prevented by the anion columns. At room temperature the intermolecular intra- and interstack Se...Se distances were similar. However, as the

temperature was lowered the distances between chains decreased almost by twice as much as the distances between TMTSF molecules within each stack. This led to increased interchain bonding and electronic delocalisation through the selenium atom network for low temperatures.

Another modification of the TTF molecule occurred in 1978 when bisethylenedithio-tetrathiafulvalene BEDT-TTF or ET was first reported by Mizuno *et al.* [12]. The (BEDT-TTF)$_2$ClO$_4$ (1,1,2-trichloroethane)$_{0.5}$ salt was the first in the sulphur based system to exhibit metallic behaviour over the temperature range 298-1.4K [13]. Superconductivity was subsequently discovered for the ET family; first for (BEDT-TTF)$_2$ReO$_4$ at 1.4K at 4 kbar; the iodine salt β-(BEDT-TTF)$_2$I$_3$ exhibited superconductivity at ambient pressure [14]. For the latter material, the critical temperature could be increased from 1.4K to 8K by use of anisotropic pressure [15].

Up to 1986, all salts that exhibited superconductivity were based on a π-cation. The first superconducting system was found for the π-anion bis-[bis-(4,5 dimercapto-1,3-dithiole-2-thione)nickel (Ni(dmit)$_2$). The salt was TTF-[Ni(dmit)$_2$]$_2$ and had a critical temperature of 1.6K at 7 kbar [16].

One further metallic π-anion salt was synthesised by Aumüller *et al.* in 1987 [17]. The anion was 2,5-dimethyl-*N*-*N*'-dicyanoquinonediimine (2,5-DMDCNQI), based on TCNQ. The Cu(2,5-DMDCNQI)$_2$ salt exhibited metallic behaviour down to 1.3K that was not interrupted by a phase transition. The conductivity was σ_{RT} = 800 S cm^{-1} and showed a maximum of 5 x 10^5 S cm^{-1} at 3.5K.

Superconductivity was also observed for the asymmetrical organic donor dimethyl(ethylenedithio) diselenadithiafulvalene (DMET) [18]. $(DMET)_2Au(CN)_2$ had a high room temperature conductivity (2500 S cm^{-1}). This complex showed a metal-semiconductor transition at about 25K at ambient pressure but superconductivity was exhibited below 0.8K for applied pressure (5 kbar).

Kobayashi *et al.* reported, in 1987, the first molecular superconductor based on a π-acceptor molecule and closed-shell cation [19]. The salt was $Me_4N[Ni(dmit)_2]$ and had a critical temperature of 5K at 7 kbar.

By substituting sulphur with tellurium in the TTF molecule, the organic donor tetratellurafulvalene (TTeF) was synthesised [20]. The 1:1 salt with TCNQ proved to be highly conductive (σ_{RT} = 1800±300 S cm^{-1}) and was metallic down to 77K.

In 1988, two more superconducting charge transfer salts were reported. One further salt of ET, κ-$(BEDT\text{-}TTF)_2Cu(SCN)_2$ was found to exhibit ambient pressure superconductivity at a high T_c = 10.4K [21]. The other compound was based on the hybrid asymmetric molecule methylenedithiotetrathiafulvalene (MDT-TTF). The salt $(MDT\text{-}TTF)_2AuI_2$ was superconducting at T_c = 3.5K at ambient pressure [22(a)]. According to Kini *et al.* the value of T_c could be raised to 4.5K [22(b)].

The first electron donor containing oxygen was synthesised in 1990. Wudl *et al.*, substituted the four outer sulphurs for oxygen atoms [23]. The resulting molecule, BEDO-TTF, formed an organic metal when combined with iodine in $(BEDO\text{-}TTF)_{2.4}I_3$ with a room temperature conductivity of 100-280 S cm^{-1}. The same year, Beno *et al.* reported

superconductivity in a BEDO-TTF salt. $(BEDO\text{-}TTF)_3Cu_2(NCS)_3$ was found to be an ambient pressure superconductor with $T_c = 1.06K$ [24].

The superconducting organic materials possessing the higher T_c currently are based on ET. The salts are $\kappa\text{-}ET_2Cu[N(CN)_2]$ X for X = Cl, Br. The bromide salt had a $T_c = 11.6K$ at ambient pressure while for the chloride salt $T_c = 12.5K$ at 0.3 kbar [25].

Recently, superconductivity has also been reported for the $(TMTTF)_2X$ family. Balicas *et al.* suppressed the metal-insulator transition in $(TMTTF)_2Br$ by applying the relatively high pressure of 26 kbar. A transition to the superconducting state was seen at 0.8K [26].

In 1977, it was discovered that the conductivity of polyacetylene $(CH)_x$ could be increased by 13 orders of magnitude upon doping with various donor and acceptor species to give *n*- or *p*-type conductors [27]. Conductivities approaching 10^6 S cm^{-1} were found in doped $(CH)_x$ (e.g. $[CH(AsF_6)_{0.1}]_x$). This initiated research into the field of conjugated organic polymers. Although variants of $(CH)_x$ have been since investigated, none has approached the high conductivity of doped polyacetylene. However, research in this field continues.

2.2 Tetrathiafulvalene Salts

The most widely investigated TTF salt is probably TTF-TCNQ [6]. Here, TTF and TCNQ form segregated stacks, both contributing to the electrical conductivity. The degree of charge-transfer has been determined to be $\rho = 0.59$, which means that on average, -0.59e

(-e is the electron charge) was transferred from TTF to TCNQ molecules. The salt exhibited a one-dimensional character, the electrical conductivity in the least favourable direction (perpendicular to the stacking axis) being about 2×10^{-3} of the value along the stacking axis (~ 500 S cm^{-1}). This complex generated a lot of interest due to its metallic character down to 60K.

In 1976, Jacobsen *et al.* reported the synthesis of the TTF-MTCNQ salt, where MTCNQ stands for Methyl-TCNQ [28]. This salt was also found to be highly conductive, σ_{RT} = 200-500 S cm^{-1}. The temperature dependence of conductivity displayed a broad maximum near T = 210K ($\sigma_{max}/\sigma_{300K} \approx 1.2$) and the conductivity was thermally activated below this region.

Another organic acceptor, 11,11,12,12-tetracyanonaptho-2,6-quinodimethane, TNAP (Figure 3.2), produced a charge-transfer compound when combined with TTF [29]. The salt was 1:1 stoichiometry and exhibited a room temperature conductivity of 40 S cm^{-1}. A sharp drop in the value of σ was seen at 185K, below which the conductivity was thermally activated with $\Delta E = 0.1$ eV.

A series of conductive TTF salts have been synthesised by combining TTF with halides or pseudohalides. These complexes are quasi-one-dimensional compounds containing cation radicals only, in contrast with a cation-anion-radical system such as TTF-TCNQ. The charge carriers are holes and conduction takes place only along the TTF chains. Due to the high electron affinity of the acceptor molecules, the degree of charge-transfer ρ can be derived straight from stoichiometry. Somoano *et al.* have reported salts with thiocyanate (SCN) and selenocyanate (SeCN) in the stoichiometry $(TTF)_{12}(SCN)_7$ and $(TTF)_{12}(SeCN)_7$

[30]. Both salts were found to be conductive with σ_{RT} =550±250 S cm^{-1} and σ_{RT} = 750±250 S cm^{-1} for the thiocyanate and the selenocyanate salt, respectively. Metal-like characteristics were noted above 200K but both compounds underwent a metal-semiconductor transition around 170K. $(TTF)X_n$, where X = Cl, Br, I have been synthesised and studied for different values of n.

$\underline{(TTF)I_n}$

For the iodide salt, n has taken the values of 0.70-0.72, 2, 3 while the simple salt (n=1) could not be prepared [31-33]. $(TTF)I_{0.70\text{-}0.72}$ proved to be the most highly conductive (σ_{RT} ~ 100-450 S cm^{-1}). The structure was monoclinic, the TTF molecules forming segregated eclipsed stacks in which the plane of TTF was approximately perpendicular to the stacking axis. Parallel to the TTF stacks were columns of equally spaced halogen atoms. These were considered not to contribute to the conduction because the distances between the halogen atoms were too large to allow considerable interaction. In Figure 2.5, the temperature dependence of conductivity is shown [32(b)]. This decreased slightly with decreasing temperature in the high temperature region T > 210K, at which temperature a transition is evident. This transition, that led to a less conducting state, was attributed to intrachain interactions. Below 210K, the activation energy varied from 0.12 eV at 170K to 0.084 eV at lower temperatures. A hysteresis loop was evident during warming up. It has been suggested that this results from a weak interstack coupling. Due to weak coupling between stacks, the individual chains did not go through the transition at the same temperature [32(b)].

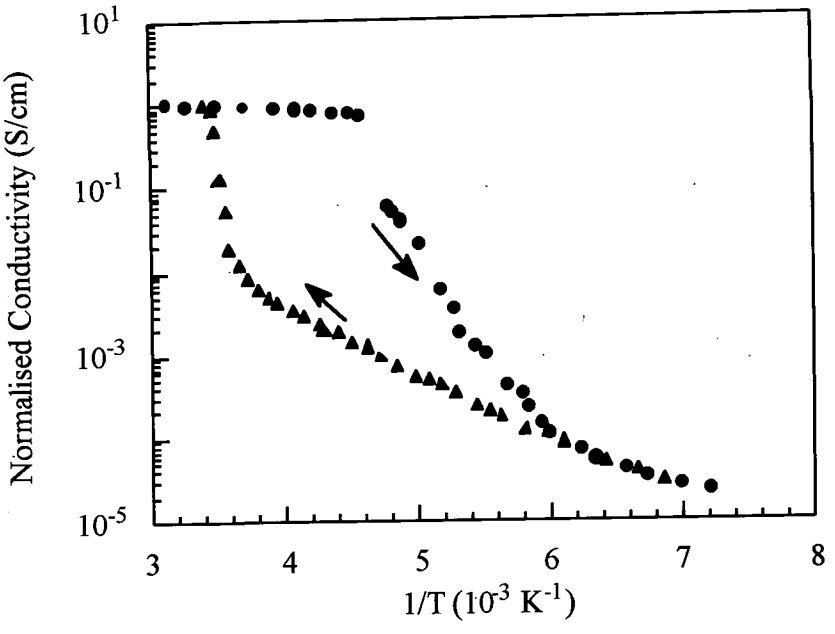

Figure 2.5: Temperature dependence of the normalised conductivity of $(TTF)I_{0.70\text{-}0.72}$ measured along the stacking axis (taken from Ref. 32(b)).

In the iodide salt formed for n=2, the TTF molecules formed segregated stacks as before, but the iodine columns now contained small polyiodide species, predominately I_3^- [33]. The conductivity along the stacking axis was found to be 10^{-3} S cm^{-1} and was thermally activated with $\Delta E = 0.24$ eV. For the salt formed for n=3, again the iodine columns consisted of I_3^- ions. The compound could be written as $(TTF^+)(I_3^-)$ and was not very conductive ($\sigma \sim 10^{-5}$ S cm^{-1}) [33].

<u>$(TTF)Br_n$&$(TTF)Cl_n$</u>

Bromide and chloride salts of TTF of different stoichiometries have been studied [33,34]. The most conductive salts were obtained for n = 0.77 and n = 0.71-0.76 for the chloride and

bromide salts, respectively. The structures of the these salts were found to be similar to that of the $(TTF)I_{0.70-0.72}$ (monoclinic with the TTF and Br molecules forming segregated stacks). The conductivities were 100-500 S cm^{-1} and 200-500 S cm^{-1} at room temperature for the chlorine and bromine salts, respectively. For $(TTF)Br_{0.71-0.76}$ the conductivity underwent a transition to an semiconducting state at 180K, below which it was thermally activated with $\Delta E = 0.081$ eV. No hysteresis was observed during the warming up cycle.

In the (TTF)Br and (TTF)Cl salts, the TTF molecules formed eclipsed cation dimers interspaced with pairs of halogen ions [33]. As expected from stoichiometry, full charge-transfer occurred between the acceptor and donor molecules. The conductivity was found to be low, as expected for fully oxidised compounds, with $\sigma < 10^{-4}$ S cm^{-1}. The relatively high value of σ (~ 0.3 S cm^{-1}), originally reported from Wudl *et al.* for (TTF)Cl [5(b)], suggests that these salts were impure and contaminated by other halide phases. The salts prepared with n = 2 were also insulating.

2.3 Dimethyl- and Trimethyl- Tetrathiafulvalene Salts

Another derivative of TTF was combined with TCNQ in an attempt to suppress the phase transition in TTF-TCNQ. Symmetrical dimethyltetrathiafulvalene, DiMe-TTF, was first prepared by Prinzbach *et al.* in 1965 [35]. The cis- and trans-isomers are shown in Figure 2.6a. The room temperature conductivity of the simple salt DiMe-TTF-TCNQ was the same for both isomers (σ_{RT} = 50 S cm^{-1}). A decrease in the transition temperature was seen for the cis- (58K) and the trans-(50K) isomers [36].

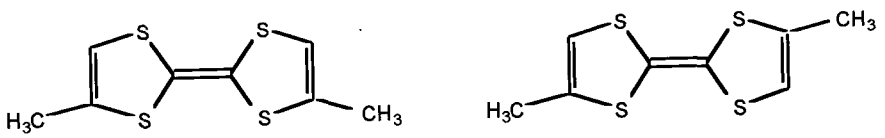

(a)

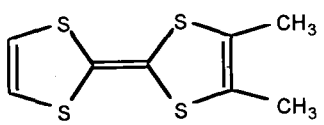

(b)

Figure 2.6: (a) Cis and trans-isomers of symmetrical DiMe-TTF and (b) unsymmetrical DiMe-TTF.

In 1977, Wudl *et al.* reported the synthesis of unsymmetrical DiMe-TTF, in which the methyl groups were located on the same side of the molecule (Figure 2.6b) [37]. As an electron donor, this molecule is superior to TTF as its ionisation potential is lower. A series of radical cation salts based on this DiMe-TTF have been reported [38]. Their stoichiometry has been determined to be 2:1, in contrast with the TTF salts but in agreement with the $(TMTSF)_2X$ salts. For all compounds, the temperature dependence of the conductivity measured along the stacking axis was very similar to that of $(TTF)_{12}(SC)_7$. A smooth maximum for σ was observed below room temperature but a metal-semiconductor transition occurred at lower temperatures. An exception was seen for the thiocyanate salt which exhibited semiconducting behaviour over the entire temperature range. Conductivity data for these compounds are summarised in Table 2.1.

	Cl^-	Br^-	I^-	PF_6^-	BF_4^-	SCN^-
σ_{295K} ($S\ cm^{-1}$)	50-100	150	100	250-300	100-150	2-10
T_{max} (K)	255	215	200	265	240	–

Table 2.1: Electrical conduction of the DiMe-TTF salts. T_{max} is the temperature at which maximum conductivity was observed.

The synthesis of TriMe-TTF was first reported in 1995 [39], and its salts have not yet been synthesised.

2.4 Bis(ethylenedithio)tetrathiafulvalene Salts

A second family of organic materials exhibiting superconductivity was found in the ET family. Most of these salts were found to be two-dimensional with some of the interstack S...S distances being shorter that the intrastack molecular distances. Thus, conduction could take place in two-dimensional sheets instead of one-dimensional stacks.

The iodine salt of ET produced a lot of interest due to its numerous crystalline phases. Ten phases, with different physical properties, have been identified by X-ray analysis. The electrical behaviour of these is summarised in Table 2.2

ET polyiodides	σ_{295K} (S cm^{-1})	Properties	Ref.
α-$(ET)_2I_3$	20	Metallic >130K	40
β-$(ET)_2I_3$	30	Superconductor (T_c = 1.4-8K)	41
θ-$(ET)_2I_3$	30	Superconductor (T_c = 3.6K)	42
κ-$(ET)_2I_3$	40-150	Superconductor (T_c = 3.6K)	42
γ-$(ET)_3(I_3)_{2.5}$	15	Superconductor (T_c = 2.5K)	43
η-$(ET)I_3$	10^{-4}	Semiconductor	44
δ-$(ET)\ I_3(C_2H_3Cl_3)_{0.333}$	15	Metallic > 160K	44
ε-$(ET)I_3(I_8)_{0.5}$	10^{-4}	Semiconductor	44
λ-$(ET)_2I_3I_5$	10^{-1}	Semiconductor	44
ζ-$(ET)_2I_{10}$	10^{-1}	Semiconductor	45

Table 2.2: Cation-radical salts in the (ET) iodide system.

The transition to the superconducting state occurred for most of the phases at ambient pressures. An exception was seen for the β-phase, where the pressure of 1 kbar increased T_c from 1.4K to 8K.

Transformation between the different phases has been achieved by specific heat treatment. For example, annealing α-phase crystals at 70-100°C for 10-20 hours produced β-phase crystals [46]. This phase, called α_t-phase to distinguish it from β, is an ambient

pressure superconductor at 8K. On heating phases with large iodine content, i.e. ε and ζ, iodine is lost resulting in conversion to the β-phase. In these cases, the resultant crystals exhibit superconductivity at a higher critical temperature of T_c= 7.5K [47]. By annealing the β-phase a new one, called β_t was discovered [48]. An increase in the transition temperature was also seen, being 7K for this crystal.

Other salts of ET range from being semiconductors to superconductors. For example, α-$(ET)_2IBr_2$ was found to be a semiconductor but β-$(ET)_2IBr_2$ was superconducting with T_c = 2-2.8K [44]. The β-$(ET)_2ICl_2$ salt was metallic but a transition to the superconducting state was not observed down to 1.3K. The $(ET)_3CuBr_3$ salt was also found to be semiconducting (σ = 0.6 S cm^{-1}) [49].

2.5 Summary

The major landmarks of the development of organic conductors have been presented in chronological order. The materials, that were of interest in this work, and the physical properties of their salts have also been discussed in detail.

References

1. H. Akamatu, H. Inokuchi and Y. Matsunaga, 'Electrical Conductivity of the Perylene-Bromine Complex', *Nature*, **173** (1954) 168.
2. H.N. McCoy and W.C. Moore, 'Organic Amalgams: Substances with Metallic Properties Composed in Part of Non-Metallic Elements', *J. Am. Chem. Soc.*, **33** (1911) 1273.
3. L.R. Melby, R.J. Harder, W.R. Hertler, W. Mahler, R.E. Benson and W.E. Mochel, 'Substituted Quinodimethans, II. Anion-Radical Derivatives and Complexes of 7,7,8,8,Tetracyanoquinodimethan', *J. Am. Chem. Soc.*, **84** (1962) 3374.

4. D.S. Acker, R.J. Harder, W.R. Hertler, W. Mahler, L.R. Melby, R.E. Benson and W.E. Mochel, '7,7,8,8-Tetracyanoquinodimethane and its Electrically Conducting Anion-Radical Derivatives', *J. Am. Chem. Soc.*, **82** (1960) 6408.

5. (a) F. Wudl, G.M. Smith and E.J. Hufnagel, 'Bis-1,3-Dithiolium Chloride: An Unusually Stable Organic Radical Cation' , *JSC Chem. Comm.*, (1970) 1453; (b) F. Wudl, D. Wobschall and E.J. Hufnagel, 'Electrical Conductivity by the Bis-1,3-dithiole-Bis-1,3-dithiolium System', *J. Am. Chem. Soc.*, **94** (1972) 670.

6. J. Ferrraris, D.O. Cowan, V. Walayka and J.H. Perlstein, 'Electron Transfer in a New Highly Conducting Donor-Acceptor Salt', *J. Am. Chem. Soc.*, **95** (1973) 948.

7. E.M. Engler and V.V. Patel, 'Structure Control in Organic Metals. Synthesis of Tetraselenofulvalene and its Charge-Transfer Salt with Tetracyano-*p*-quinodimethane', *J. Am. Chem. Soc.*, **96** (1974) 7376.

8. A.N. Bloch, D.O. Cowan, K. Bechgaard, R.E. Pyle and R.H. Banks, 'Low-Temperature Metallic Behaviour and Resistance Minimum in a New Quasi One-Dimensional Organic Conductor', *Phys. Rev. Lett.*, **34** (1975) 1561.

9. (a) C.S. Jaconbsen, K. Mortesen, J.R. Andersen and K. Bechgaard, 'Transport Properties of Some Derivatives of Tetrathiafulvalene-Tetracyano-*p*-quinodimethane', *Phys. Rev. B*, **18** (1978) 905; (b) A. Andrieux, P.M. Chaikin, C. Duroure, D. Jérome, C. Weyl, K. Bechgaard and J.R. Andersen, 'Transport Properties of The Metallic Salt of TMTSF-DMTCNQ', *J. Physiq.*, **40** (1979) 1199.

10. J.B. Torrance, J.J. Mayerle, V.Y. Lee and K. Bechgaard, 'A New Class of Highly Conducting Organic Materials: Charge-Transfer Salts of The Tetrathiafulvalenes with the Tetrahalo-*p*-benzoquinones', *J. Am. Chem. Soc.*, **101** (1979) 4747.

11. (a) K. Bechgaard, C.S. Jaconsen, K. Mortesen, H.J. Pedersen and N. Thorup, 'The Properties of Five Conducting Salts: $(TMTSF)_2X$, $X=PF_6^-$, AsF_6^-, BF_4^-, NO_3^- Derived From Tetramethyltetraselenafulvalene (TMTSF)', *Sol. Stat. Comm.*, **33** (1980) 1119; (b) D. Jérome, A. Mazaud, M. Ribault and K. Bechgaard, 'Superconductivity in a Synthetic Organic Conductor $(TMTSF)_2PF_6$', *J. Phys. Lett.*, **41** (1980) L95; (c) K. Bechgaard, K. Carneiro, F.B. Rasmussen, M. Olsen, G. Rindorf, C.S. Jacobsen, H.J. Pedersen and J.C. Scott, 'Superconductivity in an Organic-Solid - Synthesis, Structure and Conductivity of Bis(Tetramethyltetraselenafulvalenium) Perchlorate, $(TMTSF)_2ClO_4$', *J. Am. Chem. Soc.*, **103** (1981) 2440.

12. M. Mizuno, A.F. Garito and M.P. Cava, 'Organic Metals: Alkylthio Substitution Effects in Tetrathiafulvalene-Tetracyanoquinodimethane Charge-Transfer Complexes', *JSC Chem. Comm.*, (1978) 18.

13. G. Saito, T. Enoki, K. Toriumi and H. Inokuchi, 'Two-Dimensionality and Suppression of Metal-Semiconductor Transition in a New Organic Metal With Alkylthio Substituted TTF and Perchlorate', *Sol. Stat. Comm.*, **42** (1982) 557.

14. E.B. Yagubskii, I.F. Shchegolev, V.N. Laukhin, P.A. Kononovich, M.V. Karatsovnik, A.V. Zvarykina and L.I. Buravov, 'Normal-Pressure Superconductivity in an Organic Metal $(BEDT\text{-}TTF)_2I_3$[bis(ethyleledithio) Tetrathiofulvalene Triiodide]', *JETP Lett.*, **39** (1984) 12.

15. J.E. Schirber, L.J. Azevedo, J.F. Kwak, E.L. Venturini, P.C.W. Leung, M.A. Beno, H.H. Wang and J.M. Williams, 'Shear-Induced Superconductivity in β-di[bis (ethylenedithio)tetrathiafulvalene [β-(BEDT-TTF)$_2$I$_3$]', *Phys. Rev. B*, **33** (1986) 1987.

16. L. Brossard, M. Ribault, L. Valade and P. Cassoux, 'The First 3D Molecular Superconductor Under Pressure ? : TTF[Ni(dmit)$_2$]$_2$', *Physica B*, **143** (1986) 378.

17. A. Aumüller, P. Erk, G. Klebe, S. Hünig, J.U. Schütz and H.-P. Werner, 'A Radical Anion Salt of 2,5,-Dimethyl-*N*-*N*'-dicyanoquinonediimine with Extremely High Electrical Conductivity', *Angew. Chem. Int. Ed. Engl.*, **25** (1986) 740.

18. K. Kikuchi, T. Namiki, K. Saito, I. Ikemoto, K. Murata, T. Ishiguro and K. Kobayashi, 'New Organic Superconductor (DMET)$_2$Au(CN)$_2$', *Chem. Lett.*, (1987) 931.

19. A. Kobayashi, H. Kim, Y. Sasaki, R. Kato, H. Kobayashi, S. Moriyama, Y. Nishio, K. Kajita and W. Sasaki, 'The First Molecular Superconductor Based on a π-Acceptor Molecules and Closed-Shell Cations, [(CH$_3$)$_4$N] [Ni(dmit)$_2$]$_2$, Low temperature X-Ray Studies and Superconducting Transition', *Chem. Lett.*, (1987) 1819.

20. M.D. Mays, R.D. McCullough, D.O. Cowan, T.O. Pehler, W.A. Bryden and T.J. Kistenmacher, 'Intitial Studies of a New Tellurium Containing Organic Metal: Tetratellurafulvalene-Tetracyanoquinodimethane (TTeF-TCNQ)', *Sol. Stat. Comm.*, **65** (1988) 1089.

21. H. Urayama, H. Yamochi, G. Saito, K. Nozawa, T. Sugan, M. Kinoshita, S. Sato, K. Oshima, A. Kawamoto and J. Tanaka, 'A New Ambient Pressure Organic Superconductor Based on BEDT-TTF with T_c Higher than 10K (T_c = 10.4K)', *Chem. Lett.*, (1988) 55.

22. (a) G.C. Papavassiliou, G.A. Mousdis, J.S. Zambounis, A. Terzis, A. Hountas, B. Hilti, C.W. Mayer and J. Pfeiffer, 'Low Temperature Measurements of the Electrical Conductivities of Some Charge Salts with Asymmetric Donors MDT-TTF, EDT-TTF and EDT-DSDTF. (MDT-TTF)$_2$AuI$_2$, A New Superconductor (T_c=3.5K at Ambient Pressure', *Synth. Met.*, **27** (1988) B379; (b) A.M. Kini, M.A. Beno, D. Son, H.H. Wang, K.D. Carlson, L.C. Potter, U. Welp, B.A. Vogt and J.M. Williams, '(MDT-TTF)$_2$AuI$_2$ - An Ambient Pressure Organic Superconductor (T_c = 4.5K) Based on an Asymetrical Electron Donor', *Sol. Stat. Comm.*, **69** (1989) 503.

23. F. Wudl, H. Yamochi, T. Suzuki, H. Isotalo, C. Fite, H. Kasmai, K. Liou and G. Srdanov, '(BEDO)$_{2.4}$ I$_3$: The First Robust Organic Metal of BEDO-TTF', *Inorg. Chem.*, **112** (1990) 2461.

24. M.A. Beno, H.H. Wang, A.M. Kini, K.D. Carlson, U. Geiser, W.K. Kwok, J.E. Thomson, J.M. Williams, J. Ren and M.-H. Whangbo, 'The First Ambient Pressure Organic Superconductor Containing the Oxygen Donor Molecule β-M-(BEDO-TTF)$_3$Cu$_2$(NCS)$_3$, T_c=1.06K', *Inorg. Chem.*, **29** (1990) 1599.

25. A.M. Kini, U. Geiser, H.H. Wang, K.D. Carlson, J.M. Williams, W.K. Kwok, K.G. Vandervoort, J.E. Thomson, D.L. Stupka, D. Jung and M.-H. Wang, 'A New Ambient-Pressure Organic Superconductor, κ-ET$_2$Cu[N(CN)$_2$] Br, with the Highest Transition Temperature yet Observed (Inducive Onset T_c=11.6K, Resistive Onset T_c=12.5K)', *Inorg. Chem.*, **29** (1990) 2555; (b) J.M. Williams, A.M. Kini, H.H. Wang, K.D. Carlson,

U. Geiser, L.K. Montgomery, G.J. Pyrka, D.M. Watkins, J.M. Kommers, S.J. Boryschul, A.V.S. Crouch, W.K. Kwok, J.E. Schrirber, D.L. Overmyer, D. Jung and M.-H Whangbo, 'From Semiconductor- Semiconductor Transition (42K) to the Highest - T_c Organic Superconductor. κ-$ET_2Cu[N(CN)_2]$ Cl (T_c=12.5K)', *Inorg. Chem.*, **29** (1990) 3272.

26. L. Balicas, K. Behnia, W. Kang, P. uban-Senzier, E. Canadell, D. Jérome, M. Ribault and J.-M Fabre, '$(TMTTF)_2Br$: The First Organic Superconductor in the $(TMTTF)_2X$ Family', *Adv. Mat.*, **6** (1994) 762.

27. H. Shirakawa, E.J. Louis, A.G. MacDiarmid, C.K. Chiang and A.J. Heeger, 'Synthesis and Electrically Conducting Organic Polymers: Halogen Derivatives of Polyacetylene, $(CH)_x$', *J.C.S. Chem. Comm.*, (1977) 578.

28. C.S. Jacobsen, J.R. Andersen, K. Bechgaard and C. Berg, 'Organic Conductors: Electrical and Magnetic Properties of Tetrathiafulvalenium-Tetracyanoquinodimethanide (TTF-MTCNQ)', *Sol. Stat. Comm.*, **19** (1976) 1209.

29. D.J. Dahm, G.R. Johnson, M.G. Giles and J.D. Wilson, 'Structure, Conductivity and Electron Spin Resonance of Tetrathiafulvalene 11,11,12,12-tetracyanonaphtho-2,6,quinodimethane (TTF)(TNAP)', *Phys. Rev. B*, **12** (1975) 4085.

30. R.B. Somoano, A. Gupta, V. Hadek, M. Novotny, M. Jones, T. Datta, R. Deck and A.M. Hermann, 'Electrical Magnetic and Optical Properties of the Tetrathiafulvalene (TTF) pseudiohalides, $(TTF)_{12}(SCN)_7$ and $(TTF)_{12}(SeCN)_7$', *Phys. Rev. B*, **15** (1977) 595.

31. R.J. Warmack, T.A. Calcott and C.R. Watson, 'DC Conductivity of Tetrathiofulvalene Bromide (TTF-Br_n) and TTF-I_n Single Crystals', *Phys. Rev. B*, **12** (1975) 3336;

32. (a) J.J. Daly and F. Sanz, 'Hepta(tetrathiafulvalene) Pentaiodide: The Projected Structure', *Acta Cryst.*, **B31** (1975) 620; (b) R.B. Somoano, A. Gupta, V. Hadek, T. Data, M. Jones, R. Deck and A.M. Hermann, 'The Electrical and Magnetic Properties of $(TTF)(I)_{0.71}$', *J. Chem. Phys.*, **63** (1975) 4970.

33. B.A. Scott, S.J. La Placa, J.B. Torrance, B.D. Silverman and B. Welber, 'The Crystal Chemistry of Organic Metals. Composition, Structure and Stability in the Tetrathiafulvalenium-Halide Systems', *J. Am. Chem. Soc.*, **99** (1977) 6631.

34. S.J. La Placa, P.W.R. Cornfield, R. Thomas and B.A. Scott, 'Non Integral Charge Transfer in an Organic Metal: The Structure and Stability Range of $(TTF)Br_{0.71-0.76}$', *Sol. Stat. Comm.*, **17** (1975) 635.

35. H. Prinzbach, H. Berger and A. Lüttringhaus, 'Proton Activity of the 1,3-Dithiolium System', *Angew. Chem.*, **4** (1965) 435.

36. J.S. Miller, 'Design and Synthesis of Highly Conducting One-Dimensional Materials', *Ann. N. Y. Acad. Sci.*, **313** (1978) 25.

37. F. Wudl, A.A. Kruger, M.L. Kaplan and R.S. Hutton, 'Unsymmetrical Dimethyltetrathiafulvalene', *J. Org. Chem.*, **42** (1977) 768.

38. A. Abderraba, R. Laversanne, E. Dupart, C. Coulon, P. Delthaes and C. Hauw, 'Electrocrystallisation and Physical Properties of Dimethyltetrathiafulvalenium Salts', *J. Phys.Coll. 3*, **44** (1983) 1243.

39. A.J. Moore, M.R. Bryce, A.S. Batsanov, J.C. Cole, J.A.K. Howard, 'Functionalised Trimethyltetrathiafulvalene (TriMe-TTF) Derivatives via Reactions of Trimethyltetrathiafulvalenyllithium with Electrophiles: X-ray Crystal Structures of Benzoyl-TriMe-TTF and Benzoylthio-TriMe-TTF', *Synthesis*, **74** (1995) 675.

40. E.B. Yagubskii, I.F. Shchegolev, V.N. Laukhin, R.P. Shibaeva, E.E. Kostyuchenko, A.K. Khomenko, Yu.V. Sushko and A.V. Zvarykina, 'Superconducting Transition in the Dielectric α Phase of Iodine-Doped (BEDT-TTF)$_2$I$_3$ Compound', *JETP Lett.*, **40** (1984) 1201.

41. (a) E.B. Yagubskii, I.F. Shchegolev, V.N. Laukhin, P.A. Kononovich, M.V. Karatsovnik, A.V. Zvarykina and L.I. Buravov, 'Normal-Pressure Superconductivity in an Organic Metal (BEDT-TTF)$_2$I$_3$ [bis(ethylenedithiolo) Tetrathiafulvalene Triiodide], *JETP Lett.*, **39** (1984) 13; (b) V.N. Laukhin, E.E. Kostyuchenko, Yu.V. Sushko, I.F. Shchegolev and E.B. Yagubskii, 'Effect of Pressure on the Superconductivity of β-(BEDT-TTF)$_2$I$_3$', *JETP Lett.*, **41** (1985) 81.

42. K. Kajita, Y. Nishio, S. Moriyama, W.W. Sasaki, R. Kato, H. Kobayashi and A. Kobayashi, 'New-Organic Superconductors κ- and θ-(BEDT-TTF)$_2$I$_3$: Transport Property', *Sol. Stat. Comm.*, **64** (1987) 1279.

43. E.B. Yagubskii, I.F. Shchegolev, S.I. Petsotskii, V.N. Laukhin, P.A. Kononovich, M. V. Kartsovnik and A.V. Zvarykina, 'Superconducting Properties of the Orthorhombic Phase of Bis(ethylenedithio)tetrathiafulvalene Triiodide', *JETP Lett.*, **39** (1984) 328.

44. E.B. Yagubskii and R.P. Shibaeva, 'Organic Conductors and Superconductors Based on Bis(ethylenedithio)tetrathiafulvalene and its Derivatives', *J. Molec. Electr.*, **5** (1989) 25.

45. M.A. Beno, U. Geiser, K.L. Kostka, H.H. Wang, K.S. Webb, M.A. Firestone, K.D. Karlson, L. Lunez, Z.M. Williams and M.H. Whangno, 'Synthesis and Structure of ζ-(BEDT-TTF)$_2$(I$_3$)(I$_5$) and (BEDT-TTF)$_2$(I$_3$)(TIL$_4$)-Comparison of the Electrical Properties of Organic Conductors Derived from Chemical Oxidation vs Electrocrystallisation', *Inorg. Chem.*, **26** (1987) 1912.

46. D. Schweitzer, P. Bele, H. Brummer, E. Gogu, U. Haeberlen, I. Hennig, I. Klutz, R. Swietlik and H.J. Keller, 'A Stable Superconducting State at 8 K and Ambient Pressure in α_t-(BEDT-TTF)$_2$I$_3$', *Z. Phys. B Cond. Matt.*, **67** (1987) 489.

47. V.A. Merzhanov, E.E. Kostyuchenko, V.N. Laukhin, R.M. Lobkovskaya, M.K. Makova, R.P. Shibaeva, I.F. Shchegolev and E.V. Yagubskii, 'An Increase in the Superconducting-Transition Temperature of β-(BEDT-TTF)$_2$I$_3$ to 6-7K at a Normal Pressure', *JETP Lett.*, **41** (1985) 181.

48. S. Kahlich, D. Schweitzer and H.J. Keller, 'Investigations of the Transport Properties of the Organic Superconductors β-(BEDT-TTF)$_2$I$_3$ and β_t-(BEDT-TTF)$_2$I$_3$', *Sol. Stat. Comm.*, **76** (1990) 933.

49. T. More, F. Sakai, G. Saito and H. Inokuchi, 'Structural and Electrical Properties of (ET)$_3$CuBr$_3$', *Chem. Lett.*, (1987) 927.

CHAPTER THREE

THIN FILMS

3.0 Introduction

This chapter is divided into three sections. First, a general introduction to thin films is given, followed by some of the experimental techniques for film formation. Thermal evaporation, the method used in this project is discussed in detail, while other techniques are briefly mentioned. Previous work on organic thin films deposited by thermal evaporation is then considered. Finally, the development and history of organic thin film transistors (TFTs) is outlined.

3.1 Thin Films

Historically, the physical dimension of thickness was used to draw a distinction between thick and thin films. A thickness of 1 μm (1000 nm) was often accepted as the boundary. A recent viewpoint is that a film can be considered thin or thick depending on whether it exhibits surface-like or bulk-like properties. Another view classifies a film according to its usage: being thin if it is exploited for surface properties and thick for bulk properties. The same coating material can therefore be a thin or a thick film depending upon the application.

Thin films have a very large surface to volume ratio and thus, can be regarded as 'all surface'. The surface of a material may have quite different properties from the bulk. There

can be many reasons for this but these mostly concern the fact that the surface atoms are not surrounded on all sides by similar atoms (as are interior atoms).

Thin films have found applications in many fields, the main ones are summarised below:

Optically Functional: Laser optics, reflective and anti-reflective coatings, selective solar absorbers.

Electrically Functional: Electrical conductors, active solid state devices, electrical insulators and solar cells

Mechanically Functional: Wear and erosion resistant coatings, hard coatings for cutting tools.

Chemically Functional: Corrosion resistance coatings, engine blades and vanes, marine equipment.

3.2 Thin Film Deposition Techniques

3.2.1 Thermal Evaporation

Thermal evaporation is one of the physical vapour deposition (PVD) techniques. Historically, the first evaporated thin films were probably prepared by Faraday in 1857 when he exploded metal wires in a vacuum [1]. In PVD methods, atoms are removed from the source by thermal means. There are three stages to such processes.

Step 1: Creation of vapour phase species.

Step 2: Material transport from the source to the substrate in the vapour phase.

Step 3: Condensation and film growth on the substrate.

The transformation of a condensed phase into vapour involves the conversion of the thermal energy supplied to the evaporant to mechanical energy as represented by the expansion into vapour. The change in the equilibrium vapour pressure with temperature is given by the Clausius-Clapeyron equation [2]

$$\ln p \approx -\frac{\Delta H}{RT} + \text{const} \tag{3.1}$$

where p is the vapour pressure assumes that the heat of evaporation (ΔH) is constant, T the temperature, R the universal gas constant and H the enthalpy (Equation 3.1). The process takes place in a vacuum environment. The use of low pressures serves to reduce the amount of impurities in the film and it also enhances the probability of straight line propagation for the evaporant (see chapter 5). As more vapour atoms arrive on the substrate, the vapour pressure (at the substrate) increases. When this reaches the equilibrium vapour pressure, condensation takes place and a film is deposited. Some of the most important features of thin film formation by thermal evaporation are discussed in the sections below.

Film Thickness Uniformity

The thickness uniformity of the films resulting from thermal evaporation is an important factor. Consider evaporation from either a point or a small surface source onto a parallel plane-receiving substrate surface, as indicated in Figure 3.1. The film thickness t is given by

$$t = \frac{1}{\rho}\frac{dM_s}{dA} \tag{3.2}$$

where M_s and ρ stand for the mass and the density of the deposited material, respectively, while A is its surface area. For the point source

$$t = \frac{M\cos\theta}{4\pi\rho r^2} = \frac{Mh}{4\pi\rho r^3} = \frac{Mh}{4\pi\rho(h^2 + l^2)^{3/2}} \tag{3.3}$$

where M is the total mass of the evaporated material, θ the angle of incidence, h the source-substrate distance and l the distance on the substrate as seen in Fig. 3.1. The thickest deposit (t_0) occurs at $l = 0$, in which case $t_0 = M / 4\pi\rho h^2$ and thus

$$\frac{t}{t_0} = \frac{1}{\{1+(l/h)^2\}^{3/2}} \tag{3.4}$$

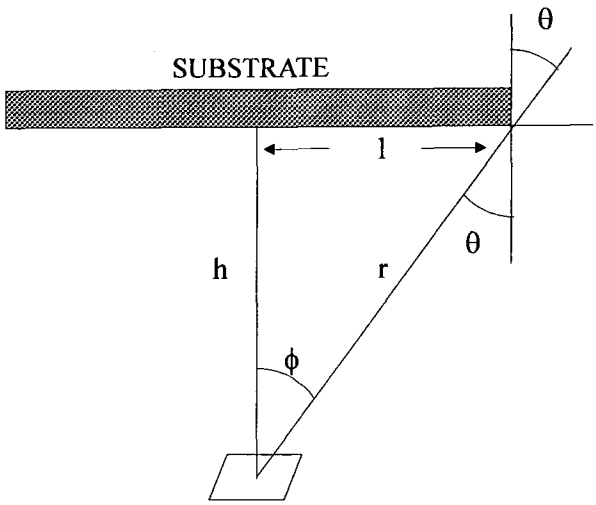

Figure 3.1: Geometry of evaporation onto parallel plane substrate from a surface source.

Similarly, for a surface source

$$t = \frac{M\cos\theta\cos\phi}{\pi\rho r^2} = \frac{M}{\pi\rho r^2}\frac{h}{r}\frac{h}{r} = \frac{M\,h^2}{\pi\rho(h^2+l^2)^2} \tag{3.5}$$

where ϕ is the angle of emission. For a parallel substrate θ=φ and so $\cos\theta = \cos\phi = h/r$. When normalised to the thickest dimensions, or $t_0 = M/\pi\rho h^2$

$$\frac{t}{t_0} = \frac{1}{\{1+(l/h)^2\}^2} \tag{3.6}$$

For example, consider l=1.75 cm and h=5.5 cm. This gives a thickness decrease at the edges of the sample of 18 %, i.e., if t_0=1 μm then t= 0.82 μm.

Film Formation

Interest in thin film formation processes dates at least to the 1920s. During research at the Cavendish laboratories on evaporated thin films, the concepts of nucleation, coalescence and growth were advanced [3].

Condensation is the transformation of a gas into a liquid or solid. Thermodynamically, the only requirement for condensation is that the partial pressure of the film material in the gas phase be equal to or larger than its vapour pressure in the condensed phase at the same temperature, i.e. vapour is saturated. However, this is true only if condensation takes place on film material already condensed on a substrate of the same substance. In the case where the substrate has a different chemical nature, a third phase, the adsorbed phase, in which vapour atoms are adsorbed on the substrate but have not yet combined with other adsorbed atoms, exists. Condensation is initiated by the formation of small clusters and through combination of several adsorbed atoms. These clusters are called nuclei and the process of cluster formation is called nucleation. The process of enlargement and coalescence of the nuclei to finally form a coherent film is termed growth. Frequently, nucleation and growth occur simultaneously during film formation.

There are three basic growth modes [4] (illustrated in Figure 3.2):

(i) Three-dimensional (3-D) island, or Volmer-Weber, growth, during which small clusters are nucleated directly on the substrate surface. The clusters then grow into islands which in turn coalesce to form a continuous film. This type of growth occurs when the film atoms are more strongly bound to each other that to the substrate.

(ii) Two-dimensional (2-D) layer-by-layer, or Frankvan der Merwe, growth occurs when the binding between film atoms is equal to or less than that between the film atoms and the substrate.

(iii) The Stranski-Krastanov mode is a combination of the previous two. In this case, after forming one or two monolayers, further layer growth becomes unfavourable and 3-D islands form.

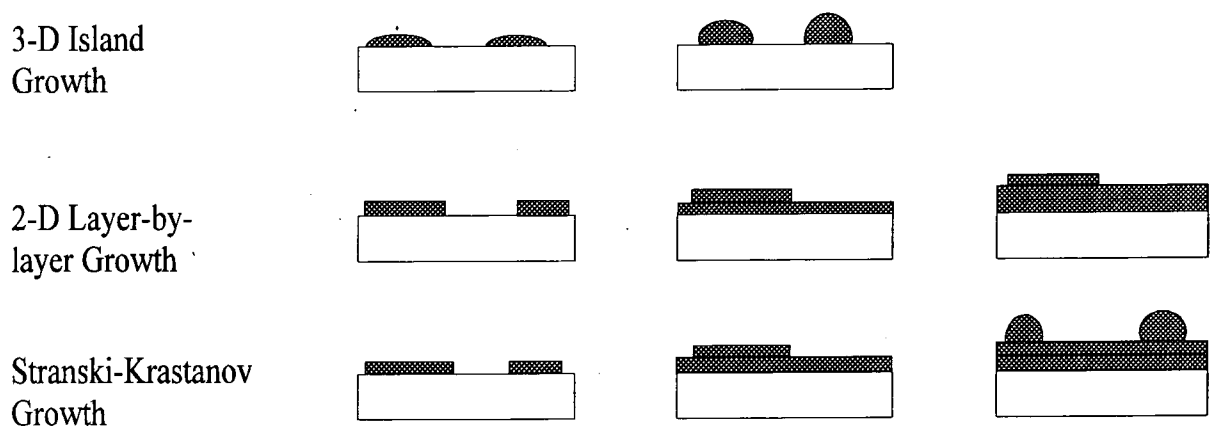

Figure 3.2: Schematic representation of the three film growth modes.

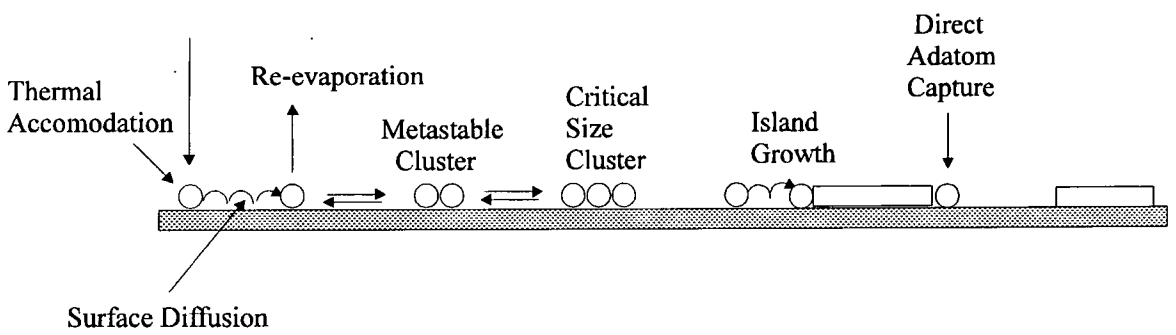

Figure 3.3: Schematic representation of processes leading to three-dimensional nucleation and film growth.

Figure 3.3 illustrates the mechanism involved in 3-D nucleation and growth. An impinging flux must be first thermally accommodated on the substrate. This typically occurs within a few vibrational periods of the surface atoms. The adatoms (adsorbed atoms) can then diffuse on the surface to interact with other adatoms or re-evaporate. Clusters smaller than the critical size could dissolve; clusters bigger than the critical size, will continue growing and thus become islands which in turn coalesce to form a continuous film.

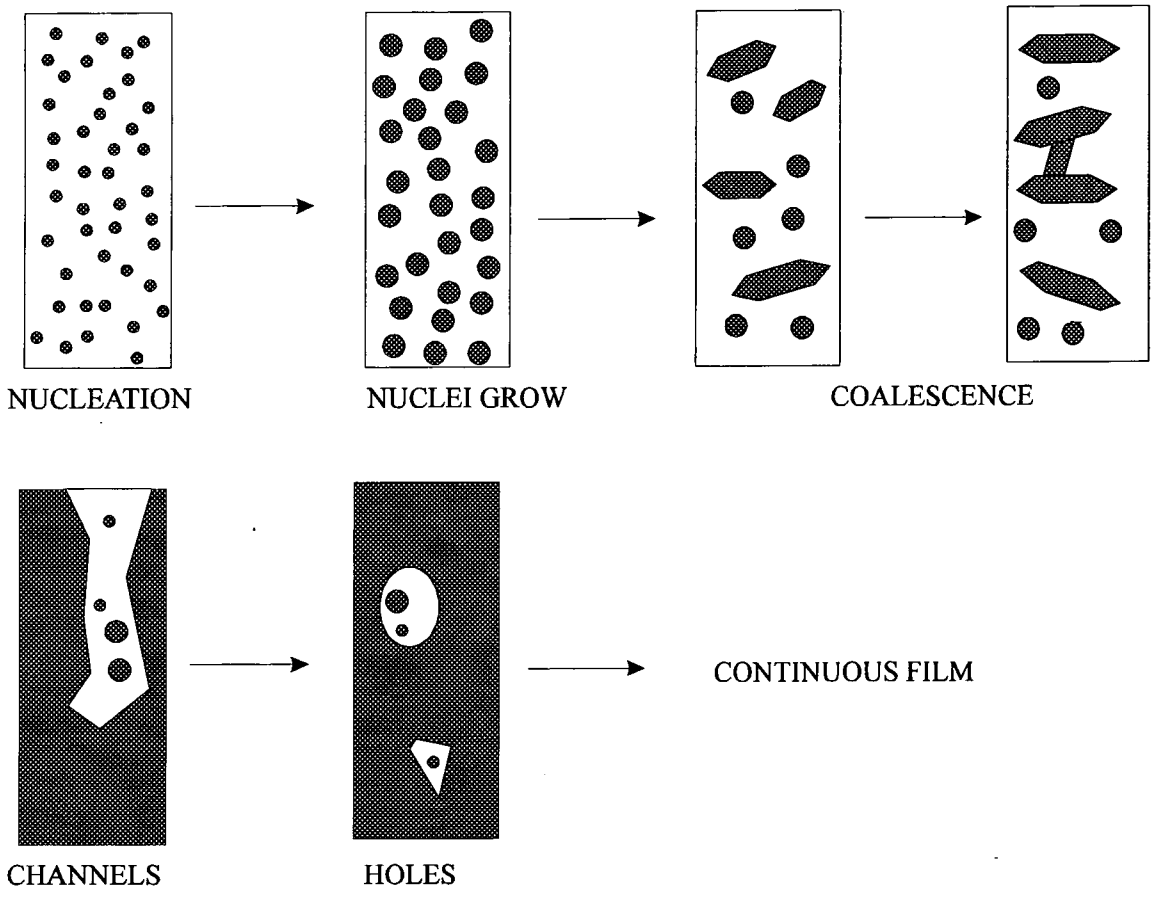

Figure 3.4: Schematic illustration of sequential steps during nucleation and the early stages of film growth [Ref. 5].

Figure 3.4 illustrates the various steps involved in thin film formation. Large islands continue to grow by capture of mobile adatoms and small clusters and/or by coalescence with nearby smaller islands and occasionally with other larger islands. Thus, the film becomes

semi-continuous with a network of channels and holes. Secondary nucleation, nuclei growth and island coalescence can also occur in the voids. The secondary islands are then incorporated into the growing film as it becomes continuous. The point at which this occurs depends both on the evaporant and the substrate; for example, a film of gold evaporated on a glass substrate at room temperature becomes continuous at an average thickness of about 30 nm.

Important Deposition Parameters

The first stages of nucleation and growth depend upon the deposition parameters. The effect of some of these is described below:

Substrate Surface: Thin films tend, in the first instance, to replicate the substrate on which they are evaporated (epitaxy). Dust particles on the surface produce pinholes in the film (the term pinholes is used to express a number of defects in the film, the simplest being a hole).

Substrate Temperature (T_s): This is one of the most important parameters in film growth. The energy of the incident atoms is already high and consists of two parts, the latent heat of evaporation (ΔH in Equation 3.1) and the thermal velocity attained by the hot vapour source. The energy retained by the molecules condensing on the substrate depends on the binding energy or heat of adsorption. If this is low compared with the latent heat of evaporation possessed by the condensed molecule, then the molecule retains high energy and may be mobile on the surface. A high T_s provides additional kinetic energy, so that a molecule may migrate to sites of lower surface potential and form a preferred structure. So, a discontinuous island structure is predicted to persist and a continuous film will take longer to

develop for these values of T_S. At much higher substrate temperature there may be sufficient energy available for re-evaporation to occur.

An example has been given for gold and silver thin films [6]. On a cold substrate, these are highly disordered but the nucleation rate is high and continuous films are formed at low average thicknesses. As T_S approaches ambient, the structure is more aggregated but there are signs of a preferred crystal orientation in the aggregates. At higher T_S, a more pronounced orientation is observed.

Deposition Rate: (affected by the source temperature) Levinstein [7] used the techniques of electron diffraction and electron microscopy to study the surface of evaporated metal films. He came to the conclusion that when the rate of arrival at a surface is high, there are many atoms migrating across the surface and the rate of nuclei formation is high. Films formed at high deposition rates therefore tend to have a smaller grain size than films deposited slowly. At sufficiently high deposition rates, the film is amorphous. This occurs since the adatoms do not have enough time to diffuse across the surface and find low energy sites before they are buried by subsequently deposited adatoms.

Residual Gas Atmosphere: This determines principally the quantity of gas that will be trapped in the film structure. The use of low pressures reduces this quantity and also guarantees that chemical reactions between the gas and the evaporant will not take place.

The Co-evaporation Technique

The incorporation of two or more sources for the evaporation of different materials in the same vacuum is widely used to produce multilayer films. By operating two sources

simultaneously, it is possible to deposit multiconstituent films which are not amenable to direct evaporation. The types of sources used are the same as in single-source evaporation.

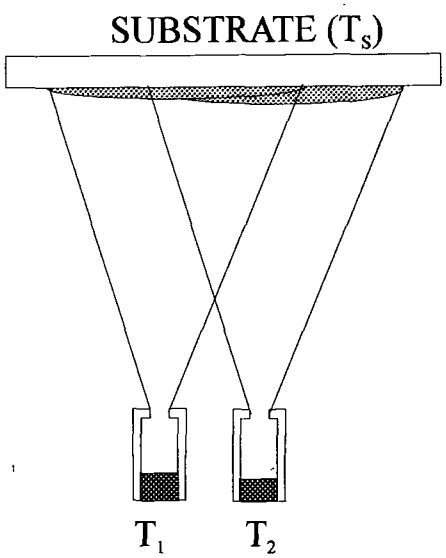

Figure 3.5: Two-source evaporation arrangement.

As the two materials evaporate, their vapours meet in the vicinity of the substrate. The constituent vapour pressures are lower over the compound than over the pure elements. Thus, the vapour pressure of the compound becomes saturated and a film is deposited. The degree of saturation needed to deposit the compound but not the pure elements depends on the condensation coefficients, i.e. on the substrate temperature T_S. Often, the individual compounds cannot deposit in a specific T_S range. An example is CdSe, compound formation is only possible within a restricted range of T_S values [2].

The objective of two-source evaporation is the deposition of films having one particular stoichiometry. Therefore, the central problem in this technique is the control of the rate of the constituent vapours. This rate can be partly controlled by adjusting the source temperatures T_1 and T_2.

3.2.2 Other Techniques

In the following, some of the most widely used other deposition techniques are briefly reviewed.

Chemical Vapour Deposition (CVD): CVD is the process of chemically reacting a volatile compound of a material to be deposited with other gases, to produce a non-volatile solid that deposits atomistically on a suitable substrate. The deposited film thickness uniformity depends on the delivery of equal amounts of reactants to all surface areas. By varying the experimental conditions such as substrate material and temperature, composition of the reaction gas mixture, total pressure gas flows, etc., films with defined properties can be grown.

Sputtering: The ejection of atoms from the surface of a material by bombardment with fast heavy particles is called sputtering. The process is one of momentum transfer. Sputtered species (atoms or clusters of atoms) can be condensed onto a substrate in vacuum, as with thermal evaporation. There are several variations of the basic sputtering process. For example, if the material is vaporised by irradiation of a laser beam, then the technique is called laser induced evaporation.

Langmuir-Blodgett (LB) Technique: Langmuir films are formed by depositing a small amount of a suitable material in a volatile solvent on the surface of a highly pure subphase, usually water. When the solvent evaporates, it leaves an expanded monolayer on the water surface. By slowly compressing the film, this forms an ordered surface layer one molecule thick. To form LB films, a suitable substrate must be repeatedly passed through the surface layer. The materials used are normally amphiphilic, i.e. they posses a hydrophilic head group and a hydrophobic tail.

Spinning: One of the simplest and quickest means of depositing uniform thin films is by spin-coating. The material deposited is first dissolved in a suitable solvent and is then filtered to remove particulate matter; finally spreading and spinning at a predetermined speed and time takes place. Materials deposited by this method do not require to be amphiphilic, as for LB films. The quality of the films can be controlled by adjusting the substrate temperature during spinning, the spinning speed and time.

3.3 Evaporated Thin Films of Organic Charge-Transfer Complexes

Though the evaporation technique has been used widely for metals and other inorganic materials, thin film formation of charge-transfer complexes has not yet been studied widely. These compounds are generally composed of two kinds of chemical species and it can be difficult to control their stoichiometries in the resultant complex.

3.3.1 Tetrathiafulvalene (TTF)

Yudasaka *et al.* [8-10], have reported the preparation of (TTF) iodide thin films by thermal evaporation. Iodine and TTF were evaporated simultaneously in high vacuum, using the co-evaporation technique. The source temperature for TTF was kept between 50°C and 70°C and deposition rates were maintained between unity and several tens of nm min^{-1}. Films were deposited on mica and their structure was found to depend strongly on the substrate temperature T_S. For $T_S < 0°C$, uncomplexed TTF coexisted with TTF_7I_5; for $T_S > 25°C$, nothing was deposited; for T_S between 0°C and 25°C polycrystalline films of TTF_7I_5, identified by X-ray analysis, were obtained. In the latter case, highly orientated rod-like

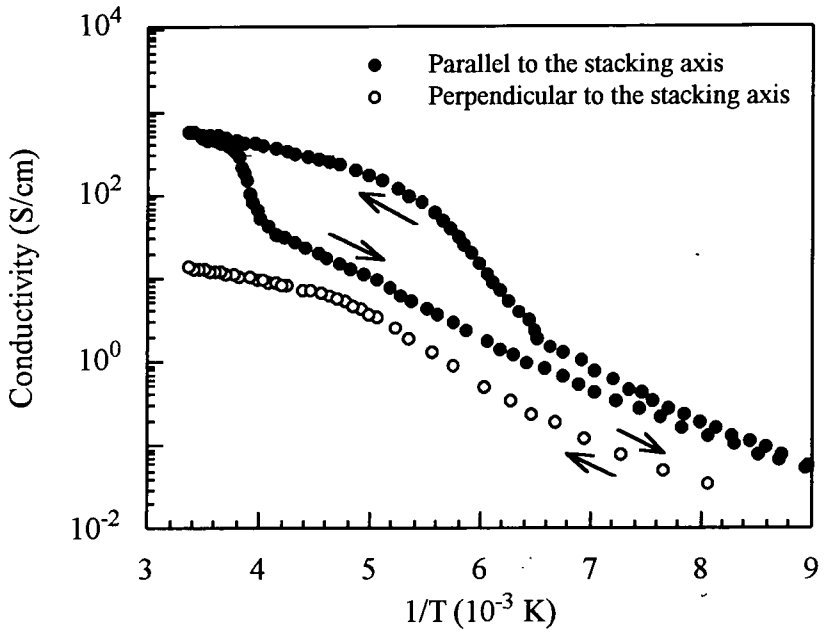

Figure 3.6: Electrical conductivities of an evaporated $(TTF)_7I_5$ thin film, measured parallel and perpendicular the stacking axis, as a function of temperature (taken from Ref. 10).

crystals were evident by scanning electron/tunnelling microscopy [11]. The dc room temperature conductivity, σ, showed anisotropic behaviour. Measured parallel to the column axis c, this was several hundreds S cm^{-1} and exhibited a hysteresis loop in its temperature dependence. Measured perpendicular to the stacking axis, σ~10 S cm^{-1} and showed no hysteresis in its temperature dependence. In the latter case, examining the shape of the curve, three different regions can be identified with transitions at 210K and 150K, Figure 3.6. The activation energy was 0.055 eV for temperatures between 300K and 210K, 0.15 eV between 200 K and 150 K and 0.01 eV between 190K and 120K.

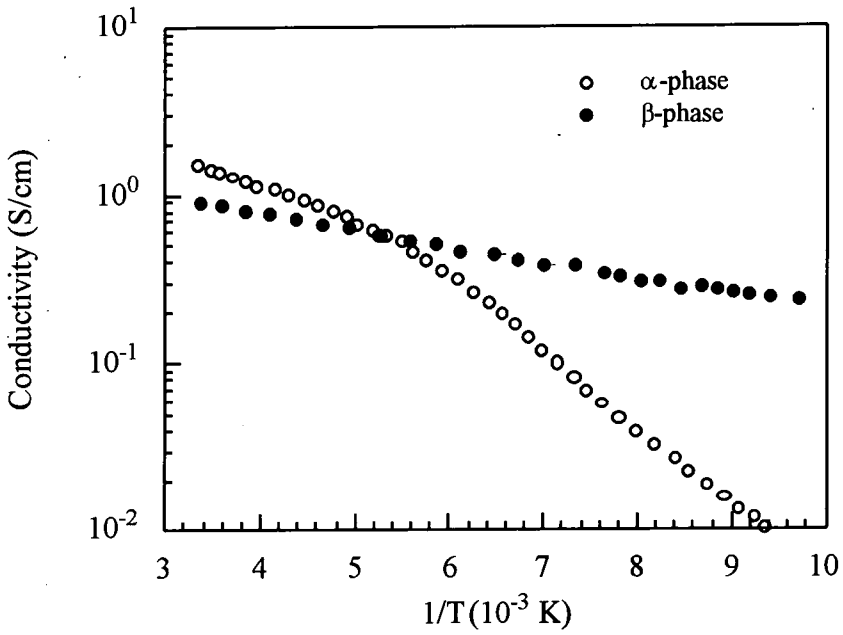

Figure 3.7: Electrical conductivities of the α-phase (open circles) and the β-phase (full circles) of an evaporated $(BEDT\text{-}TTF)_2I_3$ film as a function of temperature (taken from Ref. 12).

3.3.2 Bis(ethylenedithio)tetrathiafulvalene (BEDT-TTF)

Kawabata *et al.* [12,13], have prepared (BEDT-TTF) iodide thin films by evaporation. BEDT-TTF powder doped with iodine, prepared by direct reaction, was used as the starting material. Films were deposited on a glass substrate and showed dependence on the source-substrate distance h. For h greater than 3 cm, the resulting films consisted solely of (BEDT-TTF) molecules. When h was smaller than 3 cm, a strong dependence of the film structure on the substrate temperature, as for TTF, was seen; for $T_s < 50°C$, amorphous films of (BEDT-TTF) iodide were obtained. These were conducting with $\sigma = 0.01$ S cm^{-1}. For $T_s = 70°C$, films consisted of the α-phase ($\sigma = 1$ S cm^{-1}); for $T_s = 80°C$, films consisted of β-phase ($\sigma \sim 1$ S cm^{-1}); for $T_s > 100°C$ no iodine was found in the samples.

Figure 3.7 shows the temperature dependence of the conductivities for the α- and β- phases. By annealing the α-phase at 90°C for 40 hours, films consisting of the superconducting α_t-phase were obtained, exhibiting $\sigma \sim 0.5$ S cm^{-1} [14,15] An island structure was seen after examination under the STM, with dimensions ~ 1 μm and 0.1 μm for the α and the α_t-phase, respectively [16].

3.3.3 TCNQ Salts

In 1974, Chaudari *et al.* [17] reported epitaxial films of TCNQ-TTF from acetonitrile solution on NaCl substrates. Polycrystalline films were obtained when T_s was kept at or near room temperature; for T_s = 70°C only two kinds of crystal orientation were seen (biorientated films) while deposition on a substrate with particular orientation and for 70°C < T_s < 95°C single positioned grains were identified. These layers exhibited a conductivity of $\sigma_{RT} \sim 30$ S cm^{-1}. For the biorientated films, this value was an order of magnitude smaller.

The method of co-evaporation has also been used to produce thin films of TTF-TCNQ [18]. The ratio of TTF:TCNQ for films on SiO_2 was examined for different T_s; for 31°C <T_s < 42°C, this was found to constant with a value of unity; below this T_s region the ratio was greater than one (TTF rich films) and above, less than one (TCNQ rich films). It was assumed that the morphology of the films consisted of single crystals, in between which there was amorphous phase. Conductivity values were between 1 S cm^{-1} and 100 S cm^{-1}.

A derivative of TCNQ, 2,5-bis-methylthio-7,7',8,8'-tetracyanoquinodimethane (BMT-TCNQ) has also been evaporated [19]. Films on quartz, polyethyleneterephthalate

(PET) and KBr were crystalline and were in the same phase as that of single crystals, according to X-ray diffraction analysis. No special care was taken with the substrate temperature, i.e. substrate was at ambient temperature. The room temperature conductivity value was $\sigma = 2 \times 10^{-5}$ S cm^{-1}.

3.3.4 Phthalocyanines

Vacuum deposited thin films of metal phthalocyanines, formed by the single source method, have been widely investigated. The effect of the substrate temperature has also been studied for these materials. Uyeda *et al.* [20], have evaporated platinum-, copper- and zinc-phthalocyanines. Films deposited on mica were found to have a different structure for different values of T_S. For 150°C < T_S < 170°C, well-defined single-directional orientations were found; for T_S = 250°C, and for 200°C < T_S < 250°C double-directional and triple-directional orientations were observed, respectively. Yudasaka *et al.* [21,22] reported on evaporated films of $Si(Pc)(OH)_n$ on mica and glass, obtaining $Si(Pc)(OH)_2$ for T_S < 200°C while polymerisation was formed for T_S > 200°C. Lead-phthalocyanine (PbPc) on alumina showed a structural dependence on the source temperature, the molecules were found to fragment if this was above 670K [23]. Christen *et al.* [24] have also reported evaporated films of PbPc. In this study, films were deposited on NaCl crystals and consisted predominantly of the monoclinic form for T_S = 520K and of the triclinic form for T_S = 590K. Tanaka *et al.* [25] reported films of $PbPcI_X$ on mica by evaporating PbPc and subsequently doping with iodine. T_S was set to 50°C for these films. A difference in structure of poly(fluoroaluminium phthalocyanine) evaporated films was seen for slow or rapid formation

rates; an amorphous structure resulted from a rapid evaporation while partially crystalline layers were obtained for a low deposition rate (0.2 nm sec^{-1}) [26]. One application for evaporated metal phthalocyanine films is in gas and vapour sensors [27-28].

The co-evaporation technique has also been used for the formation of phthalocyanine films. Yudasaka *et al.* [30] have reported iodinated nickel phthalocyanine thin films on quartz by double source evaporation of iodine and nickel phthalocyanine. These films were conductive with a value of σ_{RT}~ 0.1-1 S cm^{-1} (conductivities in single crystals vary from one to several hundreds S cm^{-1}). This value was found to decrease with time, becoming one order of magnitude less over a period of 60 days.

3.4 Organic Thin Film Transistors

Many transistor devices that exploit the properties of inorganic semiconductors have been fabricated, e.g. JFET, MISFET, MOSFET. The most widely used transistor structure incorporating organic layers is shown in Fig. 3.8. This device is termed a thin film transistor (TFT).

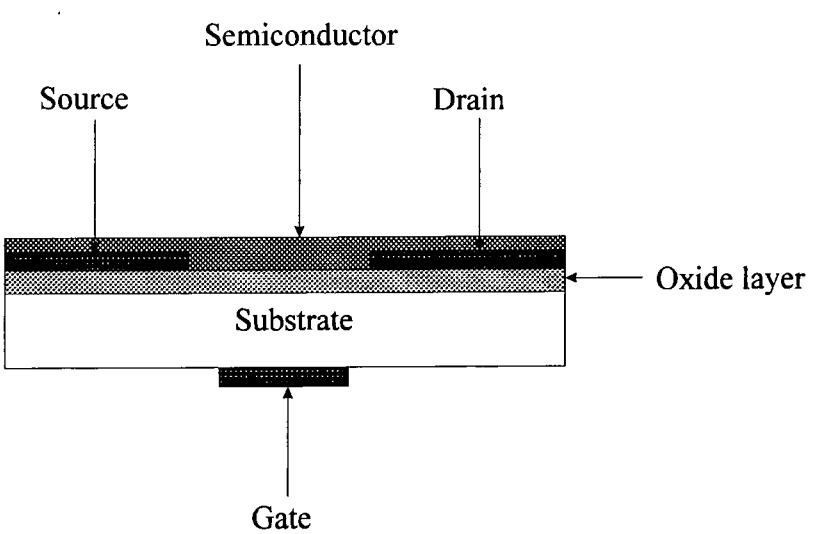

Figure 3.8: Schematic view of the TFT structure.

The arrangement in Figure 3.8 is preferred to other structures as the addition of the organic film is the final component in the fabrication process. In theory, the gate insulator (oxide layer in Figure 3.8) should not affect the conduction mechanism in the transistor, which takes place only through the organic material. The current-voltage characteristics of a TFT are similar to those of a conventional MOSFET.

Mobility μ is an important parameter of the carrier transport. This describes how strongly the motion of a charge carrier is influenced by an applied field E, and relates the field to the drift velocity v by

$$v = \mu E \tag{3.5}$$

The transistor's operating mechanism will be discussed in detail in Chapter 8. In Table 3.1, a summary of the materials that have been used for organic TFT devices is given.

Material Deposition Method	**Gate Insulator**	**Conductivity ($S\ cm^{-1}$)**	**Mobility ($cm^2\ V^{-1}\ s^{-1}$)**	**Comment**
Polyacetylene				
Direct synthesis from C_2H_2 gas	polysiloxane	1.8×10^{-5}		[31]
Spin Coating	SiO2			[32]
Poly (N-methylpyrrole)				
Chemical polymerisation	SiO_2	2×10^{-5}	10^{-2}-1	[33]
Polythiophene				
Electrochemical Synthesis	SiO_2	10^{-8}	10^{-5}	(a) No saturation for thick film. (b) No field-effect for th as-grown film. [34-36]

Lutetium bisphthalocyanine				
Vacuum evaporation	zinc phthalocyanine on SiO_2	10^{-5}	10^{-4}-6	SCLC region
	SiO_2			No field-effect [37,38]
	Si_3N_4 on SiO_2	2.5×10^{-5}	3×10^{-3}	[39]
Thulium Phthalocyanine				
Vacuum evaporation	Si_3N_4 on SiO_2	10^{-5}	1.5×10^{-2}	[39]
Poly(3-hexylthiophene)				
Spin coating	SiO_2	10^{-8}	10^{-7}-10^{-4}	[40]
Scandium diphthalocyanine				
Vacuum evaporation	nickel phthalocyanine on SiO_2		10^{-3}	[41]
	SiO_2	10^{-6}		No field-effect
α-sexithienyl				
Vacuum evaporation	SiO_2	10^{-7}	2.1×10^{-3}	[42]
	cyanoethylpullulan		3.4×10^{-2}	[43]
	polystyrene			No field-effect [43]
	polymethylmetha-crylate			No field-effect [43]
	polyvinylalcohol		9.3×10^{-4}	
	polyvinylchloride			No field-effect [43]
	cyanoethylpullulan		4.1×10^{-1}	[44]
	SiO_2		10^{-5}-10^{-4}	[45]
poly(3-hexylthiophene) /arachidic acid				
Langmuir-Blodgett	SiO_2	4×10^{-7}	7×10^{-7}	[46]

Quinquethiophene/ arachidic acid Langmuir-Blodgett	SiO_2	3×10^{-7}	1×10^{-5}	[46]
Tetracene Vacuum evaporation	SiO_2	10^{-10}		[47] No field-effect was seen
Pentacene Vacuum evaporation Spin coating	SiO_2 Si_3N_4	10^{-6} 10^{-5}	2×10^{-3} 10^{-3}	[47] [48]
Poly(3-butylthiophene) Spin coating	SiO_2		10^{-4}	[49]
Poly(3-hexylthiophene) Spin coating	SiO_2		1×10^{-4}	[49]
Poly(3-octylthiophene) Spin coating	SiO_2		3×10^{-6}	[49]
Poly(3-decylthiophene) Spin coating	SiO_2		6×10^{-7}	[49]
Erbium diphthalocyanine Vacuum evaporation	Si_3N_4			[50] No field effect
Lead phthalocyanine Vacuum evaporation	Si_3N_4			[50] SCLC region No saturation was seen
Terthiophene Vacuum evaporation	SiO_2	10^{-9}		[51] No field effect
Quaterthiophene Vacuum evaporation	SiO_2	10^{-9}	2×10^{-7}	[51]
Quinquethiophene Vacuum evaporation	SiO_2	10^{-8}	10^{-5}	[51]

Polythienylenevinylene Spin Coating	SiO_2	10^{-5}-10^{-6}	2.2×10^{-1}	[52]
$Ni(dmit)_2$ Langmuir Blodgett	SiO_2		2.4×10^{-5} 1.8×10^{-1}	[53] As-deposited After iodine-doping
$EDT(SC18)_2$ Langmuir-Blodgett	Silica	0.1-1		[54] SCLC region No saturation was seen

Table 3.1: A summary of the organic TFTs and their properties.

The values of mobility found in these devices range from 10^{-7} to 10^{-1} cm^2 V^{-1} s^{-1}. These are considerably smaller than those observed in inorganic semiconductors (1400 cm^2 V^{-1} s^{-1} and 8000 cm^2 V^{-1} s^{-1} for electrons in Si and GaAs, respectively). The highest value of mobility (~1 cm^2 V^{-1} s^{-1}) was found for the poly(N-methylpyrrole) TFT. Figure 3.9 shows the current-voltage characteristic for a successful organic TFT [41]. V_{DS} is the drain-source voltage, I_D the drain-source current and V_G the gate voltage. However, saturation characteristics (i.e. constant I_D) are not always observed and sometimes evidence for space-charge limited conduction (SCLC) is noted. Such behaviour is shown in Figure 3.10 [50].

As evident from Table 3.1, the choice of the gate insulator can affect markedly the properties of the TFT. For example, for lutetium bisphthalocyanine no field effect was observed for a TFT using SiO_2 as the gate insulator [38]. In contrast, a mobility as high as 10^{-3} cm^2 V^{-1} s^{-1} was exhibited for a TFT incorporating an additional insulating layer on top of the SiO_2 [39]. The effect of the insulating layer on the TFT properties was also observed

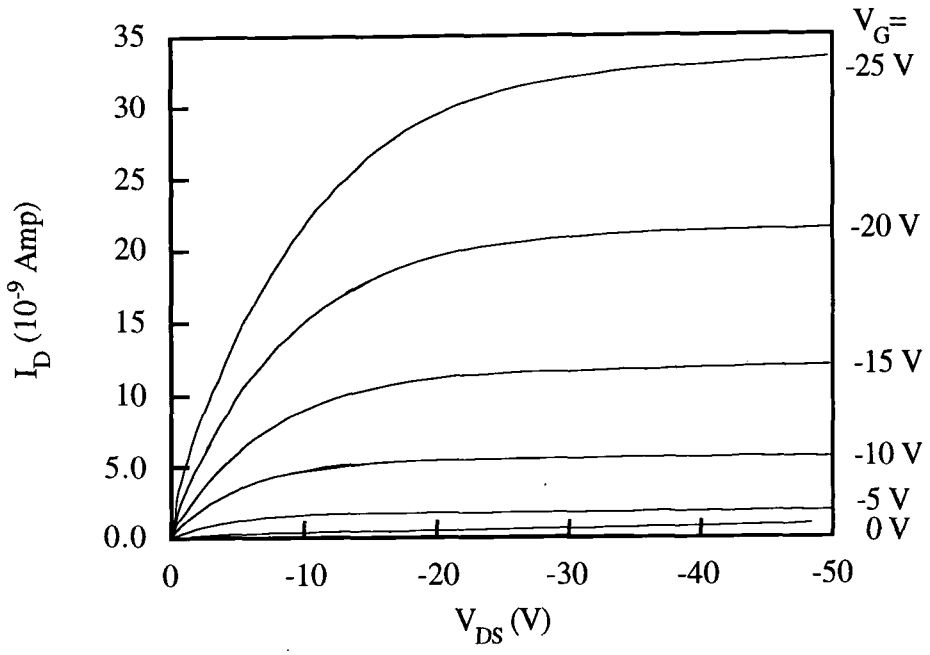

Figure 3.9: Drain current I_D versus drain voltage V_{DS} for various values of gate voltage V_G for an scandium phthalocyanine thin film transistor (taken from Ref. 41).

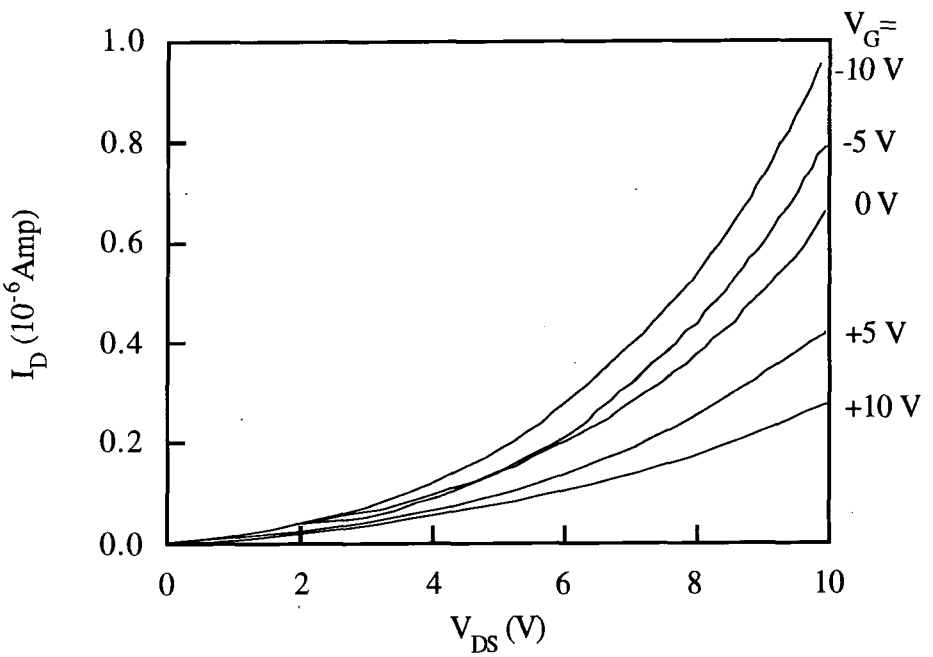

Figure 3.10: Drain current I_D versus drain voltage V_{DS} for various values of gate voltage V_G for a lead phthalocyanine thin film transistor. The supralinear behaviour (SCLC region) is evident (taken from Ref. 50).

for α-sexithienyl; an increase in the mobility from 10^{-4} cm^2 V^{-1} s^{-1} to 10^{-1} cm^2 V^{-1} s^{-1} was seen using different insulators [42-45]. This phenomenon has been attributed to carrier trapping states at the insulator surface. It has been suggested that these surface states can neutralise the charged species formed in the organic layer by the gate voltage.

3.5 Summary

The deposition method, physical vapour deposition, used for thin film formation in this work has been discussed. Other formation techniques have also been described briefly. The growth mechanism of evaporated films, from nucleation to a continuous film, has been given. This was followed by a history of evaporated organic charge-transfer materials and an outline of the organic thin film transistor.

References

1. M. Ohring, 'The Materials Science of Thin Films', *Academic Press*, San Diego (1992) pp. 79-81, and the references therein.
2. L.I. Maissel and R. Glang, 'Handbook of Thin Film Technology', McGraw & Hill, USA (1970), pp. 1-7 - 1.25 and 1-85 - 1-95.
3. B. Lewis and J.C. Anderson, 'Nucleation and Growth of Thin Films', *Academic Press*, London (1978).
4. R.F. Bunshah, 'Handbook of Deposition technologies for Films and Coatings', *Noyes Publications*, New Jersey (1994), pp.681-734.
5. C.A. Neugebauel, 'Handbook of Thin Film Physics', *McGraw Hill*, New York (1970).
6. L. Holland, 'Thin Film Microelectronics', *Chapman & Hall Ltd.*, London (1965) pp. 1-7.
7. H.J. Levinstein, 'The Growth and Structure of Thin Metallic Films', *J. Appl. Phys.*, **20** (1949) 306.
8. M. Yudasaka, K. Hironaga, H. Yamochi, K. Nakamishi and G. Saito, 'Formation of Highly Orientated Thin Films of TTF_7I_5 and Their Properties', *Synth. Met.*, **41-43** (1991) 1527.

9. M. Yudasaka, K. Hironaga, H. Yamochi, K. Nakamishi and G. Saito, 'Thin Film Formations of Charge-Transfer Complexes with Metallic Properties by Vacuum Deposition Method', *Mat. Res. Symp. Proc.*, **173** (1990) 137.

10. M. Yudasaka, K. Hironaga, H. Yamochi, K. Nakamishi and G. Saito, 'Highly Orientated Thin Films of Hepta-(Tetrathiafulvalene) Pentaiodide Formed by Double-Source Evaporation of Tetrathiafulvalene and Iodine', *J. Appl. Phys.*, **70** (1991) 3501.

11. J.J. Breen, J.S. Tolman and G.W. Flynn, 'Scanning Tunneling Microscopy Studies of Vapour Deposited Films of Tetrathiafulvalene with Iodine', *Appl. Phys. Lett.*, **62** (1993) 1074.

12. K. Kawabata, K. Tanaka and M. Mizutani, 'Thin Films of (BEDT-TTF) Iodide Prepared by Evaporation Method', *Synth. Met.*, **41-43** (1991) 2097.

13. K. Kawabata, K. Tanaka and M. Mizutani, 'Conducting Thin Films of α-(BEDT-TTF)$_2$I$_3$ by Evaporation Method', *Sol. Stat. Comm.*, **74** (1990) 83.

14. K. Kawabata, K. Tanaka and M. Mizutani, 'Superconducting Thin Films of (BEDT-TTF) Iodide', *Synth. Met.*, **39** (1990) 191.

15. K. Kawabata, K. Tanaka and M. Mizutani, 'Superconducting Organic Thin Films Prepared Using an Evaporation Technique', *Adv. Mat.*, **3** (1991) 157.

16. M. Yoshimura, H. Shigekawa, K. Kawabata, Y. Saito and A. Kawazu, 'STM Study of Organic Films of BEDT-TTF iodide', *Appl. Surf. Sci.*, **60** (1992) 317.

17. P. Chaudhari, B.A. Scott, R.B. Laibowitz, Y. Tomkiewitcz and J.B. Torrance, 'Characterisation of Epitaxially Grown Films of (TTF) (TCNQ)', *Appl. Phys. Lett.*, **24** (1974) 439.

18. T. Sumimoto, K. Kudo, T. Nagashima, S. Kuniyoshi and K. Tanaka, 'Formation of TTF-TCNQ Charge-Transfer Complex in Co-Evaporated Films', *Synth. Met.*, **70** (1995) 1251.

19. J.S. Zambounis, J. Mizugughi, G. Rihs, O. Chauvet and L. Zuppirolli, 'Optical and Electrical Properties of Evaporated 2,5-methylthio-7,7',8,8'-tetracyanoquinodimethane', *J. Appl. Phys.*, **76** (1994) 1824.

20. N. Uyeda, M. Ashida and Eiji Suito, 'Orientation Overgrowth of Condensed Polycyclic Aromatic Compounds Vacuum-Evaporated onto Cleaved Face of Mica', *J. Appl. Phys.*, **36** (1965) 1453.

21. M. Yudasaka, M. Kawai, S. Kurita, K. Nakanishi and Y. Kuwae, 'Formation of Si(phthalocyaninato)(OH)$_2$ and [Si(phthalocyaninato)O]$_n$ Films and their Optical and Electrical Properties', *Thin Solid Films*, **151** (1987) L115-L119.

22. M. Yudasaka, Y. Kuwae, M. Kawai, K. Nakanishi and S. Kurita, 'Optical and Electrical Properties of Deposited Films of Si(Phthalocyanine)(OH)$_2$', *Thin Solid Films*, **157** (1988) 189-194.

23. H. Mockert, K. Graf, D. Schmeisser, W. Göpel, L.H. Ahmad, P.B.M. Archer, A.V. Chadwick and J.D. Wright, 'Characterisation of Gas-Sensitive Lead Phthalocyanine Film Surfaces by X-ray Photoelectron Spectroscopy', *Sensors and Actuators B*, **2** (1990) 133-141.

24. D. Christen, V. Hoffman, A. Rager and W. Göpel, 'Oriented Structures of Lead Phthalocyanine Thin Films: IR studies and Normal Coordinate Calculations of the Non-Planar Porphin Ring System', *Thin Solid Films*, **208** (1992) 284-289.

25. M. Tanaka, H. Tsuyoshi, M. Yudasaka and S. Kurita, 'Uniaxial Stress Effect on the Charge Transfer of Highly orientated Films of Iodinated Palladium Phthalocyanine', *Phys. Stat. Sol. B*, **168** (1991) 39.

26. Berthet, J.P. Blanc, J-P. Germain, A. Larbi, C. Maleysson and H. Robert, 'Electroactive Polymers in Thin Layers: A Potential Application as a Gas Sensor', *Synth. Met.*, **18**(1987) 715-720.

27. B. Bott and T.A. Jones, 'Highly Sensitive NO_2 Sensor Based on Electrical Conductivity Changes in Phthlocyanine Films', *Sensors and Actuators*, **5** (1984) 43-53.

28. S. Dogo, J-P. Germain, C. Maleysson and A. Pauli, 'Gas-Sensing Properties of Metallo-Phthalocyanine Thin Films as a Function of their Crystalline Structure', *Sensors and Actuators B*, **8** (1992) 257-259.

29. M. Passard, A. Pauli, J-P. Blanc, S. Dogo, J-P. Germain and C. Maleysson, 'Doping Mechanisms of Phthalocyanines by Oxidizing Gases: Applications to Gas Sensors', *Thin Sol. Films*, **237**(1994) 272-276.

30. M. Yudasaka, K. Hironaga and K. Nakamishi, 'Formation of Iodinated Nickel Phthalocyanine Thin Films by Double-Source Evaporation of Iodine and Nickel Phthalocyanine', *J. Appl. Phys.*, **69** (1991) 3402.

31. F. Ebisawa, T. Kurowawa and S. Nara, 'Electrical Properties of Polyacetylene/Polysiloxane Interface', *J. Appl. Phys.*, **54** (1983) 3255.

32. J.H. Burroughes, C.A. Jones and R.H. Friend, 'New Semiconductor Physics in Polymer Diodes and Transistors', *Nature*, **355** (1988) 137.

33. A. Tsumura, H. Koezuka, S. Tsunoda and T. Ando, 'Chemically Prepared Poly(n-Methylpyrrole) Thin Film', *Chem. Lett.*, (1986) 863.

34. A. Tsumura, H. Koezuka and T. Ando, 'Macromolecular Electronic Device: Field-Effect Transistor With a Polythiophene Thin Film', *Appl. Phys. Lett.*, **49** (1986) 1210.

35. A. Tsumura, H. Koezuka and T. Ando. ' Field-Effect Transistor With Polythiophene Thin Film', *Synth. Met.*, **18** (1987) 699.

36. A. Tsumura, H. Koezuka and T. Ando, 'Polythiophene Field-Effect Transistor: Its Characteristics and Application System', *Synth. Met.*, **25** (1988) 11.

37. M. Madru, G. Guillard, M. Al Sadoun, M. Maitrot, C. Clarisse. M. Le Contellec, J.-J. André and J. Simon, 'The First Field-Effect Transistor Based on an Intrinsic Semiconductor', *Chem. Phys. Lett.*, **142** (1987) 103.

38. M. Madru, G. Guillard, M. Al Sadoun, M. Maitrot, J.-J. André, J. Simon and R. Even, 'A Well-Behaved Field Effect Transistor Based on an Intrinsic Molecular Semiconductor', *Chem. Phys. Lett.*, **145** (1988) 343.

39. G. Guillard, M. Al Sadoun, M. Maitrot, J. Simon and M. Bouvet, 'Field-Effect Transistors Based on Intrinsic Molecular Semiconductors', *Chem. Phys. Lett.*, **167** (1990) 503.

40. A. Assadi, C. Svensson, M. Willander and O. Inganäs, 'Field-Effect Mobility of Poly(3-hexylthiophene)', *Appl. Phys. Lett.*, **53** (1988) 195.

41. C. Clarisse, M.T. Riou, M. Gauneau and M. Le Contellec, 'Field-Effect Transistor with Diphthalocyanine Thin Film', *Electron. Lett.*, **24** (1988) 674.

42. G. Horowitz, D. Fichou, X. Peng, Z. Xu and F. Garnier, 'A Field-Effect Transistor Based on Conjugated Alpha-Sexithienyl', *Sol. Stat. Comm.*, **72** (1989) 381.

43. X. Peng, G. Horowitz, D. Fichou and F. Garnier, 'All-Organic Thin Film Transistors Made of Alpha-Sexithienyl Semiconducting and Various Polymeric Insulating Layers', *Appl. Phys. Lett.*, **57** (1990) 2013.

44. F. Garnier, G. Horowitz, X. Peng and D. Fichou, 'An All-Organic Thin Film Transistor With Very High Carrier Mobility', *Adv. Mat.*, **2** (1990) 592.

45. P. Ostoja, S. Guerri, S. Rossini, M. Servidori, C. Taliani and R. Zamboni, 'Electrical Characteristics of Field-Effect Transistors Formed with Ordered α-sexithienyl', *Synth. Met.*, **54** (1993) 447.

46. J. Paloheimo, P. Kuivalainen, H. Stubb, E. Vuorimaa and P. Yli-Lahti, 'Molecular Field-Effect Transistors Using Conducting Polymer Langmuir-Blodgett Films', *Appl. Phys. Lett.*, **56** (1990) 1157.

47. G. Horowitz, D. Fichou, X.Z. Peng, and F. Garnier, 'Thin-Film Transistors Based on Alpha-Conjugated Oligomers', *Synth. Met.*, **41-43** (1991) 1127.

48. A.R. Brown, A. Pomp, C.M. Hart and D.M. de Leeuv, 'Logic Gates Made from Polymer Transistors and Their Use in Ring Oscillators', *Science*, **270** (1995) 972.

49. J. Paloheimo, H. Stubb, P. Yli-Lahti and P. Kuivalainen, 'Field-Effect Conduction in Polyalkylthiophenes', *Synth. Met.*, **41-43**(1991) 563.

50. C. Hamann, M. Müller, A. Mrwa, M. Starke and w. Vollman, 'Organic Thin Films - Deposition Structure Properties - Electronic Devices', *Synth. Met.*, **41-43** (1991) 1081.

51. G. Horowitz, X.Z. Peng, D. Fichou and F. Garnier, 'Role of the Semiconductor/Interface in the Characteristics of π-Conjugated-Oligomer-Based Thin-Film Transistors', *Synth. Met.*, **51** (1992) 419.

52. H. Fuchigami, A. Tsumura and H. Koezuka, 'Polythienylenevinylene Thin-Film Transistor with High Carrier Mobility', *Appl. Phys. Lett.*, **63** (1993) 1372.

53. C. Pearson, A.J. Moore, J.E. Gibson, M.R. Bryce and M.C. Petty, 'A Field-Effect Transistor Based on Langmuir-Blodgett Films of an $Ni(dmit)_2$ Charge Transfer Complex', *Thin Soid Films*, **244** (19940 932.

54. P. Hesto, L. Aguilhon, G. Tremblay, J.P. Bourgoing, M. Vandevyver and A. Barraud, 'Field-Effect Induced Modulation of Conduction in Langmuir-Blodgett Films of Ethylenedithiotetrathiofulvalene Derivatives', *Thin Solid Films*, **242** (1994) 7.

CHAPTER FOUR

EXPERIMENTAL DETAILS

4.0 Introduction

This chapter provides a description of the techniques used for characterisation of the semiconducting evaporated layers. Section 4.1 describes the preparation of the substrates prior to the evaporation of the thin film. The thermal evaporation method has already been discussed in the previous chapter and the vacuum system purpose built for this work will be described in the following chapter. Sections 4.2 and 4.3 outline the techniques used for the optical, structural and electrical characterisation of the samples.

4.1 Substrate Preparation

Evaporated films were mainly deposited on glass microscope slides of dimensions 2.5x1.5 cm^2 ; in some cases mica was also used. The cleaning procedure followed was the same for both substrates. These were first degreased using Decon 90 and rinsed thoroughly with deionised water before being ultrasonically agitated in pure water for 30 min [1]. Gold electrodes were then deposited on the clean substrates. The evaporation was performed in an Edwards E306A vacuum coating system, at pressures less that 10^{-5} mbar, using a resistively heated tungsten boat as an evaporation source. A layer of chromium was deposited first to improve the adhesion of the gold on the glass/mica. Evaporation thicknesses were controlled

using a crystal oscillator and a mechanical shutter. Electrodes consisted of a 40 nm gold layer deposited on 15 nm of chromium.

4.2 Optical and Structural Characterisation

4.2.1 Optical Microscopy

A Vickers M17 optical microscope with reflected and transmitted modes available was used to study the surface of the evaporated films. The microscope could magnify up to 800 times and was equipped with a camera with which micrographs could be obtained.

4.2.2 Infrared/Visible Spectroscopy

The intensity of light passing through an absorbing material is reduced according to Beer's Law [2]

$$I = I_0 e^{-\alpha l} \tag{4.1}$$

where I is the measured intensity after passing through the material, I_0 is the initial intensity, α is the absorption coefficient and l is the path length. Eq. (4.1) is often written as

$$A = -\log_{10}\left(\frac{I_0}{I}\right) \tag{4.2}$$

where A is the absorbance of the sample and is given by $A = (\log_{10} e)\alpha l = 0.43\alpha l$.

The optical absorption spectra were measured on a Perkin Elmer Lambda 19 ultraviolet/visible/near-infrared spectrophotometer. An uncoated glass substrate placed in the reference beam was used for background correction.

4.2.3 Scanning Electron Microscopy

To study the morphology of the films in more detail, scanning electron micrographs were recorded using a Cambridge Stereoscan 600 system. This was used in secondary mode with the electron beam accelerated through 25 kV. The samples were pasted onto aluminium stubs using conducting silver which helped earth and stabilise the sample during study. Highly insulating samples were coated with a layer of gold to avoid charging under the electron beam [3]. This gold film was deposited by glow discharge sputtering using a Polaron Instrument SEM coating unit.

4.3 Electrical Characterisation

4.3.1 Elimination of the Contact Resistance

The resistance R of a material between two electrodes is defined as

$$R = \frac{V}{I} \tag{4.3}$$

where V is the potential difference and I the current flowing between the two electrodes. Consider first the two-terminal arrangement shown at Figure 4.1(a) where each electrode serves both as a current and a voltage contact.

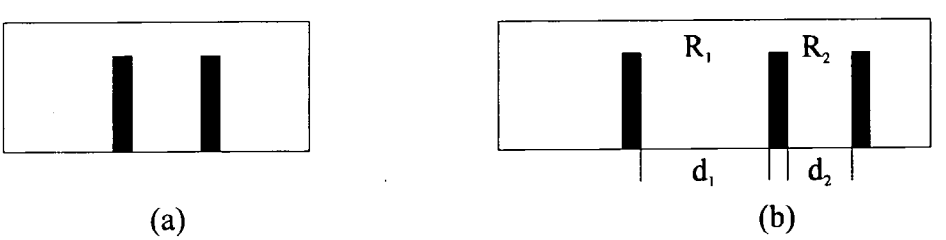

Figure 4.1: a) Two-terminal and b) Three-terminal contact arrangements.

The total resistance is given by

$$R = \frac{V}{I} = 2R_C + R_S \tag{4.4}$$

where R_S is the semiconductor resistance and R_C is the contact resistance, defined as the resistance at the metal/semiconductor interface. To evaluate R_S, R_C must either be known or $R_C << R_S$.

To overcome this problem, a three-terminal arrangement, shown in Figure 4.1(b) was developed [4]. Three identical contacts were made with spacings d_1 and d_2. Assuming identical contact resistances for all three contacts allows the total resistance to be written as

$$R_i = R_{si} + 2R_C \tag{4.5}$$

where i=1,2, R_{Si} and R_i are the semiconductor and the total resistances between different electrodes, as shown in Figure 4.1. Combining the two equations that derive from Eq. (4.5) for i=1,2, gives

$$\frac{R_1 - 2R_C}{R_2 - 2R_C} = \frac{R_{S1}}{R_{S2}} \tag{4.6}$$

But $R_{S1}/R_{S2} = d_1/d_2$, and by substituting this in Eq. (4.6)

$$\frac{R_1 - 2R_C}{R_2 - 2R_C} = \frac{d_1}{d_2} \tag{4.7}$$

Solving for R_C gives

$$R_C = \frac{(R_2 d_1 - R_1 d_2)}{2(d_1 - d_2)} \tag{4.8}$$

The value of R_c was then subtracted from the measured resistance to give an accurate value of the resistance of the evaporated film. The three-terminal contact method was used throughout this work with $d_1 = 4.46$ mm and $d_2 = 1.46$ mm. The electrodes length and width were 5.9 mm and 1.5 mm, respectively. Apart from evaporated gold, electrical contacts were also established after deposition of the semiconducting film, using either air drying silver paint (Acheson 915 electrodag) or carbon cement (Neubauer Chemikalien Leit-C).

4.3.2 Electrical Measurements

Electrical measurements were performed in air in a screened sealed sample chamber which also allowed measurements to be taken under vacuum. Variable bias voltages were supplied by Time Instruments 2003S voltage calibrators. Dc currents were measured using a Keithley 410A picoammeter. The measurement circuit is shown in Figure 4.2.

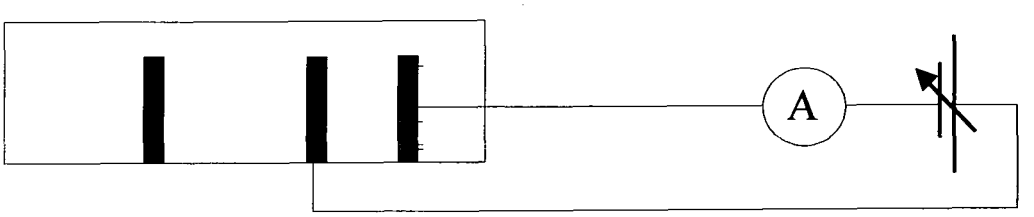

Figure 4.2: Electrical circuit used for conductivity measurements.

The dc conductivity σ was calculated from

$$\sigma = \frac{d}{R_s A} \tag{4.9}$$

where R_S is the semiconductor resistance, d the distance between the electrodes and A the cross-sectional area given by $A = lt$, where l is the length of the electrodes and t the thickness of the evaporated layer [5]. Substituting this into Eq. (4.9)

$$\sigma = \frac{d}{R_S lt} \tag{4.10}$$

An Alpha-step 200 was used to measure the thickness t of the organic layers.

4.3.3 Low Temperature Measurements

Low temperature measurements over the range 77-300K were undertaken in an Oxford Instruments DN 704 exchange gas cryostat. Figure 4.3 shows a cross section

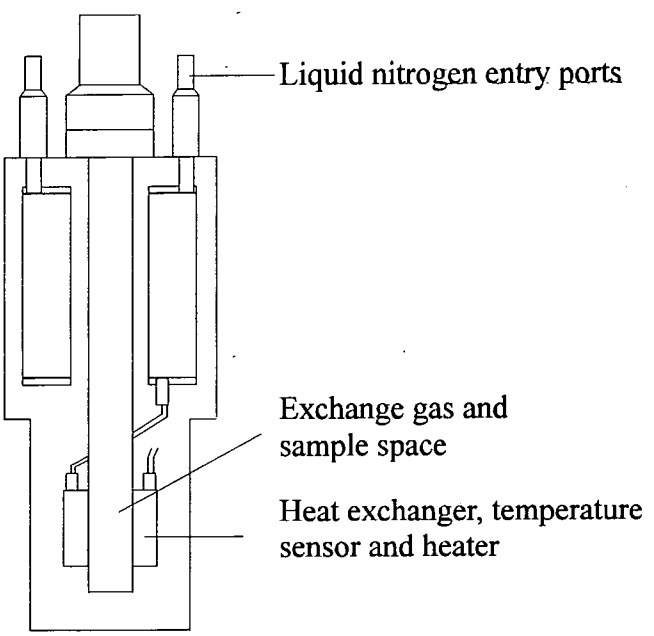

Figure 4.3: Cross section through the cryostat used.

through this system. The sample was pasted on a special holder and electrical contacts were established using air drying silver paint or carbon cement. Liquid nitrogen was used to lower

the temperature of the heat exchanger. Helium was the exchange gas between the heat exchanger and the sample. A W+W312 chart recorder was used to monitor the variation of dc current with time.

4.4 Summary

The method for substrate preparation has been described. After deposition of the organic layer, the evaporated films were characterised by optical, structural and electrical techniques.

References

1. H.K. Pulker, 'Coatings on Glass', Elsevier Science Publishers, 1984, pp. 52-56.
2. M.C. Petty, 'Langmuir-Blodgett Films', Cambridge University Press, Cambridge (1996), pp. 216-221.
3. D.K. Schroder, 'Semiconductor Material and Device Characterisation', Wiley, USA (1990), pp. 510-515.
4. D.K. Schroder, 'Semiconductor Material and Device Characterisation', Wiley, USA (1990), pp. 114-121.
5. A.R. Blythe, 'Electrical Properties of Polymers', Cambridge University Press, London (1979), pp. 132-137.

CHAPTER FIVE

DESIGN AND CONSTRUCTION OF A VACUUM SYSTEM FOR THERMAL EVAPORATION

5.0 Introduction

For the needs of the research work, a novel vacuum system was designed and built in the School of Engineering Workshop. In this chapter, this system is described in full. The vacuum environment is discussed in Section 5.1, while, in Section 5.2, a detailed description of each component's function is given. First, the components that were bought commercially are introduced and then the construction of the vacuum chamber is explained.

5.1 Vacuum Properties

The need for an operating environment for the evaporation of thin films which interferes as little as possible with the process of thin formation is essential (e.g. eliminates oxidation of metals during heating, reduces contaminants trapped in the film). Various 'degrees' of vacuum are used; their terminology with reference to operating pressure ranges, is given below.

Low vacuum.....760 - 25 Torr (1 - 0.33 bar)

Medium vacuum.....25 - 10^{-3} Torr (0.33 bar - 10^{-3} mbar)

High vacuum.....10^{-3} - 10^{-6} Torr (10^{-3} - 10^{-6} mbar)

Very high vacuum.....10^{-6} - 10^{-9} Torr (10^{-6} - 10^{-9} mbar)

Ultrahigh vacuum.....Below 10^{-9} Torr (10^{-9} mbar)

5.1.1 The Mean Free Path

In all vacuum deposition techniques, it is essential that the gaseous species travel in a straight line from the source to the substrate. At high pressures, gas molecules do not traverse large distances because of frequent collisions and deflection from their path. The mean distance travelled by particles between successive collisions is called the mean free path (mfp) λ, which depends on pressure. To calculate λ, kinetic theory is used. Here, molecules are assumed to be smooth, hard, elastic spheres of diameter σ [1]. A binary collision occurs every time the centre of one molecule approaches within a distance σ of the other. If we imagine the diameter of one molecule increased to 2σ while the other molecules are reduced to points, then in a distance λ the former sweeps out a cylindrical volume $\pi\sigma^2\lambda$. A collision will occur under the condition $\pi\sigma^2\lambda n = 1$, where n is the number of molecules per unit volume. For air at room temperature and atmospheric pressure, $\lambda \approx 50$ nm, assuming $\sigma \approx 0.5$ nm.

A molecule collides in a time given by λ/υ, where υ is its velocity, and using the relationship above, air molecules make around 10^{10} collisions sec^{-1}. Thus, gas particles do not travel in uninterrupted linear trajectories but, as a result of collisions, they are knocked to and fro, executing a zigzag motion and accomplishing little net movement. Since the number of molecules per unit volume n is directly proportional to the pressure P, a simple relation for ambient air is

$$\lambda = 3.8 \times 10^{-3}/P \qquad (5.1)$$

where λ is given in cm and P is in mbar. For pressures down to 10^{-5} mbar, λ is so large that molecules effectively collide only with the walls of the vessel.

Reduced pressures also result in a lower gas impingement flux. The latter is a measure of the frequency with which molecules impinge on, or collide with, a surface. It also expresses the time required for a surface to be coated by, and contaminated with, a monolayer of gas molecules. This issue is important when one attempts to deposit or grow films under extremely clean conditions. In air at atmospheric pressure and ambient temperature, a surface will acquire a monolayer of gas in 3.49×10^{-9} s, assuming all impinging atoms stick. On the other hand, at 10^{-10} mbar a surface will stay clean for 7.3 h.

For thin film deposition processes, thermal evaporation requires a vacuum between the high and ultrahigh regimes, whereas sputtering and low pressure chemical vapour deposition are accomplished between the medium and high vacuum ranges.

5.1.2 Materials In Vacuum

The ultimate pressure achievable in any vacuum system depends on the materials used in its construction. Outgassing and permeation are two important factors [2]. Outgassing is the release of bonded gas and vapour from a surface. Gas can interact with the surface of the solid and be taken up at it. This behaviour is called adsorption and can exist in two forms; physisorption and chemisorption. In physisorption, the adsorbate is bound to the surface by van der Waals forces due to the interaction of fluctuating dipoles. Chemisorption, which is associated with higher bonding energies than physisorption, involves a chemical reaction between the adsorbate molecule and a surface atom. Outgassing will depend greatly on the history, cleanliness and time of exposure to the atmosphere. Water vapour is the main component released when a solid surface is exposed to a vacuum.

Permeation is another means by which gas can find its way into a vacuum system. This is a three-step process. First, gas adsorbs on the outer wall of a vacuum vessel, then it diffuses through the bulk and finally desorbs from the interior wall. If equilibrium has been established, gas will desorb from the vacuum chamber at a steady rate and the process behaves exactly like a small leak. Hydrogen and helium permeate through glass, although glasses do exist that are relatively impermeable to helium. Any gas that is soluble in a metal may permeate it since permeability is directly proportional to solid solubility. Hydrogen will permeate most metals but this is least in aluminium.

Several ways of limiting the effects of outgassing and permeation on a vacuum system have been found. Outgassing can be reduced by exposing the system to atmospheric air for shorter times as possible and/or using a suitable cleaning treatment. The process of outgassing can be accelerated by baking the system at high temperatures for sufficient time. Permeation only becomes a significant factor in ultrahigh vacuums but even then its effect can be minimised by careful choice of vacuum materials.

5.2 The Vacuum System

A schematic diagram of the vacuum system used in this work is given in Figure 5.1; A photograph of the equipment is shown in Figure 5.2. There are two main parts: the pumping system, which determines the ultimate pressure and the vacuum chamber, in which evaporation takes place. The pumping system consists of the instruments that create and monitor the vacuum. The vacuum chamber is versatile and can be modified according to the wishes of the researcher.

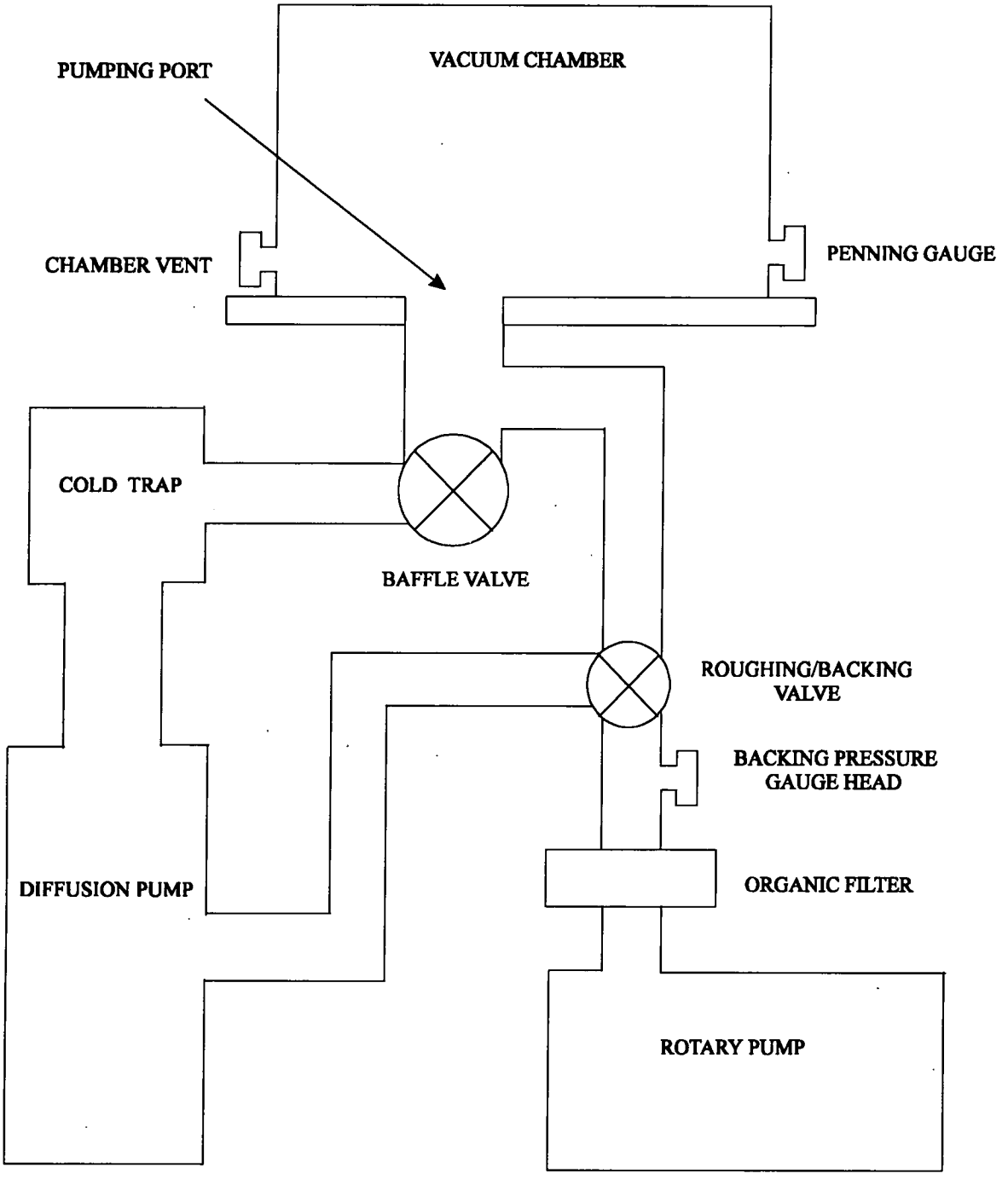

Figure 5.1: Schematic representation of a vacuum system showing all components.

Figure 5.2: Photograph of the vacuum system used in this work.

5.2.1 Basic Components

Vacua were first produced by mechanical pumps that removed a definite volume of the gas from the vessel to be exhausted, compressed it and released it to the atmosphere. For rotary oil-sealed pumps, a sliding vane pump is mainly used [3]. The action of the pump is illustrated in Figure 5.3.

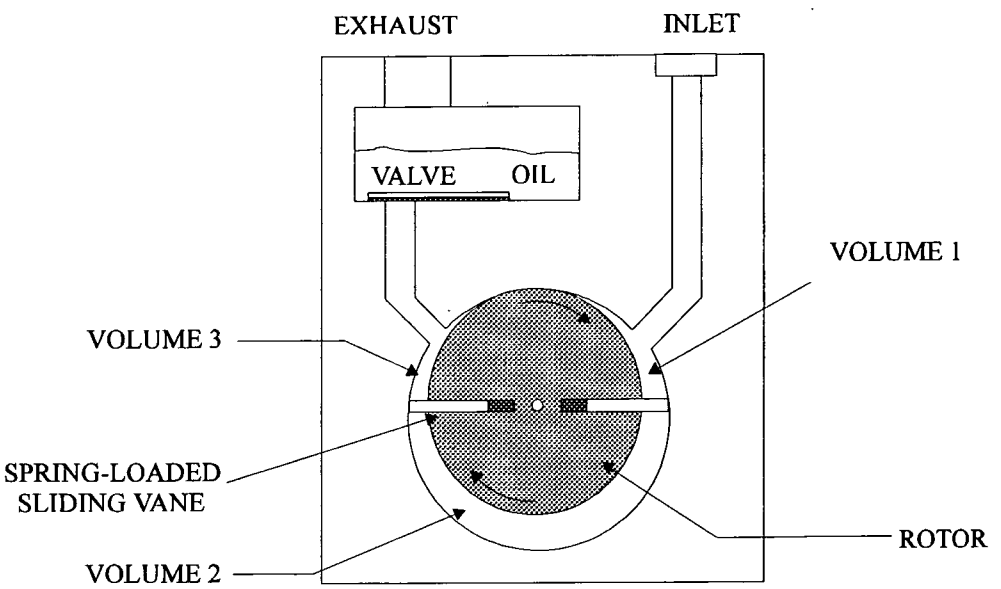

Figure 5.3: Cross section through a rotary oil pump.

The pump has a rotor located off-centre in a cylindrical housing, the stator. The top of the rotor seats against the top of the bore of the stator closely enough that the lubricating oil will form a vacuum seal at the junction line. The bore, the rotor, their junction line and the two sliding vanes form three volumes. Volume 1, connected to the inlet, is expanding. Gases in the vacuum chamber connected to the inlet can expand into this volume and are removed from the chamber. Volume 2 contains gas that has been removed from the vacuum chamber and is being compressed. Volume 3, connected to the exhaust through a flapper valve, contains gas being compressed further. When the pressure in volume 3 reaches atmospheric pressure, the gas can escape through the flapper valve and out the exhaust to the

atmosphere. For pressures below atmospheric in volume 3, the flapper valve prevents air from leaking backwards from the atmosphere into volume 3. When the vane separating volume 3 from volume 2 has passed the line connecting volume 3 to the exhaust, there is a small amount of gas entrapped. Most of the this gas, as it is further compressed, is able to leak through the vacuum seal between the spring-loaded vane and the wall of the cylindrical bore of the stator and back into the new volume 3 (formerly volume 2). Some of this gas leaks into volume 1 through the vacuum seal between the rotor and the bore and thus puts limits on both the pumping speed and the ultimate vacuum that can be achieved. If a second stage is added, by connecting the exhaust of the first stage to the intake of the second, lower pressures can be reached. The lowest pressure obtained by a single-stage rotary vane pump is about 10^{-2} mbar. However, a two-stage may reach an ultimate pressure of 10^{-4} mbar. Rotary vane pumps have an extremely high compression ratio that allows them to pump drawn-in gases against atmospheric pressure. This special feature makes these basic pumps suitable for a wide range of operations. The Edwards 2M8 rotary pump was used in our vacuum system initially for roughing the chamber down to pressures ~10^{-2} mbar and afterwards for backing the diffusion pump. Edwards 17 mineral oil was used as operating fluid. Because organic materials were evaporated in the system, an Edwards Inlet Chemical Trap ITC 20 with activated charcoal as the sorbent was connected before the pump. This provided protection against various aggressive vapours which could attack the pump or the pump oil. It also prevented high molecular weight vapours, which can cause lacquering or clogging, from reaching the pump. But even so, the rotary pump oil had to be changed approximately every four months.

When the pressure in the vacuum chamber decreases to a value where the mean free path is greater than the dimensions of this volume, the residual gas molecules experience

more collisions with the walls than with each other. In this case, it becomes necessary to wait until the gas molecules travel into the inlet of the pump and then give them a preferred direction of motion by momentum transfer. This is accomplished by the diffusion pump, the basic components of which are shown schematically in Figure 5.4 [4].

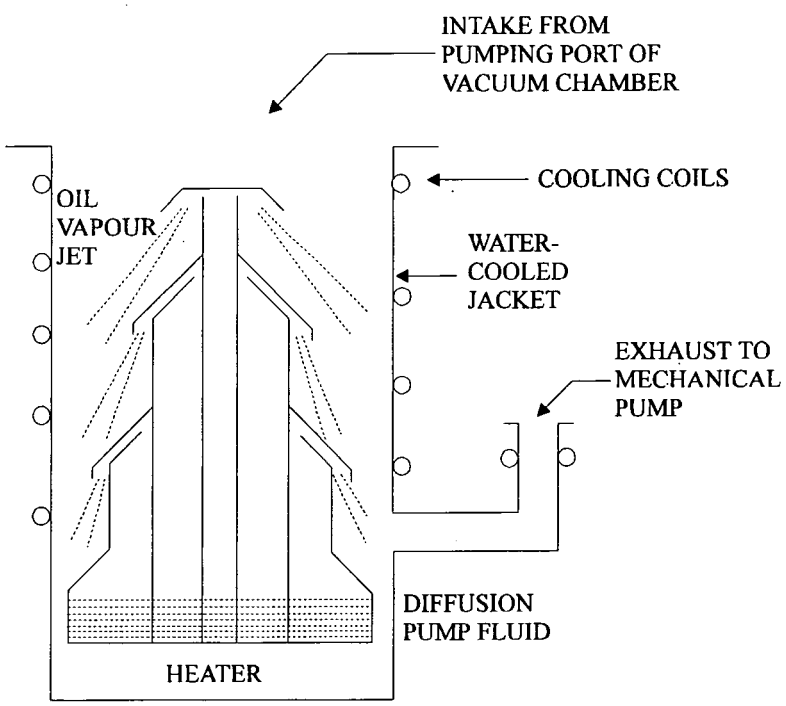

Figure 5.4: Schematic representation of a diffusion pump.

A heater causes the oil to boil and to vaporise in a flue. The vapours flow up the chimney and out through a series a nozzles. These nozzles direct the vapour stream downward and towards the water-cooled outer jacket, where it condenses and returns to the boiler. The vapour flow is supersonic and remains so until it hits the wall. Gases that diffuse into this supersonic vapour stream are, in general, given a downward momentum and ejected into a region of higher pressure. Modern pumps have several stages of compression, usually three or four. Each stage compresses the gas to a successively higher pressure than the proceeding stage as it transports it toward the outlet.

resistance wire enclosed in a glass or metal envelope is exposed to the pressure in the vacuum system while being part of a Wheatstone-bridge circuit. An identical wire in a similar but evacuated and sealed enclosure serves as a reference. The wire filament is heated by a passage of an electric current, the temperature of the wire depends on the current passing through it and the rate of heat loss by conduction, convection and radiation. If the current passing through the wire is maintained at a constant value then the rate of heat loss will depend on the thermal conduction by the gas and so on the pressure of the system.

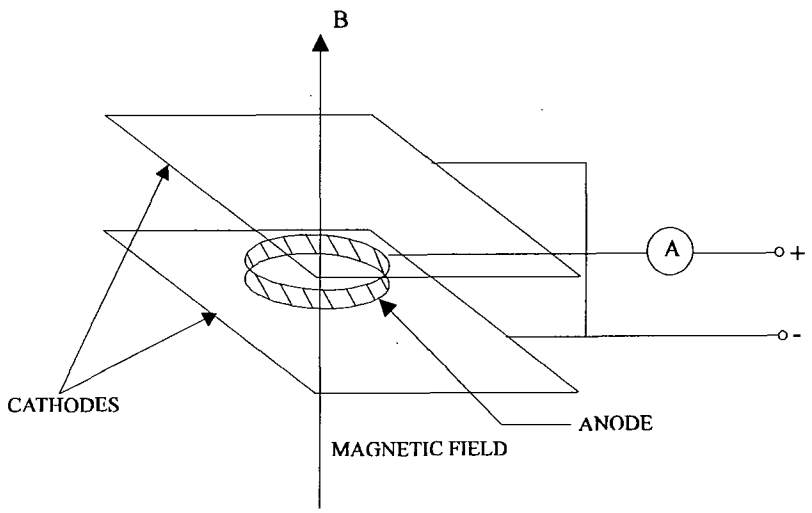

Figure 5.6: Schematic of a Penning ionisation gauge

For pressures lower than 10^{-3} mbar, a Penning gauge is used [6]. The principal arrangement is shown in Figure 5.6. A dc potential of about 2 kV is maintained between a ring-shaped anode and two cathode plates. Because of the ubiquitous presence of cosmic rays and stray radioactivity, a few secondary electrons are liberated from the electrodes. These initiate some ionisation, whereupon positive ions strike the cathode with enough energy to cause substantial secondary emission with subsequent ionisation of the gas. As a result, a self-sustaining glow discharge is obtained. The magnetic field causes the electrons to travel in long helical paths before reaching the anode and to make many ionisation collisions. The total discharge current, which consists of positive-ion and electron emission currents, is

used as a measure of the gas pressure of the gauge. There is often a heater attached to the anode to burn off surface contamination.

To monitor the pressure in our system at all times, an Edwards Pirani-Penning 1005 vacuum gauge was used. The instrument combines a Pirani PRM10K and a Penning CP25K gauge (operating ranges 200-10^{-3} mbar and 10^{-2}-10^{-7} mbar, respectively) and therefore can be used for all pressure ranges. In addition, an automatic protective switch for switching off the Penning gauge at high pressures was included.

The pumping system, as described above, could create a vacuum in the high range, with an ultimate pressure between 10^{-6} mbar and 10^{-5} mbar and thus, was suitable for the physical evaporation technique.

5.2.2 The vacuum chamber

The vacuum chamber is the most important part of a vacuum system. Modifications can provide different evaporation conditions to suit to the material that is being evaporated. The evaporation of organic materials is a relative new area of research and requires special provisions that most commercial vacuum chambers do not provide.

A novel chamber, Figure 5.7, was designed and constructed in the School of Engineering Workshop. The chamber, of anodised aluminium, was cylindrical with an outside and inside diameter of 23 cm and 20.3 cm, respectively and 20 cm of height. It consisted of three pieces: the lid, the main body and the base. The substrate holder was attached on the lid, the main body was a cylinder and the sources were located on the base. Two windows, built into the main housing, allowed viewing of the interior. These were made of 6 mm thick, 3.8 cm diameter pyrex glass. An extra cylindrical 'spacer', 5.7 cm high and

Figure 5.7: Photograph of the interior of the vacuum chamber.

also manufactured from anodised aluminium, was used to increase the source-substrate distance.

Resistive heating was used to provide the vapour. Several evaporation sources are commercially available to suit the needs of the particular material to be evaporated. These include filaments, baskets, boats and crucibles of different shapes, sizes and materials [7]. Organic materials are usually in a powder form and a combination of a filament and a crucible is needed to hold the material in place during pumping down and to provide the necessary heat for vaporisation. The arrangement used in this work is shown in Figure 5.8.

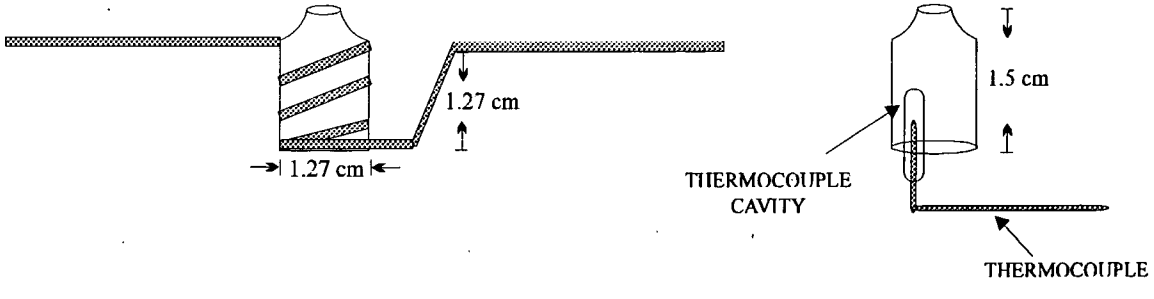

Figure 5.8: The tungsten filament and glass crucible.

The filament was purchased from Testbourne (model B8A) and was made of tungsten (melting point 3382°C). The crucible was pyrex glass, which can withstand temperatures up to 400°C, and was specially fabricated in the Durham University Glassblowing Workshop. To monitor the temperature of the powder in the crucible accurately, a special cavity, extending both on the inside and the outside of the crucible was added. To this, a thermocouple (type K of nickel-chromium/nickel-aluminium, operating range: -50°C to 400°C) was securely inserted during deposition.

The above combination (filament-crucible) was used for evaporation of TTF and ET. Iodine was also co-evaporated in the system and, as nothing was commercially available for this type of material, a special crucible was designed and built. This is shown in Figure 5.9.

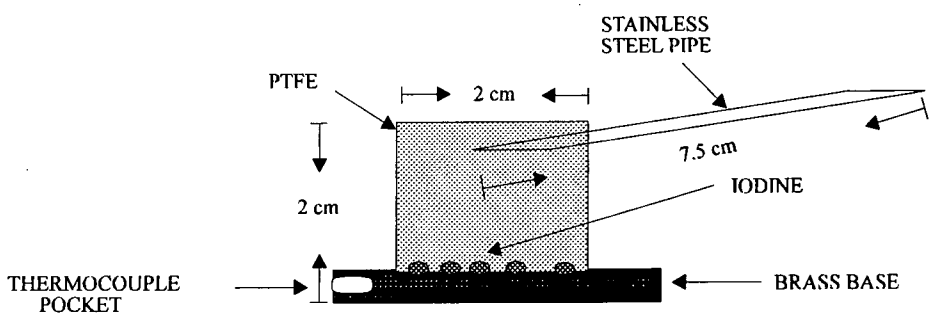

Figure 5.9: The crucible used as a source for iodine.

The crucible consisted of a brass base, onto which iodine crystals were placed, and a PTFE cylindrical top of 2 cm diameter. Iodine was vented through a stainless steel pipe (2.5 mm diameter) attached to the side. Both ends of the pipe were cut horizontally: (a) at the inside end to allow more iodine to penetrate and (b) at the outside end to direct iodine to the substrate. The temperature of the crucible was monitored by a further thermocouple (type K) that was inserted in a small hole in the brass base.

As iodine evaporates at room temperature at ambient pressures, a means to cool the iodine crucible, to below 0°C, was required. This system, had also to provide the heat necessary for iodine vaporisation during deposition. A suitable arrangement used a Peltier effect heat pump. This is based on the principle that if an electric current passes between two junctions of dissimilar materials, then heat will be evolved at one junction and absorbed at the other. The iodine crucible was bonded on a 3x3 cm^2 Radio Spares (RS) Peltier heat pump with RS heat sink compound, allowing good heat transfer. The brass base of the iodine

crucible was easily cooled or heated. During co-evaporation, the filament source and the iodine source were quite close, so that the temperature of the one could affect the other. The temperature of the TTF/ET crucible was monitored accurately by the thermocouple attached to it. To minimise the effect on the iodine source, the top of the latter was made of PTFE, a poor thermal conductor.

As clear from the discussion above, simultaneous evaporation of more than one material, was possible. This could be either two materials in the powder form, in which case two filament-crucible combinations, as shown in Figure 5.8, were used, or one filament-crucible and iodine. A small modification also allowed simultaneous evaporation from all three different sources.

The substrate holder is shown in Figure 5.10. It was a cylindrical block, 7.5 cm in diameter, made of chromium plated brass. This was attached to the chamber lid via two stainless steel pipes that extended to the outside of the chamber. The pipes were not fixed but could move vertically to allow an increase/decrease in the source-substrate distance. For many organic materials it is necessary to cool or heat the substrate to obtain high quality thin films. An 4x4 cm^2 Peltier device, on which the glass/mica substrate was bonded was used here (as for the iodine crucible). Heat sink compound provided an adhesive bond between both the substrate holder and the Peltier device, and the Peltier and the substrate holder. Mechanical leaf springs made sure that the substrate would remain in place. To monitor the temperature of the substrate, a thermocouple (type T of copper/copper-nickel operating range: -200°C to 400°C) was attached, via a mechanical clamp and heat sink compound, to a separate substrate piece of smaller dimensions.

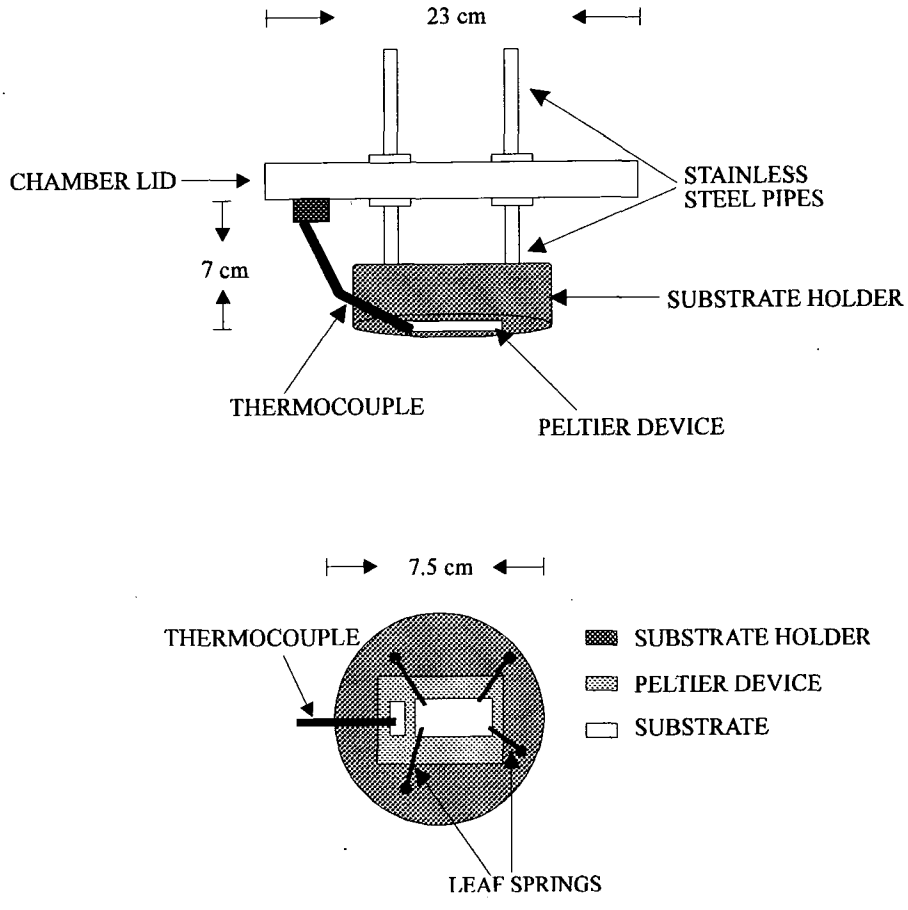

Figure 5.10: Schematic presentation of the substrate holder. On closer view the substrate configuration is evident.

A mechanical shutter was used to regulate the amount of material deposited. This was a stainless steel disc of 5 cm diameter and of adjustable height. It was placed about 1 cm below the sample and was removed during evaporation.

To maintain uniform temperature in Peltier devices it is necessary to extract heat from one side while supplying it from the other. As both Peltier devices (for the substrate and for the iodine source) were used mainly for maintaining temperatures below 0°C, heat was removed from their back side by circulating cool water. A reservoir to hold a small quantity of fluid was placed behind each Peltier. Water was cooled and circulated by a BIO-RAD 4875 refrigerated circulator. The ultimate negative temperature that could be achieved at one

surface of the Peltier device was related to the temperature on the other side, the maximum difference being 67°C. The devices have a maximum operating temperature of 110 °C, while in theory no limit exists for negative temperatures. By using water at 5°C, the ultimate cooling temperature of both the substrate and iodine source was -25°C. Using special oils, the temperature of the cooling fluid could be lowered below 5°C and thus, the temperature of the substrate/iodine crucible could be lowered further.

Each thermocouple was connected to a CAL 9900 temperature controller. For the filament and the substrate Peltier, the power was supplied by two ZENITH Z404 transformers. For the iodine Peltier, a dc power supply was designed and manufactured in the School of Engineering Electronic Workshop.

For some of the materials evaporated, the sticking coefficient was zero when the substrate was kept at ambient temperature and it was necessary that this was cooled with the help of the Peltier heat pump during deposition. To avoid water condensation on the film, nitrogen gas was introduced via a dedicated connection to the chamber. This was used first to bring the chamber to ambient pressure and then to bring the thin film to ambient temperature.

To avoid cross-contamination, the vacuum plant was dedicated to the evaporation of organic materials and the chamber was cleaned thoroughly with a solvent, mainly acetone, after an evaporation was performed.

An extractor fan was placed a short distance above the chamber to remove the vapour of the evaporated materials after the chamber was opened. As the latter were mainly organics and therefore toxic, the fan provided a fast and effective protection for the researcher. The fan was connected to a fume cupboard that removed the fumes further via a

filter and eventually released them to the atmosphere. A face mask provided further protection against toxic fumes while all handling of the chamber was carried out using rubber gloves.

5.3 System Specifications

The full specifications of the purpose-built system are summarised below. The specifications of each instrument with operating conditions are given also.

Vacuum	**Range**
Penning gauge range	10^{-2}-10^{-7} mbar
ultimate vacuum	10^{-5}-10^{-6} mbar
typical pumping time (from atmospheric to ultimate pressure)	90-120 min

TTF/ET source temperature	**Maximum value**
temperature controller limit	1800°C
source crucible limit	400°C
thermocouple (type K) limit	400°C
their combination	400°C

Iodine source temperature	**Minimum value**
Components limits	
temperature controller limit	-200°C
thermocouple (type K) limit	-50°C
cooling fluid limit	-10°C
Peltier with the above cooling fluid	-80°C
their combination	-50°C

operating conditions in this work	
cooling fluid (water)	5°C
Peltier with the above cooling fluid	-25°C
their combination	-25°C

Substrate temperature	**Min/Max value**
components limits	
temperature controller limits	-200°C/1800°C
thermocouple (type T) limits	-200°C/400°C
cooling fluid limits	-10°C/70°C
Peltier with this cooling fluid	-80°C/110°C
their combination	-80°C/110°C
operating conditions in this work (the substrate temperature was only lowered)	
cooling fluid (water)	5°C
Peltier with the above cooling fluid	-25°C
their combination	-25°C

5.3 Summary

The vacuum system used for the thermal evaporation of organic materials has been described. Components of the pumping mechanism were all purchased commercially while the chamber was designed especially for the needs for the experiment.

References

1. T.A. Delchar, 'Vacuum Physics and Techniques', Chapman & Hill, London (1993), pp. 47-77.
2. T.A. Delchar, 'Vacuum Physics and Techniques', Chapman & Hill, London (1993), pp.1-9.

3. J.F. O'Hanlon, 'A User's Guide to Vacuum Technology', Wiley, USA (1980), pp. 159-167.
4. R.V. Stuart, 'Vacuum Technology, Thin Films and Sputtering', Academic Press, London (1983), pp. 31-47.
5. L.I Maissel and R. Glang, 'Handbook of Thin Film Technology', McGraw-Hill, USA (1970), pp. 2-112-2-120.
6. L.I Maissel and R. Glang, 'Handbook of Thin Film Technology', McGraw-Hill, USA (1970), pp. 2-123 - 2-128.
7. Testbourne Ltd., 'Vaccum Evaporation Sources Catalog 1995'.

CHAPTER SIX

FORMATION OF THIN FILMS OF TTF USING THE SINGLE SOURCE AND CO-EVAPORATION TECHNIQUES: RESULTS AND DISCUSSION

6.0 Introduction

In this chapter, the structural, optical and electrical behaviour of thin films of (TTF) iodide are discussed. The effect of deposition rate on the film structure is also reported. Two different deposition methods were used for the thin film preparation: single source evaporation and co-evaporation. In the former case, doping was achieved after deposition of the film, while for the latter, doping occurred during the evaporation process.

6.1 Single Source Evaporation of TTF

6.1.1 Film deposition

TTF powder, with a melting point of 120-123°C and 97% purity, was purchased from Aldrich and used without further purification. The molecular formula of TTF is shown in Figure 6.1. A small quantity (35-50 mg) was placed in a glass crucible whose temperature was continuously monitored. It was then heated up slowly, under vacuum, and the temperature at which evaporation occurred determined by the change in the Penning gauge reading. Evaporation was found to commence at a temperature of 50°C for a background pressure of $2x10^{-5}$ mbar. To examine the effect of the source temperature, this was varied

from 50°C to 80°C in 5° steps. Glass microscope slides of dimensions 25x15 mm^2 were used as substrates. The source-substrate distance was set to 13 cm. Doping was achieved by exposing the evaporated films to iodine vapour in a sealed container.

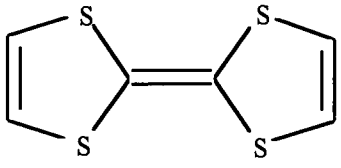

Figure 6.1: Molecular formula of TTF.

It has been reported [1], and was verified here, that the sticking coefficient of TTF is zero, i.e. no film would deposit, when the substrate was kept at temperatures above 0°C. After some experimentation with the substrate temperature (T_S), it was decided that all evaporations would be performed at T_S = -10°C. The deposition conditions are given in Table 6.1.

Source Temperature (°C)	**Thickness (μm)**	**Deposition Rate (nm min^{-1})**
50±2	1.1±0.2	73±16
55±2	1.1±0.1	100±13
60±2	1.3±0.3	140±36
65±2	1.3±0.2	170±30
70±2	2.3±0.2	230±27
75±2	0.8±0.2	400±112
80±2	1.5±0.1	480±48

Table 6.1 Relation between the source temperature and deposition rate. A summary of the films prepared.

6.1.2 Film Morphology

The structure of the thin films was polycrystalline and found to depend markedly on the deposition rate, i.e. on the source temperature (T_{sc}). Doping with iodine was accompanied by a marked change of colour from light yellow to black. A photograph of a typical (TTF) iodide evaporated thin film is shown in Figure 6.2. The morphology of the thin films was not affected by doping. The rate of film formation is determined by the number of vapour atoms reaching the substrate per unit time and this is directly proportional to the rate of evaporation. Increasing the source temperature increases the vapour flux. Films deposited at a T_{sc} = 50°C consisted mainly of needle-type crystals in between which isolated crystalline plates (platelets) could seen. Films were not uniform and the existence of pinholes was evident. Figure 6.3 shows an optical micrograph of a (TTF) iodide thin film prepared at T_{sc} = 50°C. Figure 6.4 compares electron micrographs of (TTF) iodide films evaporated at T_{sc} of 50 and 60°C, respectively. At a source temperature of 60°C, the morphology of the deposited film consists of approximately equal quantities of needles and platelets. The diameter of the crystalline needles was measured to be about 10 μm for a 1.3 μm thick film. These films were more uniform than those deposited for T_{sc}=50°C, uncoated areas were still evident but the size of these had decreased. Further increasing the source temperature resulted in films consisting solely of platelets (Figure 6.5(a)). The micrographs suggested that film formation proceeded in the 3-D island growth mode (Section 3.2.1). At a source temperature of 80°C, a change in morphology was evident, with the films consisting of flakes (Figure 6.5(b)).

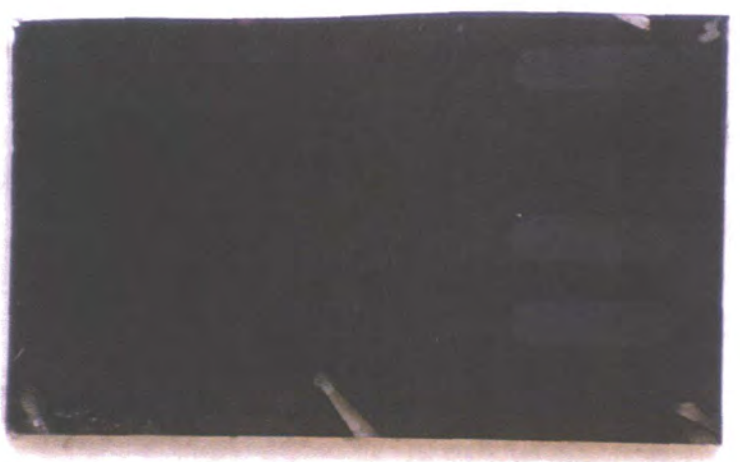

→ 2.5 cm ←

Figure 6.2: Photograph of a 1 μm (TTF) iodide deposited on a glass substrate showing the typical colour of all samples prepared.

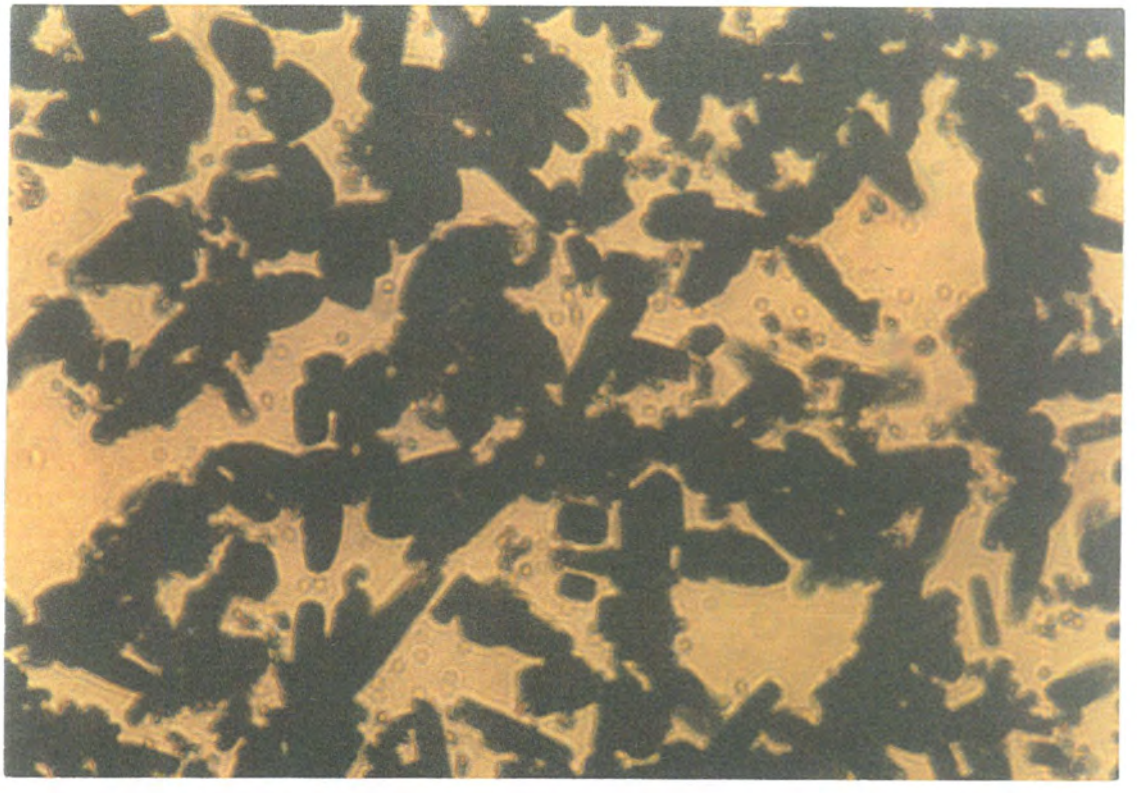

Figure 6.3: Transmission optical micrograph of a 1.1 μm thick (TTF) iodide thin film on a glass substrate deposited at a TTF source temperature of 50°C.

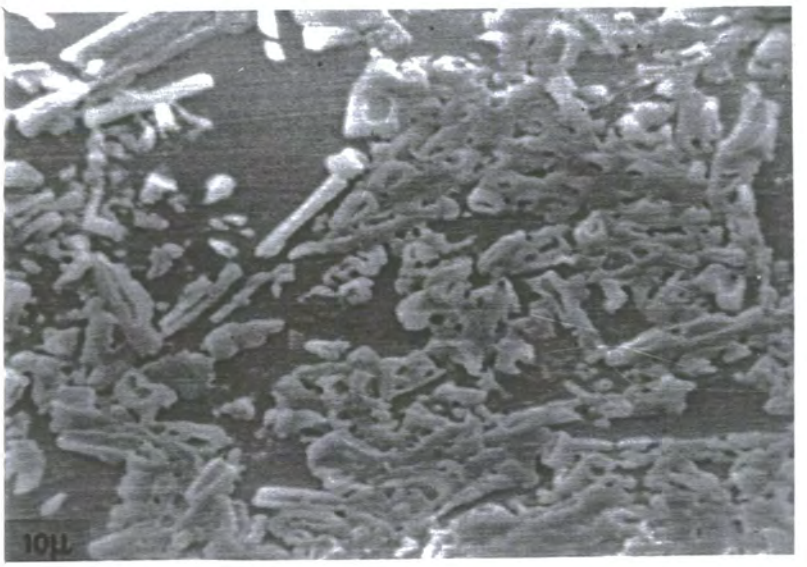

(a)

→ ← 10 μm

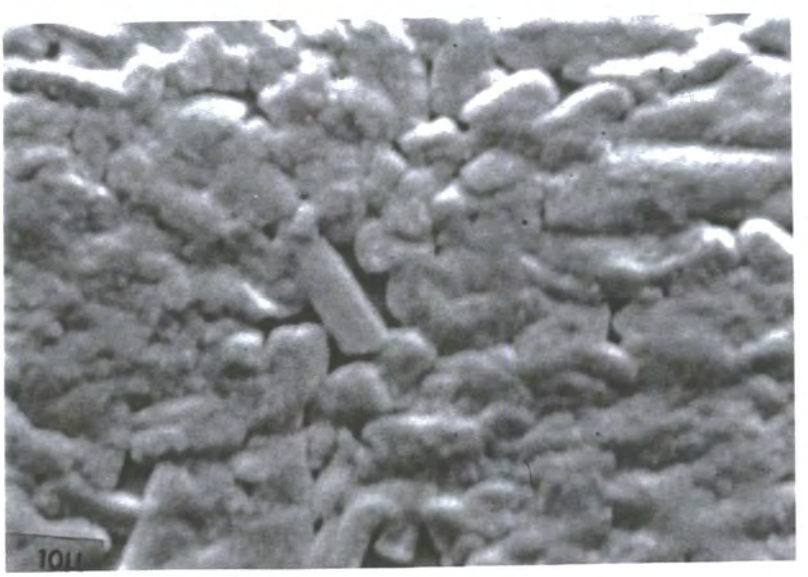

(b)

Figure 6.4: Electron micrographs of 1.1 μm and 1.3 μm thick (TTF) iodide thin films prepared at a source temperature of a) 50°C and b) 60°C, respectively.

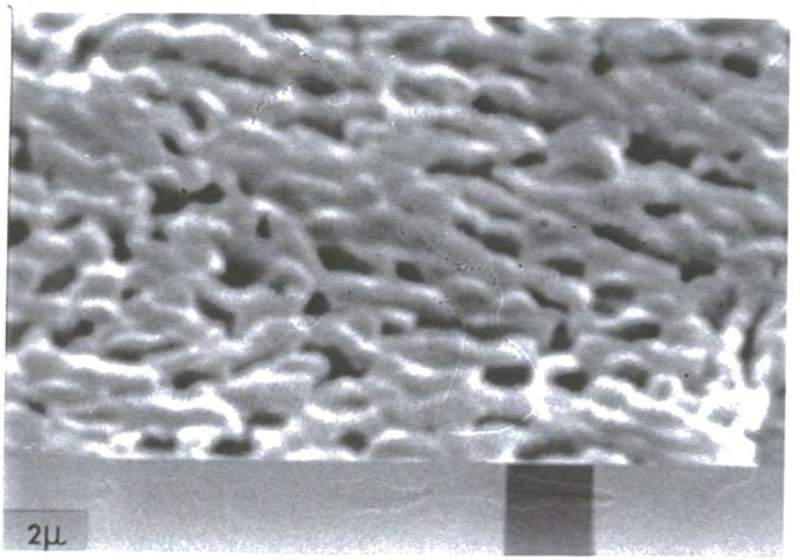

(a)

→ ←

2 μm

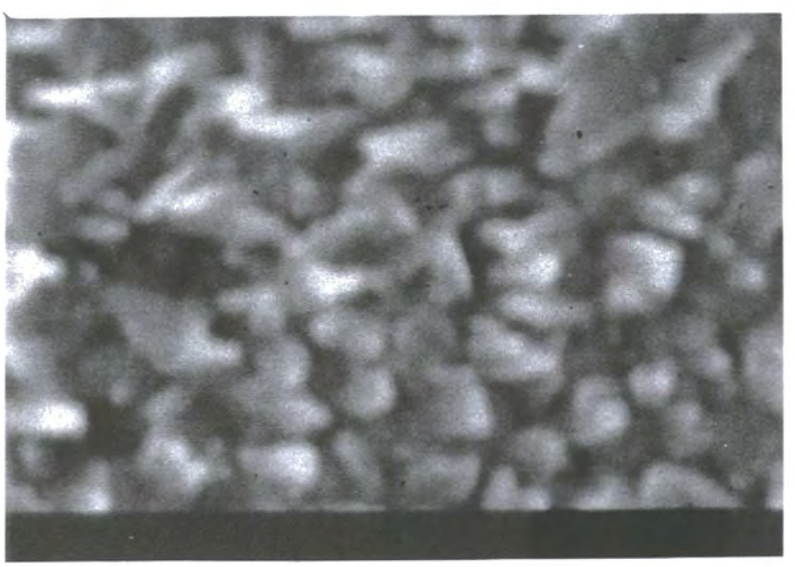

(b)

Figure 6.5: Electron micrographs of 0.8 μm and 1.5 μm thick (TTF) iodide thin films prepared at a source temperature of a) 75°C and b) 80°C, respectively.

Summarising, a change in film structure with the value of T_{sc} was observed. For low deposition rates (low values of T_{sc}), films consisted mainly of needle type crystals (large grain size). Increasing the deposition rate (high values of T_{sc}) resulted in films consisting solely of crystalline plates (finer grain size). The size of the needles (~10 μm) was found to be much greater than the size of the platelets (<4 μm). The effect of deposition rate on the film formation has been reported before for evaporated thin films of metals. In his book, Holland [2] notes that high rates of film formation results in more nuclei initially formed. This produces a fine grain structure. Ohring [3] has come to the same conclusion: '..it is clear that increasing the deposition rate results in smaller islands' (see Section 3.2.1). The higher deposition rate obtained for a T_{sc} =80°C, resulted in a completely different structure, possibly amorphous.

6.1.3 Infrared/visible spectroscopy

The films were characterised using optical absorption spectroscopy. In the literature, only the optical spectrum of TTF in solution is available [4,5]. The differences between the optical spectra of a compound in the solid state and in a solution generally arise from the fact that intermolecular interactions are much weaker in the solution phase. For the sake of comparison, the optical spectrum of powder TTF was obtained following the procedure below:

TTF powder was mixed with NUJOL to make a thick paste and was spread on a glass microscope slide. The spectrum of TTF powder, in the visible and near infrared regions was then obtained (Figure 6.6(b)).

Figure 6.6 compares the solution and solid spectra of TTF. A band at 380 nm exists in both cases but the band around 450 nm in the solution spectrum is shifted and split into two in the powder spectrum, at 490 nm and at 510 nm. Figure 6.7 shows the optical spectrum of a typical as-deposited evaporated TTF thin film. This is similar to that of powder TTF. The band at 380 nm was always present in the as-deposited films and the two closely spaced absorptions at 490 nm and 510 nm were either exhibited separately or as one broad band around 500 nm. According to Hunig *et al.* [4], all the above absorptions are attributed to intramolecular excitations within the TTF molecule.

The optical spectra of the doped samples were similar to those from the literature [5-8]. Figure 6.8 shows a typical optical spectrum of a (TTF) iodide evaporated thin film. The bands at 380 nm and 500 nm in the as-deposited spectrum are slightly shifted to 400 nm and 560 nm, respectively. Two new absorptions, at 870 nm and 1550 nm, appear in the near infrared region. According to Sugano *et al.* [5], the absorption bands around 400 nm and 560 nm are due to intramolecular transitions of $TTF^{+\cdot}$ ions and that at approximately 870 nm is attributed to intermolecular charge-transfer between $TTF^{+\cdot}$ ions within a stack. In particular, it is interpreted as an isovalence transition of the type

$$TTF^{+\cdot} + TTF^{+\cdot} \rightarrow TTF^{2+} + TTF^{0}$$

In the near infrared region, an absorption around 1500 nm can be seen. A study by Scott *et al.* [6] on powdered samples of (TTF)-halide systems reveals a band around 2000 nm which is consistent with the high conductivity ($\approx$ 400 S cm^{-1} at room temperature). This is attributed to an intervalence transition of the type

$$TTF^{0} + TTF^{+\cdot} \rightarrow TTF^{+\cdot} + TTF^{0}$$

The 1500 nm band is almost certainly associated with the mixed valence state, necessary for the compound to be electrically conductive.

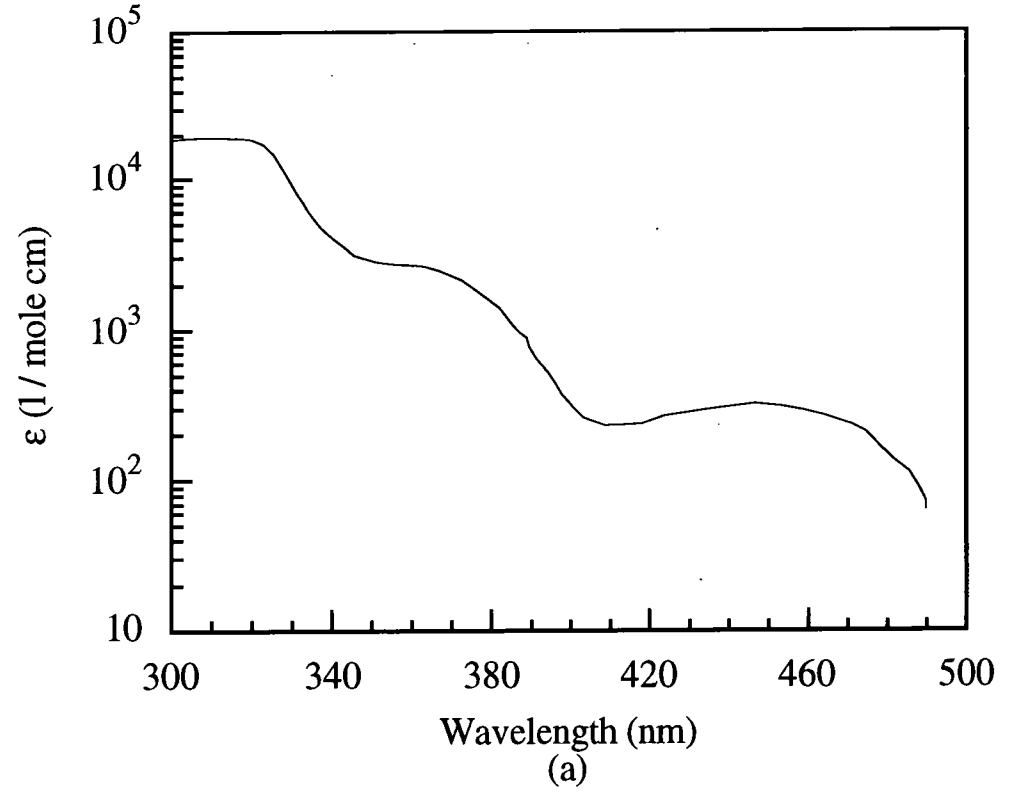

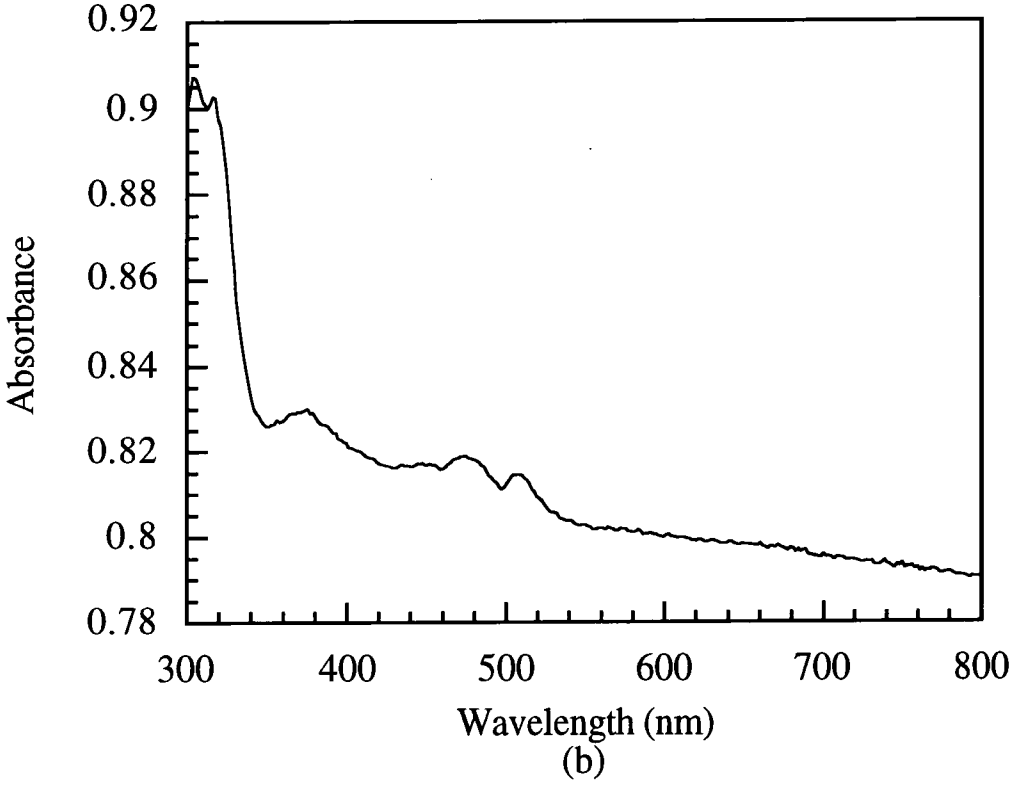

Figure 6.6: The spectrum of TTF, (a) in acetonitrile solution, as taken from Hunig *et al*. [4], and (b) in powder form as measured in this work.

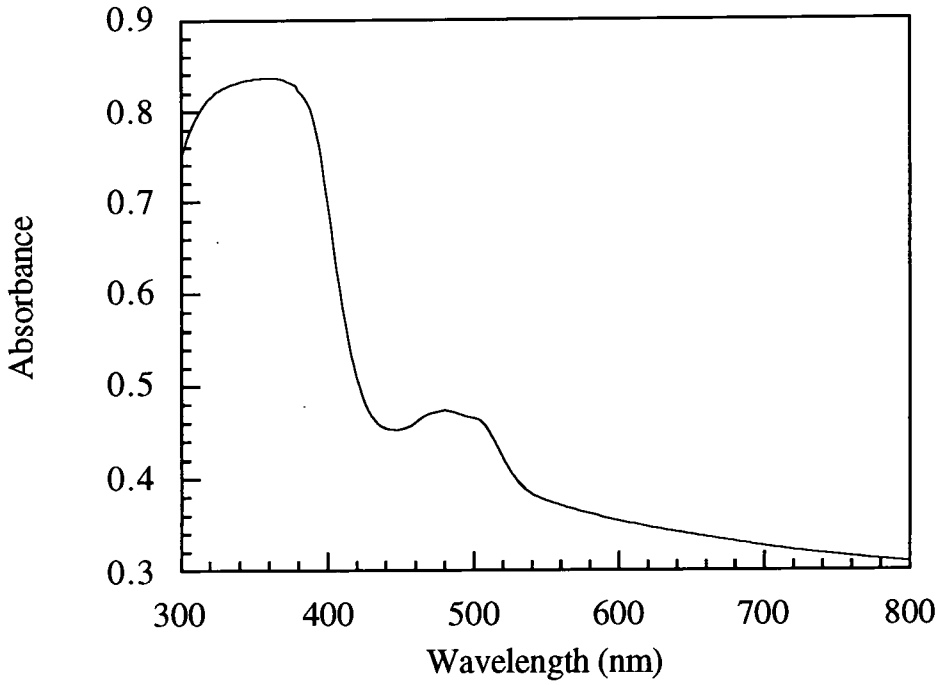

Figure 6.7: Optical spectrum of a 0.8 μm thick as-deposited TTF film deposited on a glass substrate.

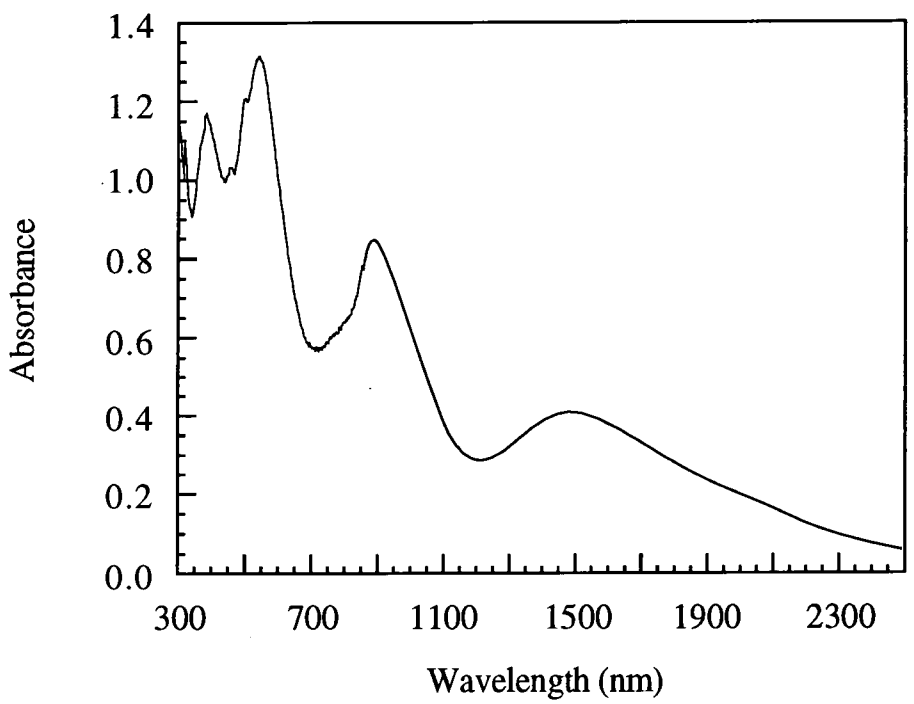

Figure 6.8: Optical spectrum of a 1.1 μm thick (TTF) iodide thin film deposited on a glass substrate.

6.1.4 Electrical Characterisation

Linear current versus voltage behaviour was noted for all TTF films investigated. Figure 6.9 shows the I-V characteristics for an evaporated TTF film, both before and after doping. Using the three point probe method (Section 4.3.1), the effect of the contact resistance was eliminated. Table 6.2 contrasts the in-plane, dc room temperature conductivity for the as-deposited and iodine doped films.

Source Temperature (°C)	In-plane, dc conductivity as-deposited σ_{as}(S cm^{-1})	In-plane, dc conductivity after iodine doping σ_{dop}(S cm^{-1})
50±2	(7.1±1.9)x10^{-7}	2.2±0.6
55±2	(7.0±1.9)x10^{-7}	2.3±0.6
60±2	(1.2±0.4)x10^{-6}	4.3±1.5
65±2	(4.9±1.7)x10^{-6}	6.1±2.1
70±2	(4.2±1.1)x10^{-7}	5.8±1.6
75±2	(3.4±1.0)x10^{-6}	8.0±2.4
80±2	(1.3±0.4)x10^{-7}	0.68±0.2

Table 6.2 In-plane, dc room temperature electrical conductivity for the undoped and iodine doped TTF thin films.

The as-deposited TTF thin films exhibited dc room temperature conductivity values in the range 1.24x10^{-7} to 4.9x10^{-6} S cm^{-1}. These figures are considerably higher than that reported by Wudl *et al.* (σ(25°C) = 10^{-12} S cm^{-1}) [9]. We believe that the reason for this is the impurities present (3%) in the TTF powder used as the starting material. Low impurity levels in inorganic semiconductors are well-known to affect the resistivity. An example is

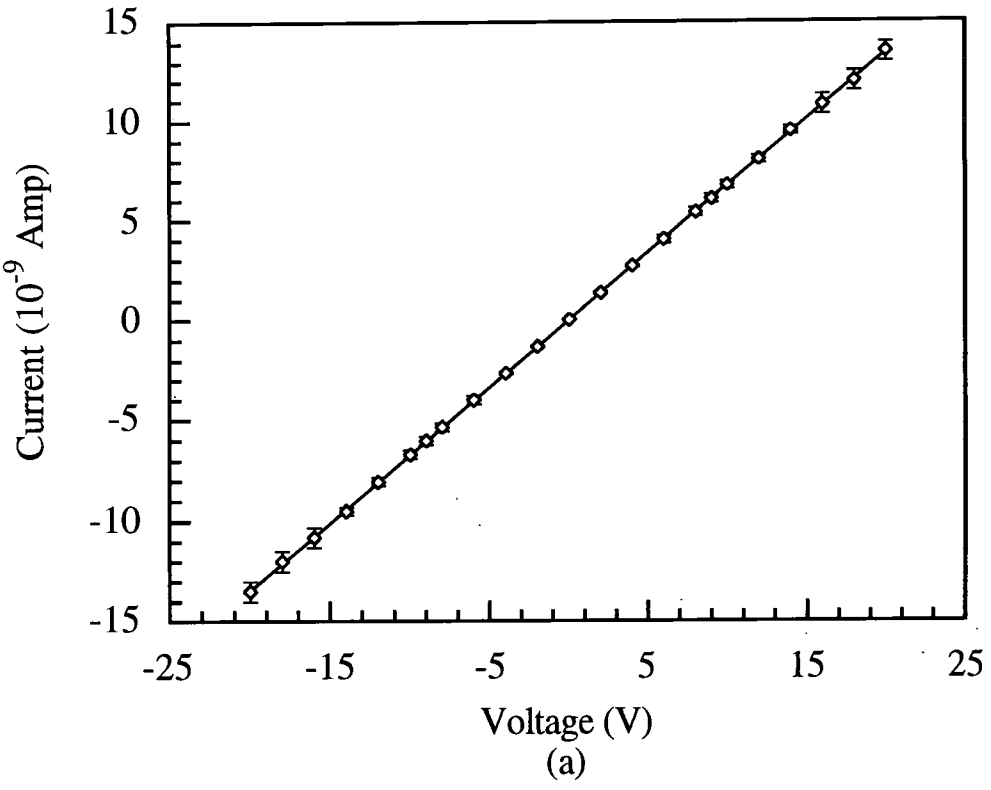

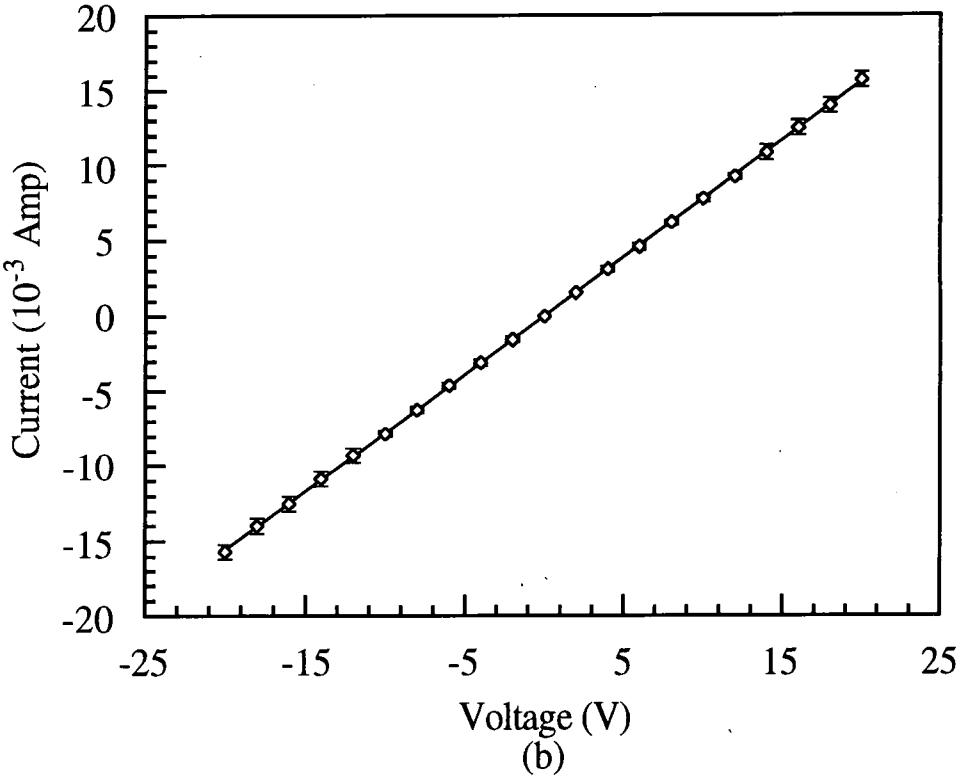

Figure 6.9: In-plane, dc room temperature current versus voltage characteristic for a 1.3 μm TTF thin film, (a) as-deposited and (b) after iodine doping.

silicon, where even an addition of 2 ppm of arsenic reduces the resistivity by a factor of 10^6 [10].

As can be seen from Table 6.2, an increase in the in-plane, dc room temperature conductivity of almost seven orders of magnitude was observed upon doping, with values ranging between 0.68 and 8.0 S cm^{-1}. This suggests that charge-transfer between the TTF molecules and iodine was established. The conductivity value also implies that the degree of charge-transfer between the donor and acceptor molecules was less than unity and that the complex was in the mixed valence state, in complete agreement with results from the optical spectra. Single crystals of (TTF) iodide [9,11,12] have exhibited much higher conductivities (100-450 S cm^{-1}) but this difference can be explained by the polycrystalline nature of the evaporated films. Grain boundaries (i.e. the interface between two adjacent single crystal regions) exist in polycrystalline films and can represent an obstacle to electron conduction.

From the Table 6.2, it is evident that the in-plane, dc room temperature conductivity of the undoped films increases (though only slightly) with increasing source temperature, until the latter reaches 80°C. At this temperature, a significant decrease is observed to a figure lower than that exhibited at a source temperature of 50°C. The conductivity of the films after iodine doping seems to follow the same pattern. One reason for this concerns the method used to measure the conductivity σ, given by

$$\sigma = \frac{Id}{Vlt} \qquad (6.1)$$

where I and V are the current and voltage, t the thickness of the film and l and d the electrode's length and separation, respectively. The electrode pattern used for electrical characterisation was the same for all films prepared. Implicit in the calculation of σ from

Equation (6.1) is that the entire area between the electrodes was uniformly covered with TTF. However, the electron micrographs suggest (Figure 6.4) that this was not true for low values of T_{sc} (i.e. existence of pinholes). The erroneous assumption leads to a lower value of σ. For high values of T_{sc}, this experimental error becomes less significant because the total uncoated area is decreased. The significant decrease in the conductivity observed for T_{sc}=80°C could result from the different morphology exhibited for this temperature (Figure 6.4(b)). This could also imply a different crystallographic phase of (TTF) iodide thin films.

Figure 6.10 shows the temperature dependence of the in-plane, dc conductivity of an (TTF) iodide thin film. Examining the shape of the curve closely, three different regions can be identified with transitions at 160K and 130K. The calculated activation energy was 0.095 eV for temperatures between 290K and 180K, 0.083 eV between 160K and 140K and 0.073 eV between 130K and 100K. If a single activation energy over the entire temperature range was assumed, a value of 0.09±0.02 eV was obtained. No hysteresis was observed during the warming up cycle. For single crystals of the monoclinic form of $(TTF)I_{0.7}$, a transition, attributed to intrachain interactions, has been reported at 210K [9,14]. Below this temperature a change in ΔE from 0.084 eV below 170K to 0.12 eV between 170K and 210K was seen. The former value compares well to that exhibited by our evaporated films for intermediate temperatures (0.083 eV). For the single crystals, a clear hysteresis loop has also been noted. The origin of this has been attributed to interchain interactions (it has been suggested that interchain coupling is weak and individual chains do not go through the transition at the same temperature [15,16]). The evaporated films reported here exhibited no such hysteresis. However, the stacking axis in our films was ill-defined (i.e. the films were polycrystalline). The conductivity measured was therefore a mixture of the conductivities

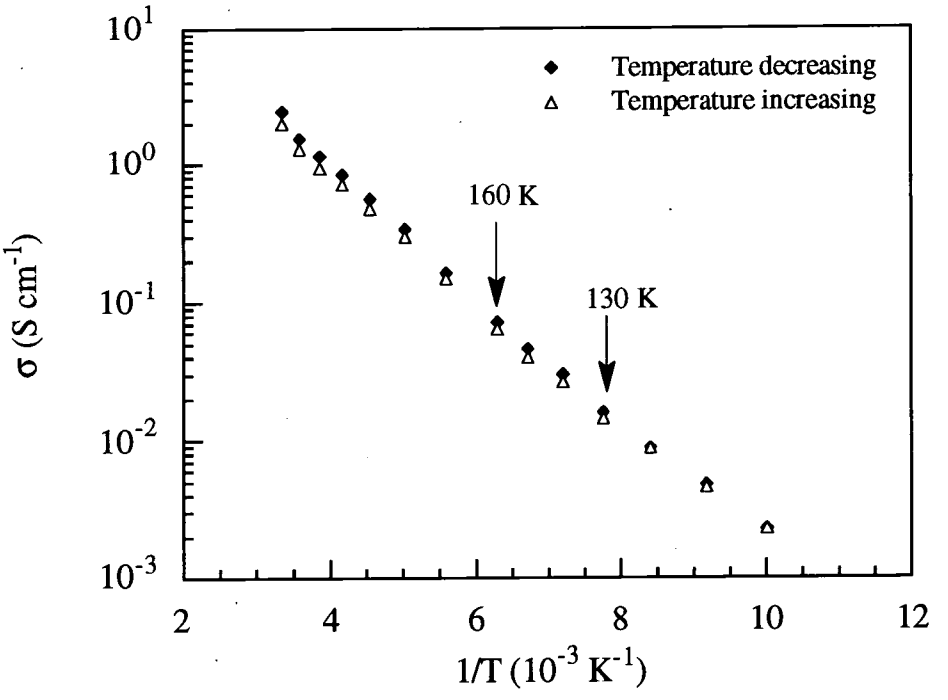

Figure 6.10: In-plane, dc room temperature conductivity versus reciprocal temperature for a 1 μm thick (TTF) iodide thin film. The arrows indicate the transition temperatures. Conductivity values were evaluated for V=5 V.

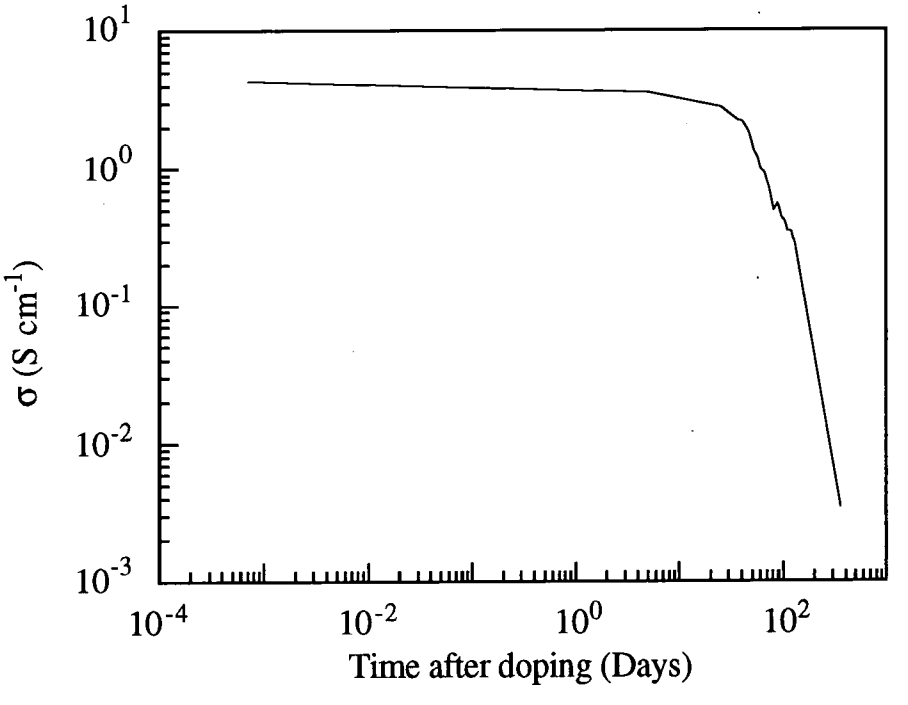

Figure 6.11: Time dependence of the in-plane, dc room temperature conductivity in air of a 1.3 μm thick (TTF) iodide thin film. Conductivity values were evaluated by measurement of I-V over the range -20 V to 20 V.

along and perpendicular the stacking axis. The temperature dependence of the conductivity of the evaporated films was the same, within experimental error, for all films prepared with T_{sc}<80°C.

The value of the in-plane, dc room temperature conductivity was found to depend on time. In particular, samples stored in air were stable over a period of 20 days, after which a decrease was seen (Figure 6.11). The conductivity was monitored for a total period of 240 days, revealing a drop of three orders of magnitude. This significant decrease cannot be attributed to a decrease in iodine content since re-doping did not restore the high conductivity. This long term degradation of the conductivity is probably associated with structural/chemical changes in the film, perhaps resulting in a different phase. However, no differences in the film morphology were apparent on examination under the SEM.

6.2 Co-evaporation of TTF and Iodine

6.2.1 Film deposition

A second evaporation source, for iodine, was added to the vacuum chamber. A crucible, as described in Section 5.2.2, was used for this. To allow comparison with films of (TTF) iodide prepared by single source evaporation, the substrate temperature was kept at -10°C (Section 6.1.1). The source-substrate distance was set to 6 cm and the chamber volume reduced to allow the two evaporating materials to mix and react before condensing on the substrate. Glass microscope slides of dimension 15x25 mm^2 were used as substrates. The chamber was maintained a pressure of $2.5x10^{-5}$ mbar. The source temperatures of both TTF and iodine sources (T_{sc}(TTF), T_{sc}(I)) were varied. Tables 6.3-6.5 show the conditions used to prepare a range of films.

$T_{sc}(I)$ (°C)	Thickness (μm)	Deposition Rate (nm min^{-1})
0±2	1.7±0.2	85±10
-10±2	1.0±0.2	33±7
-20±2	0.2±0.02	11±2

Table 6.3: A summary of the films prepared with $T_{sc}(TTF)$ = 50°C.

$T_{sc}(I)$ (°C)	Thickness (μm)	Deposition Rate (nm min^{-1})
0±2	0.7±0.2	100±28
-10±2	0.4±0.1	57±14
-20±2	0.7±0.2	70±20

Table 6.4: A summary of the films prepared with $T_{sc}(TTF)$ = 60°C.

$T_{sc}(I)$ (°C)	Thickness (μm)	Deposition Rate (nm min^{-1})
0±2	0.6±0.1	300±51
-10±2	1.2±0.1	630±60
-20±2	0.6±0.2	264±90

Table 6.5: A summary of the films prepared with $T_{sc}(TTF)$ = 70°C.

6.2.2 Film Morphology

The colour of the films varied according to the iodine content, which, in turn, was related to the iodine source temperature $T_{sc}(I)$. Films prepared at a high $T_{sc}(I)$ and low

T_{sc}(TTF) were as black as those prepared by single source evaporation, shown in Figure 6.2. Different combinations of T_{sc}(I) and T_{sc}(TTF) resulted in films with colours ranging from dark purple to dark yellow. Figure 6.12 shows a photograph of a film prepared with T_{sc}(I)= -20°C and T_{sc}(TTF)= 50°C. The morphology of the films was also found to depend on the preparation conditions. Deposition rates for the (TTF) iodide films ranged from significantly lower (11 nm min^{-1}) to higher (630 nm min^{-1}) values compared to those observed for films prepared with the single source evaporation. Figure 6.13 shows an optical micrograph of a 0.6 μm thick (TTF) iodide thin film prepared with T_{sc}(TTF) = 70°C and T_{sc}(I) = -20°C while Figure 6.14 shows electron micrographs of two (TTF) iodide samples prepared under different conditions. These suggest 3-D island growth (Section 3.2.1.). Deposition was found to be quite uniform. Pinholes still existed but the size of these had considerably reduced compared to films prepared by the single source evaporation (e.g. compare the optical micrographs in Figures 6.3 and 6.13). In general, the pattern that was followed by the (TTF) iodide films prepared by the single source evaporation was also followed by the films prepared by the co-evaporation, i.e. low deposition rates result in large grain size and higher deposition rates in smaller grain size. Figure 6.14(a) was prepared with a much higher deposition rate than (b) and the difference in the crystal size is clearly evident. In co-evaporated films, the large needle-type structure seen for films prepared by single source evaporation was not observed, the grain size was, in general, found to be smaller. This is also evident by comparing micrographs of films prepared by the two evaporation methods and with similar deposition rates. The grain (needles/platelets) size seen in Figure 6.4 (a) is larger than that (platelets) in Figure 6.14(a) even though the deposition rates were comparable (73 and 85 nm min^{-1} for the two films).

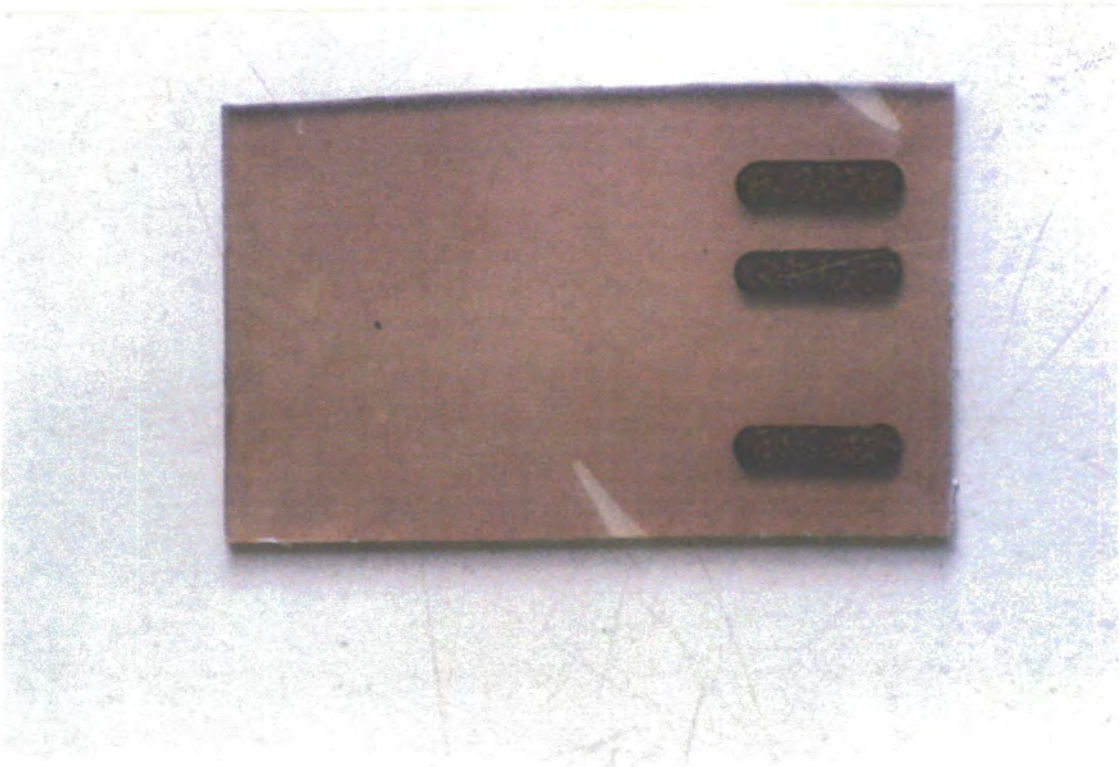

Figure 6.12: Photograph of a 0.2 μm (TTF) iodide deposited on a glass substrate prepared at $T_{sc}(TTF) = 50°C$ and $T_{sc}(I) = -20°C$.

→ ←
10 μm

Figure 6.13: Transmission optical micrograph of a 0.6 μm thick (TTF) iodide thin film on a glass substrate deposited at T_{sc}(TTF) = 70°C and T_{sc}(I) = -20°C.

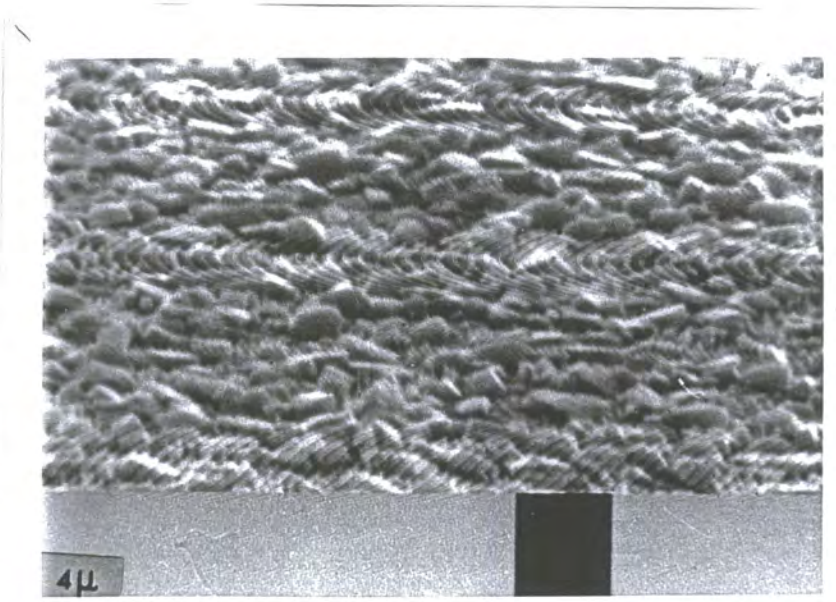

(a)

→ ← 4 μm

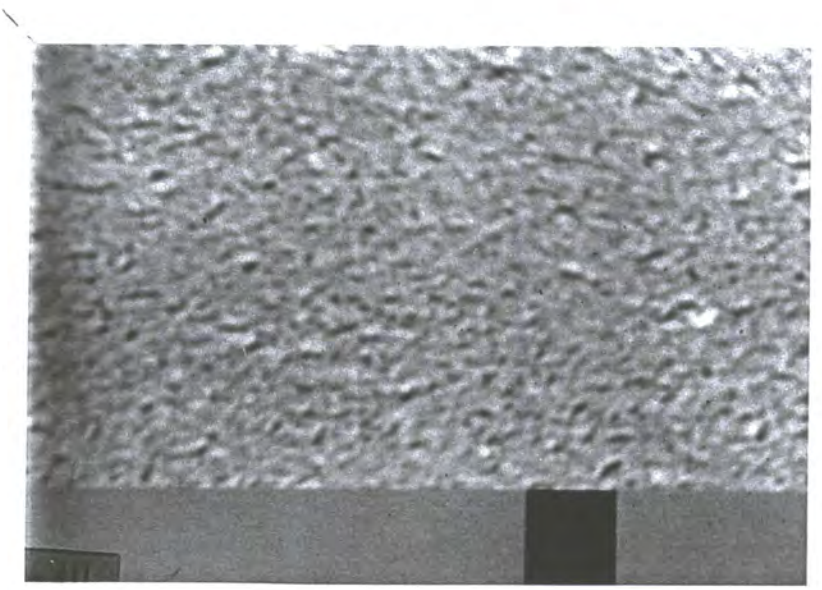

(b)

Figure 6.14: Electron micrographs of (TTF) iodide films deposited on a glass substrate prepared at a) T_{sc}(TTF) = 50°C and T_{sc}(I) = 0°C (deposition rate of 85 nm min^{-1}), 1 μm thick and b) T_{sc}(TTF) = 70°C and T_{sc}(I) = 0°C (deposition rate of 300 nm min^{-1}), 0.6 μm thick.

6.2.3 Infrared/visible spectroscopy

As expected, the optical spectra of the (TTF) iodide films prepared with the co-evaporation technique exhibited similarities to those of the (TTF) iodide films prepared with the single source evaporation technique. Figures 6.13-17 show the optical spectra of the (TTF) iodine thin films, grouped according to T_{sc}(TTF). Bands around 320, 400 and 530 nm were exhibited by all films. These are due to local excitations and their origin has been explained before (Section 6.1.3). The 870 nm absorption, present only in the spectra of some films (especially those with high T_{sc}(I)), is attributed to charge-transfer between TTF molecules. In the near infrared region a band, whose location changed from film to film, would appear. The (TTF) iodide films prepared by single source evaporation exhibited an absorption at similar wavelengths. This was attributed to transitions of the sort:

$$TTF^{+\cdot} + TTF^{0} \rightarrow TTF^{0} + TTF^{+\cdot}$$

However, for the single source evaporated (TTF) iodide films, the position of this band did not depend on the preparation conditions. This different wavelength for the maximum of this band in the co-evaporated films probably reflects the different degree of iodide doping.

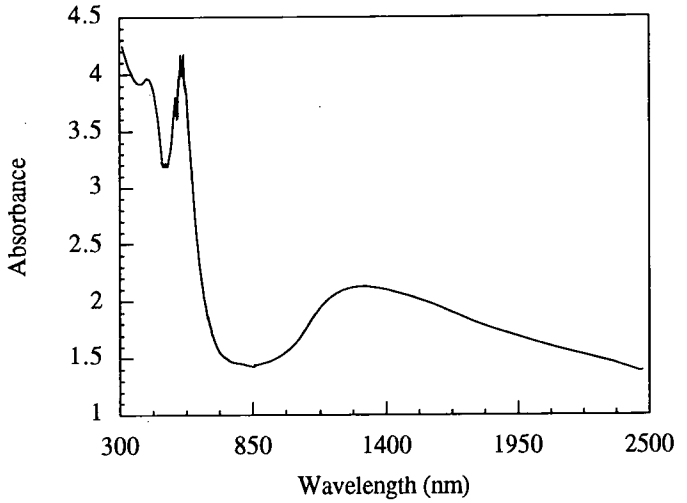

(a)

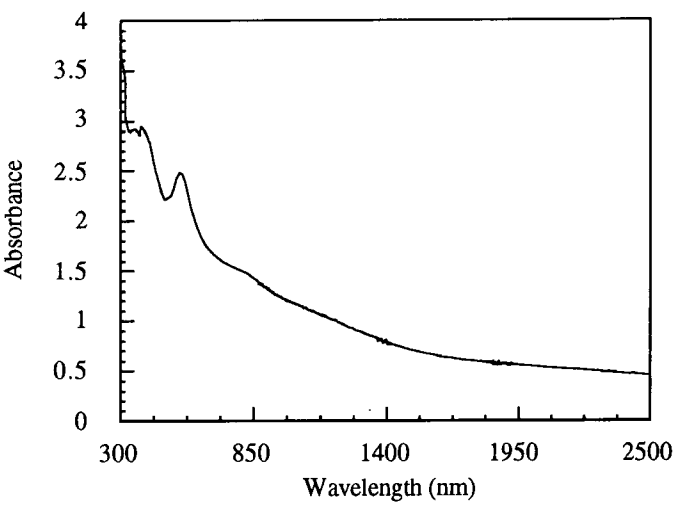

(b)

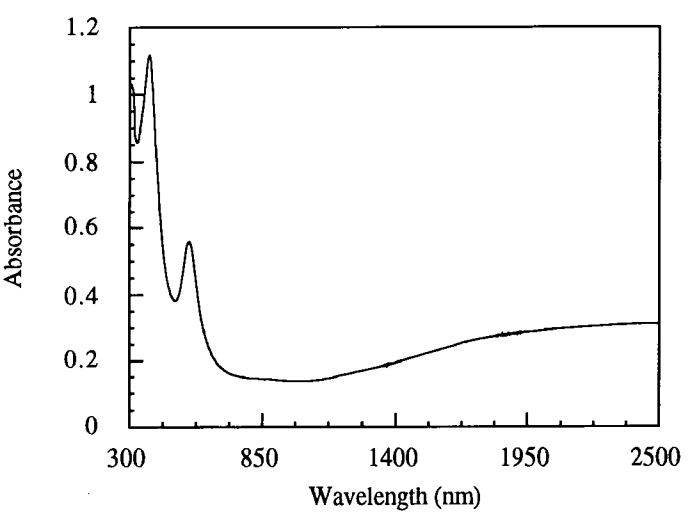

(c)

Figure 6.15: Optical spectra for (TTF) iodide films deposited on a glass substrate with T_{sc}(TTF) = 50°C, (a) 1.7 μm thick and with T_{sc}(I) = 0°C, (b) 1 μm thick and with T_{sc}(I) = -10°C and (c) 0.2 μm thick and with T_{sc}(I) = -20°C.

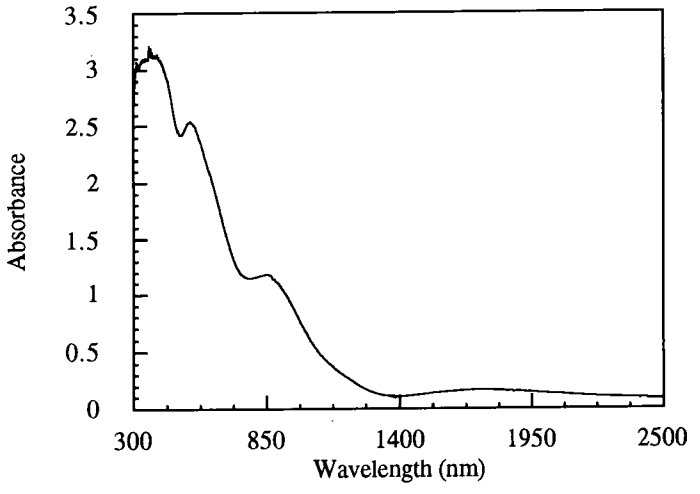

(a)

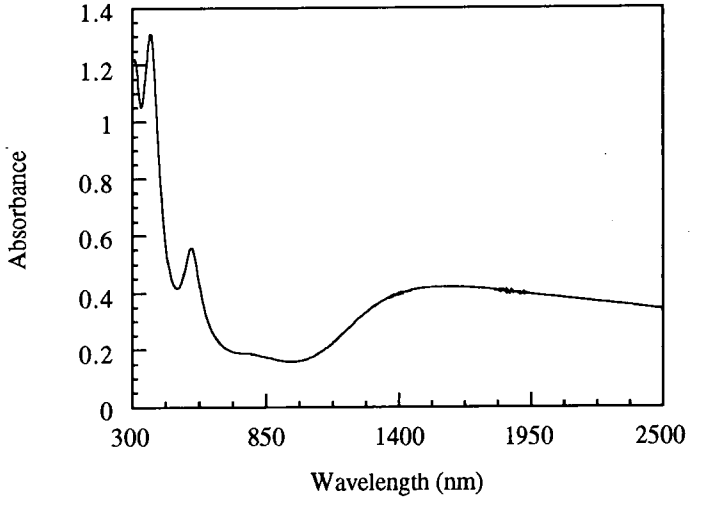

(b)

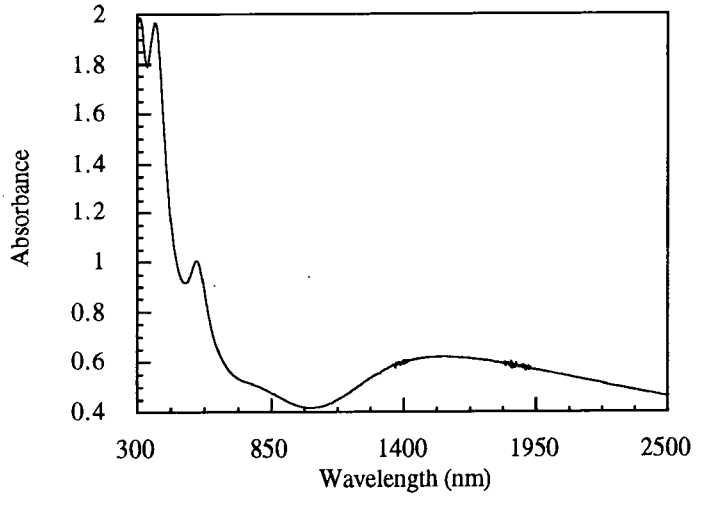

(c)

Figure 6.16: Optical spectra for (TTF) iodide films deposited on a glass substrate with T_{sc}(TTF) = 60°C, (a) 0.7 μm thick and with T_{sc}(I) = 0°C, (b) 0.4 μm thick and with T_{sc}(I) = -10°C and (c) 0.7 μm thick and with T_{sc}(I) = -20°C.

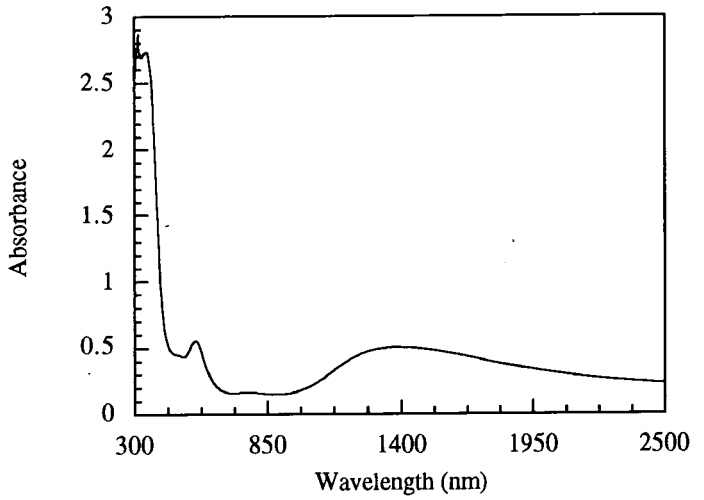

(a)

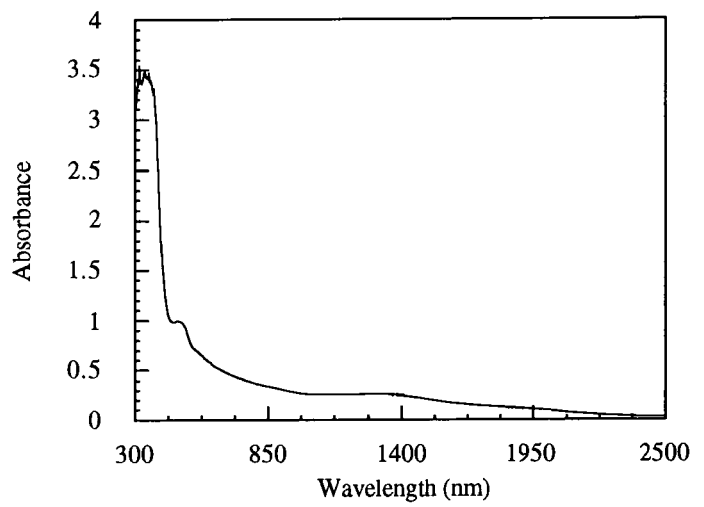

(b)

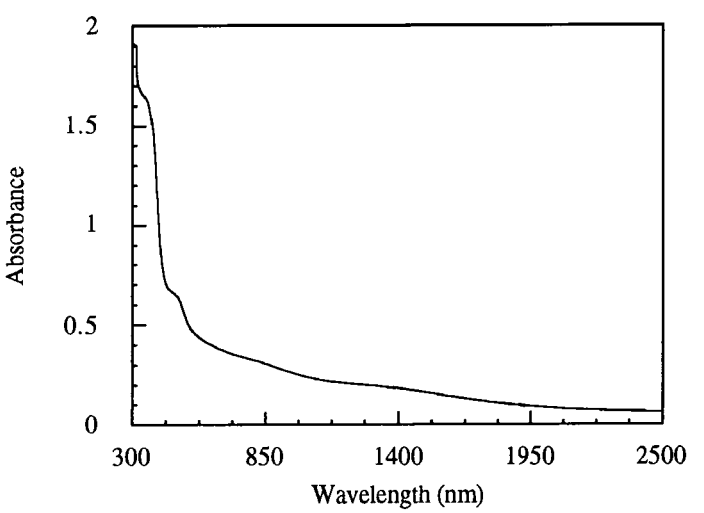

(c)

Figure 6.17: Optical spectra for (TTF) iodide films deposited on a glass substrate with T_{sc}(TTF) = 70°C, (a) 0.6 μm thick and with T_{sc}(I) = 0°C, (b) 1.2 μm thick and with T_{sc}(I) = -10°C and (c) 0.6 μm thick and with T_{sc}(I) = -20°C.

6.2.4 Electrical Characterisation

The in-plane, dc room temperature conductivity of the thin films depended on the preparation conditions. Ohmic behaviour was observed for all samples investigated (Figure 6.18).

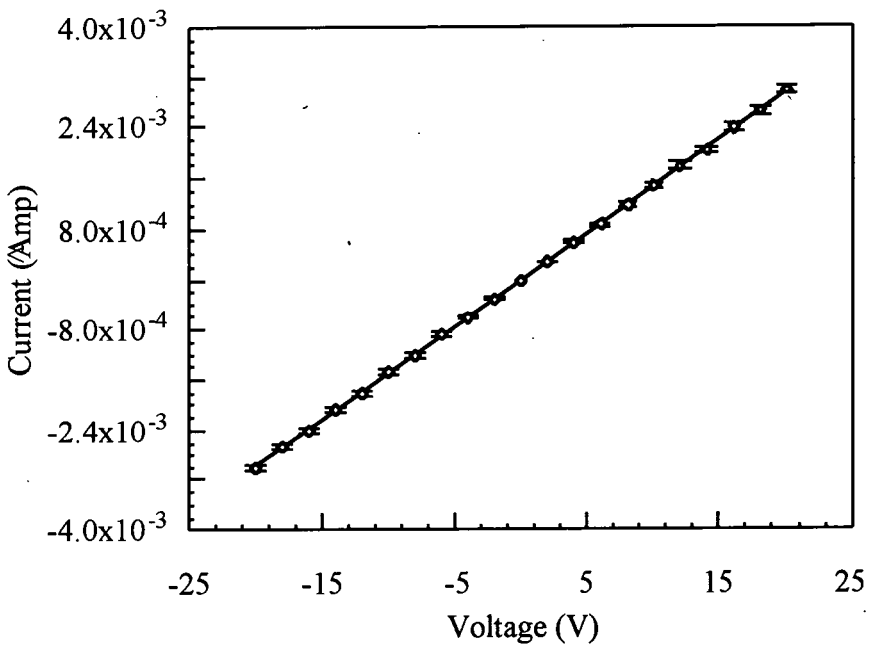

Figure 6.18: In-plane, dc room temperature current versus voltage characteristic for a 1.7 μm thick (TTF) iodide thin film prepared with T_{sc}(TTF) = 50°C and T_{sc}(I) = -10°C.

The conductivity values are summarised in tables 6.6-6.8.

T_{sc}(I) (°C)	Thickness (μm)	σ (S cm^{-1})
0±2	1.7±0.2	2.9±0.4
-10±2	1.0±0.4	1.5±0.4
-20±2	0.2±0.3	1.2±0.2

Table 6.6: In-plane, dc room temperature conductivity for samples prepared with T_{sc}(TTF) = 50°C.

$T_{sc}(I)$ (°C)	Thickness (μm)	σ (S cm^{-1})
0±2	0.7	$(1.4\pm0.4)x10^{-3}$
-10±2	0.4±0.3	0.13±0.02
-20±2	0.7±0.2	$(4.9\pm1.6)x10^{-2}$

Table 6.7: In-plane, dc room temperature conductivity for samples prepared with $T_{sc}(TTF) = 60°C$.

$T_{sc}(I)$ (°C)	Thickness (μm)	σ (S cm^{-1})
0±2	0.6±0.2	$(6.3\pm1.3)x10^{-2}$
-10±2	1.2±0.1	$(1.2\pm0.16)x10^{-4}$
-20±2	0.6±0.2	$(2.2\pm0.16)x10^{-6}$

Table 6.8: In-plane, dc room temperature conductivity for samples prepared with $T_{sc}(TTF) = 70°C$.

As can be seen from Tables 6.6-8, dc room temperature conductivity increases with increasing $T_{sc}(I)$. For $T_{sc}(TTF) = 70°C$, an increase of two orders of magnitude is observed for every 10°C increase in the $T_{sc}(I)$. This is explained by the fact that higher iodine content provides more charge carriers. The sample deposited with a $T_{sc}(I) = -20°C$, exhibits a dc room temperature conductivity very close to that of as-deposited TTF samples (Table 6.2). Evidently, not enough iodine is present in the film.

For $T_{sc}(TTF) = 60°C$, an increase is also observed for $T_{sc}(I) = -20 \rightarrow -10°C$ with a high value of conductivity exhibited for $T_{sc}(I) = -10°C$. Further increase in $T_{sc}(I)$ resulted in

a decrease in conductivity to a figure lower than exhibited for $T_{sc}(I) = -20°C$. As can be seen from Figure 6.16, all three samples prepared with $T_{sc}(TTF) = 60°C$ exhibited the full charge-transfer band around 870 nm. In the case of the film prepared at $T_{sc}(I) = 0°C$, this band was much stronger. A decrease in the value of conductivity for this film would, therefore, be expected.

For $T_{sc}(TTF) = 50°C$, no significant differences were observed for different values of $T_{sc}(I)$. We believe that the low value of $T_{sc}(TTF)$ allowed more time for the two components to react before depositing on the glass substrate. The highest value of the in-plane dc room temperature conductivity is similar to that exhibited by the (TTF) iodide films prepared by the single source evaporation technique.

The temperature dependence of the dc conductivity for two of the more conductive (TTF) iodide films ($\sigma = 2.9$ S cm^{-1} prepared with $T_{sc}(TTF) = 50°C$ and $T_{sc}(I) = 0°C$ and for $\sigma = 0.13$ S cm^{-1} prepared with $T_{sc}(TTF) = 60°C$ and $T_{sc}(I) = -10°C$) was investigated and found to be similar. This is shown in Figure 6.19. Examining the shape of the curve, two regions can be seen with a transition occurring at 120K. The activation energy varied from 0.21 eV between 300K and 130K, to 0.14 eV between 120K and 100K. If a single activation energy was assumed over the entire temperature range, its value would be 0.2±0.02 eV. This latter figure is close to that one being reported for (TTF) iodide films (0.25 eV) prepared by the LB technique [17]. It is also similar to the 0.24 eV value reported for single crystals of orthorhombic (TTF) I_2. In the latter case, the dc conductivity measured along the stacking axis was three orders of magnitude lower that the one reported here for our evaporated films [13]. A small amount of hysteresis was noted in Figure 6.19. Single crystals of (TTF) $I_{0.7}$

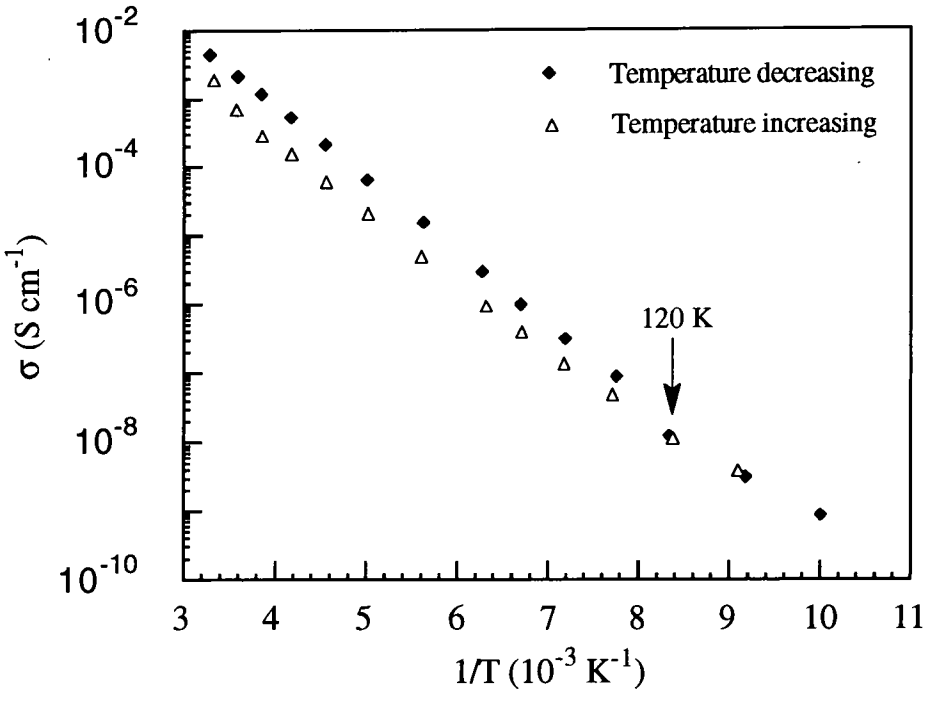

Figure 6.19: In-plane, dc room temperature conductivity versus reciprocal temperature for a 0.7 μm thick (TTF) iodide thin film prepared with T_{sc}(TTF) = 60°C and T_{sc}(I) = -10°C. The transition temperature at 120K is also shown. Conductivity values were evaluated for V=5 V.

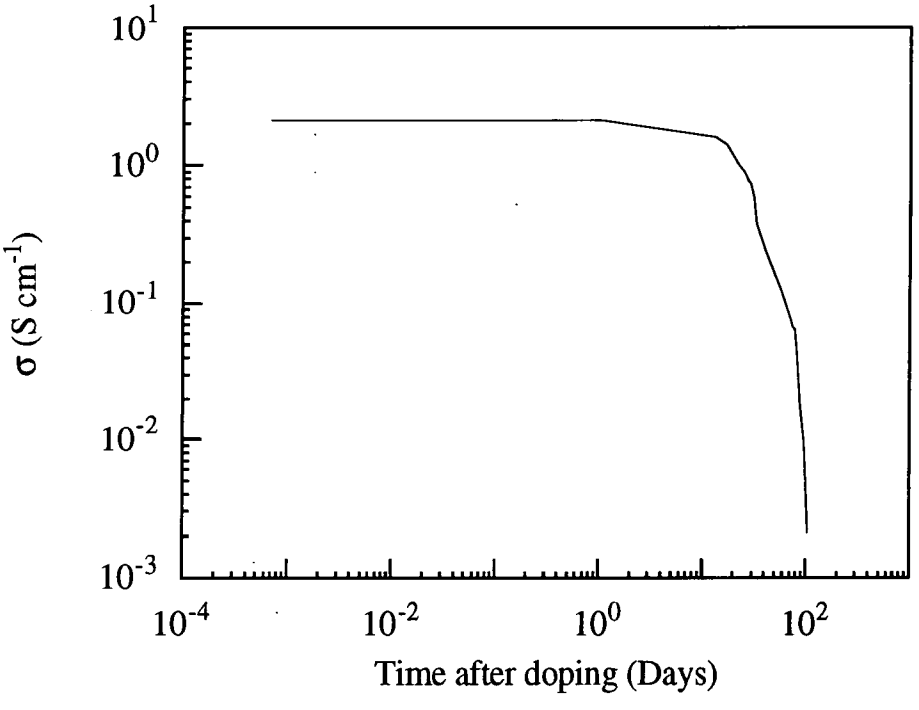

Figure 6.20: Time stability of the in-plane, dc room temperature conductivity in air for a 1.7 μm thick (TTF) iodide thin film prepared with T_{sc}(TTF) = 60°C and T_{sc}(I) = -10°C. Conductivity values were evaluated by measurement of the I-V over the range -20 V to 20 V.

have exhibited a similar but much stronger hysteresis loop in the dc conductivity measured along the stacking axis of the TTF radical cations [13,14]. Yudasaka *et al.* [1,18], have also reported (TTF) $I_{0.7}$ thin films prepared by co-evaporation. In their films, domains of highly orientated rod-like crystals were identified by scanning electron microscopy [19] and measurements of the dc conductivity along and perpendicular the stacking axis were possible. These workers reported a hysteresis loop in the temperature dependence of the conductivity along the stacking axis but a single activation energy was observed for the dc conductivity measured perpendicular to the stacking axis. Conductivity values measured along and perpendicular to the stacking axis were of the order of 500 S cm^{-1} and 10 S cm^{-1}, respectively [20]. This latter value compares well with the values exhibited for films prepared in this work, both by the single source and co-evaporation. However, the structure of our evaporated films was found to be polycrystalline. Dc conductivity values measured in this work are mixtures of the conductivities measured along and perpendicular the stacking axis. This is a possible reason for our lower conductivity observed (compared to that of Yudasaka's films along the stacking axis) and the smaller hysteresis loop exhibited.

Finally, we tried to repeat the preparation conditions of the films reported by Yudasaka *et al.* [1], these were: $T_{sc}(TTF) = 60°C$, $T_{sc}(I) = 0°C$ and $T_s = 14°C$. Samples were deposited on glass and mica but their in-plane, dc room temperature conductivity was 5-8 S cm^{-1}, in contrast with the value of 300 S cm^{-1} reported by Yudasaka *et al.* Our films were polycrystalline and we cannot be sure why the domains of highly orientated crystals observed in the films reported by Yudasaka *et al.*, were not observed in our films.

As for the (TTF) iodide films prepared by the single source evaporation, the value of the in-plane, dc room temperature conductivity of the co-evaporated films was found to

depend on time. Samples stored in air were stable for a period of 15 days after which a decrease was seen (Figure 6.20). A drop in conductivity of three orders of magnitude was observed after a period of 105 days. Re-doping did not restore the previous value of conductivity and, as for the single source evaporated (TTF) iodide films, a structural (that SEM analysis could not reveal) or a chemical change must have taken place in the film.

6.3 Comparison Between the Two Types of Films

The (TTF) iodide thin films produced by the single and co-evaporation techniques showed several similarities. The optical spectra of both exhibited the same bands in the visible region. In the near-infrared, an absorption around 1500 nm was evident for the films produced by single source evaporation. This absorption, identified as a mixed-valence band, was also present in the spectra of co-evaporated films but its location varied from 1300 nm to 2500 nm, depending on the preparation conditions. The in-plane, dc room temperature conductivity of the co-evaporated films ranged from 2.2×10^{-6} to 2.9 S cm^{-1}, the highest value being in the same order of magnitude as that exhibited by the single source evaporated films. One significant difference was noted in the activation energy values measured. The figure for the co-evaporated films (0.2 eV) was almost twice that for the single source evaporated films (0.09 eV). Both types of film were found to be polycrystalline and therefore have a limited conductivity due to grain boundaries, the density of which were greater for the co-evaporated films (due to the smaller grain size). This could explain the larger activation energy measured. On the other hand the difference in ΔE could suggest different crystallographic phases for the two types of films. The conductivity value for both films was found to depend on time but co-evaporated films were more unstable. In particular, the time

required for the same decrease of three orders of magnitude in conductivity, was for the single source evaporated films almost double (240 days) that for the co-evaporated films (105 days).

6.4 Summary

Thin films of (TTF) iodide were deposited on glass using two different vacuum evaporation techniques. First, a single source (TTF) was used and the films were doped with iodine after deposition. Films were conductive with dc room temperature conductivity values between 0.68 and 8.0 S cm^{-1}. For the second technique, TTF and iodine were evaporated simultaneously from two separate sources. For these films, the dc conductivity covered an extended range of values (10^{-6}-10 S cm^{-1}), according to the iodine content. Similarities were exhibited in the optical spectra and in the in-plane, dc room temperature conductivities for the two types of films. However, the thin layers prepared by single source evaporation were found to be more conductive, more stable and easier to produce than those prepared by co-evaporation.

References

1. M. Yudasaka, K. Hironaga, H. Yamochi, K. Nakamishi and G. Saito, 'Thin Film Formations of Charge-Transfer Complexes with Metallic Properties by Vacuum Deposition Method', *Mat. Res. Soc. Symp. Proc.*, **173** (1990) 137.
2. Holland, 'Vacuum Deposition of Thin Films', Chapman & Hall Ltd., (1963) pp. 207-208.
3. M. Ohring, 'The Materials Science of Thin Films', Academic Press, (1992), pp. 201-213.
4. S. Hunig, G. Kiesslich, H. Quast and D. Scheutzow, 'Tetrathio-äthylene and Ihre Höheren Oxidationsstufen', *Liebigs Ann. Chem.*, (1973) 310.
5. T. Sugano, K. Yakushi and H. Kuroda, 'Polarised Absorption Spectra of Single Crystals of Tetrathiafulvalenium Salts', *Bull. Chem. Soc. Jap.*, **51** (1978) 1041.

6. B.A. Scott, S.J. La Placa, J.B. Torrance, B.D. Silverman and B. Welber, 'The Crystal Chemistry of Organic Metals: Structure and Stability in the Tetrathiafulvalenium-Halide Systems', *J. Am. Chem. Soc.*, **99** (1977) 6631.

7. J.B. Torrance, B.A. Scott, B. Welber, F.B. Kaufman and P.E. Seiden, 'Optical Properties of the Radical Cation Tetrathiafulvalenium Salts (TTF^+) in its Mixed-Valence and Monovalence Halide Salts', *Phys. Rev. B*, **19** (1979) 730.

8. R.J. Warmack and T.A. Callcott, 'Single Crystal Properties of Two Forms of Tetrathiafulvalenium iodide (TTF-I_n)', *Phys. Rev. B*, **14** (1976) 3238.

9. F. Wudl, D. Wobschall and E. Hufnagel, 'Electrical Conductivity by the Bis-1,3-dithiole-Bis-1,3-dithiolium System', *J. Am. Chem. Soc.*, **92** (1972) 670.

10. W.S. Ruska, 'Microelectronic Processing, An introduction to the Manufacture of Integrated Circuits', McGraw-Hill, (1987) pp 29-33.

11. B.A. Scott, J.B. Torrance, S.J. LaPlaca, P. Cornfield, D.C. Green and S.Etemad, 'Mixed Valence Interactions in the TTF-Halide Systems', *Bull. Am. Phys. Soc.*, **20** (1975) 496.

12. G.R. Johnson, D.J. Dahm, M.G. Miles and J.D. Wilson, 'Structure and Conductivity of (TTF) Halides', *Bull. Am. Phys. Soc.*, **20** (1975) 466

13. R.J. Warmack and T.A. Calcott, 'Dc conductivity of Tetrathiafulvalene Bromide (TTF-Br_n) and TTF-I_n Single crystals', *Phys. Rev. B*, **12** (1975) 3336.

14. R.B. Somoano, A. Gupta, V. Hadek, T. Datta, M. Jones, R. Deck and A.M. Hermann, 'The Electrical and Magnetic Properties of (TTF) $(I)_{0.71}$', *J. Chem. Phys.*, **63** (1975) 4970.

15. J.J. Daly and F.Sanz, 'Hepta(tetrathiafulvalene) Pentaiodide: the Projected Structure', *Acta Cryst.*, **B31** (1975) 620.

16. F. Wudl, D.E. Schafer, W.M. Walsh, Jr. L.W. Rupp, F.J. DiSalvo, J.V. Waszczak, M.L. Kaplan and G.A. Thomas, 'A Systematic Study of an Isomorphous Series of Organic Solid State Conductors Based on Tetrathiafulvalene', *J. Chem. Phys.*, **66** (1977) 377.

17. M. Kilitziraki, C. Pearson, A.S. Dhindsa, M.R. Bryce and M.C. Petty, *Thin Solid Films, in press.*

18. M. Yudasaka, K. Hironaga , H. Yamochi and G. Saito, 'Highly Oriented Thin Films of Hepta-(tetrathiafulvalene) pentaiodide Formed by Double-Source Evaporation of Tetrathiafulvalene and Iodide', *J. Appl. Phys.*, **70** (1991) 3501.

19. J.J. Breen, J.S. Tolman and G.W. Flynn, 'Scanning Tunneling Microscopy Studies of Vapor Deposited Fims of Tetrathiafulvalene with Iodine', *Appl. Phys. Lett.*, **62** (1993) 1074.

20. M. Yudasaka, K. Hironaga, H. Yamochi, K. Nakamishi and G. Saito, 'Formation of Highly Orientated Thin Films of TTF_7I_5 and their Properties', *Synth. Met.*, **43** (1991) 1527.

CHAPTER SEVEN

OTHER MATERIALS : RESULTS AND DISCUSSION

7.0 Introduction

In this chapter, evaporated films of three related organic materials are reported. Two of these derive from TTF and were chemically synthesised in the Chemistry Department at Durham, while the third is the well-known electron donor (BEDT-TTF), obtained from a commercial source. In each case, doping with iodine resulted in the formation of a charge-transfer compound. The structural, optical and electrical properties of the thin films are presented here.

7.1 Dimethyl-Tetrathiafulvalene

7.1.1 Film Deposition Parameters

Dimethyltetrathiafulvalene (DiMe-TTF), with a melting point of 119-120°C, was provided by the Chemistry Department in Durham and used without further purification. Its molecular formula is given in Figure 7.1. This is the unsymmetrical DiMe-TTF, i.e. the methyl groups are located on the same side of the molecule [1]. A small quantity (35-50 mg) of this was placed in a glass crucible and the temperature raised to 58-60°C. Glass microscope slides of dimensions 25x15 mm^2 were used as substrates. It was found that, as for TTF, no film would deposit if the substrate was kept at ambient temperature, so T_S was set to -10°C for all evaporations attempted. The source-substrate distance was fixed at

13 cm. The vacuum chamber was kept at a pressure of 2.5×10^{-5} mbar during deposition. Film deposition rates were kept between 20 and 30 nm min^{-1} and typical film thicknesses were 0.4-0.9 μm. Chemical doping was achieved by placing the samples in a sealed iodine jar. A reaction between the DiMe-TTF film and iodine was evident, with the colour of the samples changing from light yellow to black over a period of 3-4 min.

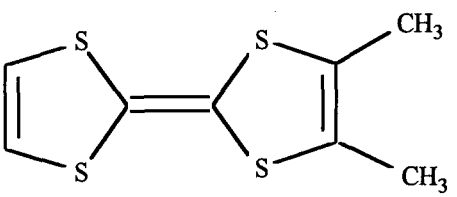

Figure 7.1: Molecular formula of DiMe-TTF.

7.1.2 Film Morphology

The morphology of the thin layers was found to be similar to that of evaporated TTF films. The films were not continuous and uncoated areas could be seen on examination under the optical microscope (Figure 7.2). A polycrystalline structure was revealed and further information was obtained using the SEM. Figure 7.3 compares electron micrographs of the same DiMe-TTF thin film, both before and after doping. A 3-D island growth is evident by the micrographs (Section 3.2.1). The as-deposited films again consisted of two types of structure: dominant needle-type crystals and crystalline plates. After doping, thickness measurements at the same point on the film revealed an irreversible thickness increase (~ 200%). We cannot be sure about the explanation for this phenomenon which has not been reported previously and was not observed for the thin films of TTF. Examined

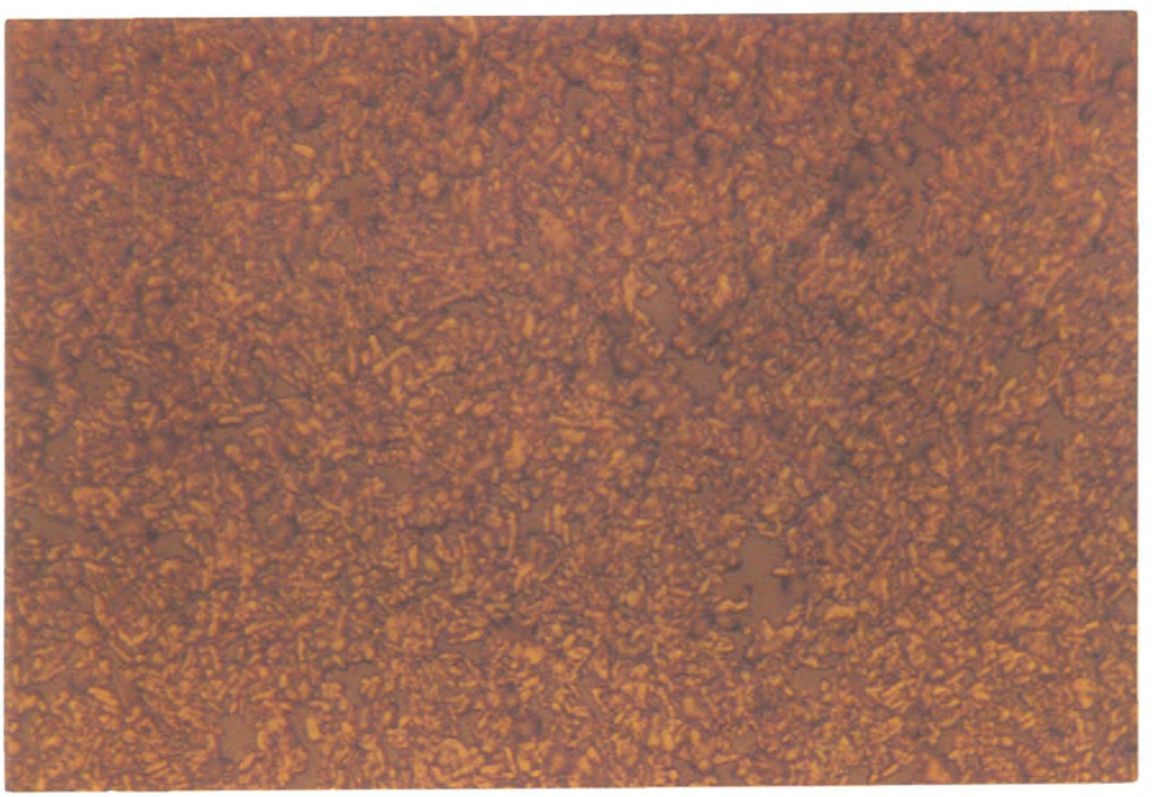

Figure 7.2: Reflection optical micrograph of a 1 μm thick (DiMe-TTF) iodide thin film deposited on a glass slide.

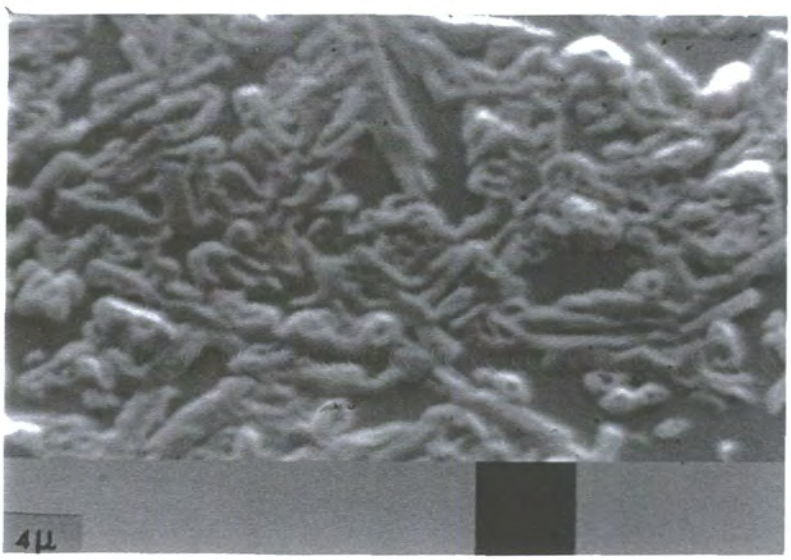

(a)

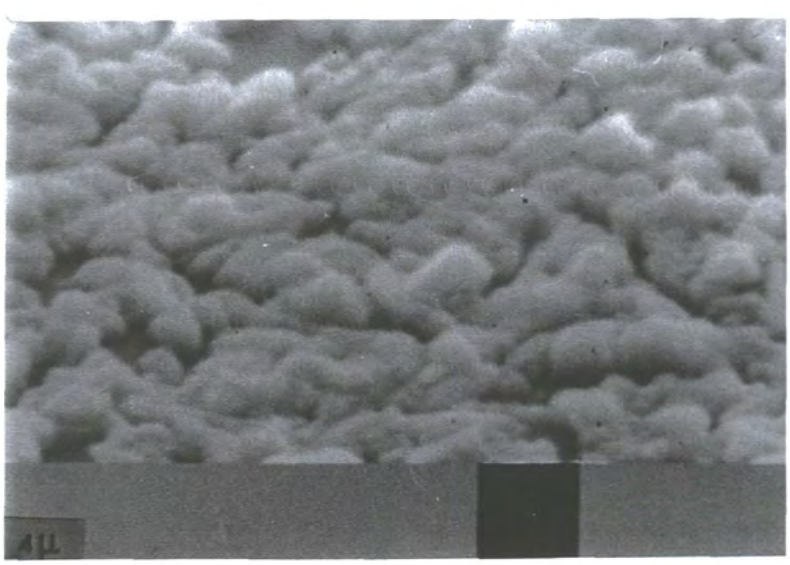

(b)

Figure 7.3: Electron micrographs of a DiMe-TTF evaporated film (a) 0.4 μm thick as-deposited and (b) the same film after iodine doping, now 1 μm thick.

under the SEM, pinholes were still evident in the doped samples but the structure was different. The crystalline plates were now dominant although needle-type crystals could still be seen. A change in crystal orientation was also evident. Such changes in the film morphology upon doping (i.e. from needle to plate-type crystals and the change in crystal orientation) could be a possible explanation for the thickness increase.

The composition of the films was investigated using EDAX analysis. For undoped films, the sulphur peak was dominant while the presence of the iodine in doped samples revealed that chemical doping had been achieved (Figure 7.4). The strong silicon peak originated from the glass substrate.

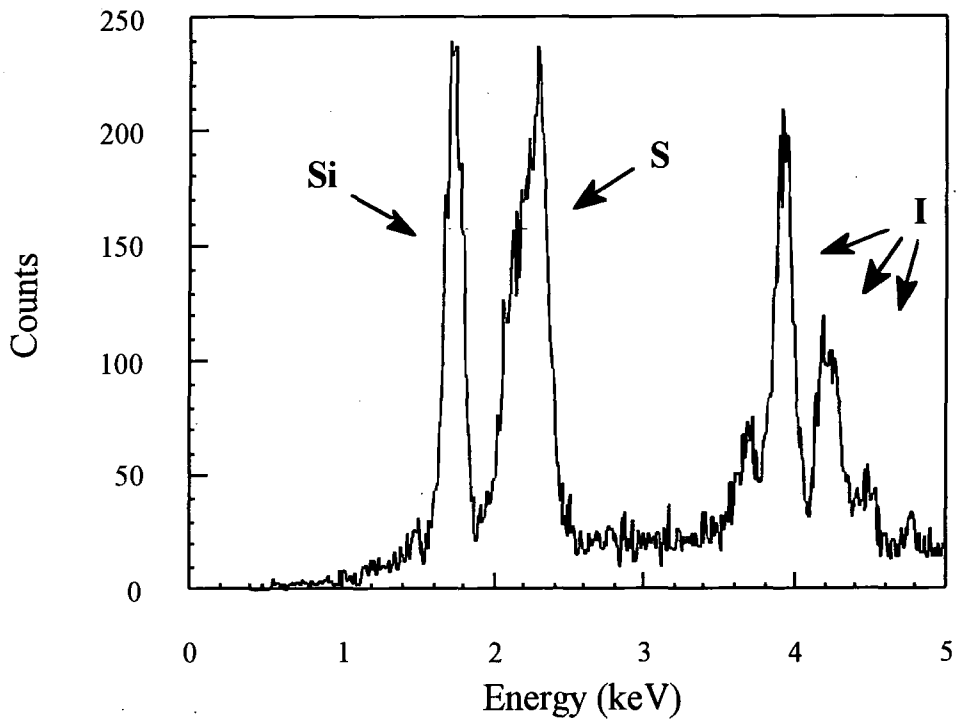

Figure 7.4: EDAX analysis for a 0.9 μm (DiMe-TTF) iodide thin film deposited on a glass substrate.

7.1.3 Optical and Electrical Properties

The substitution of the acidic hydrogen atoms with methyl groups did not change the optical properties markedly. According to Torrance *et al.*, the methyl substitution of the hydrogens results only in a slight decrease in the energy of the low frequency absorption peaks [2]. Figure 7.5 compares optical spectra of a DiMe-TTF thin film, before and after doping. The IR/Visible spectra of the undoped DiMe-TTF thin films were found to be very similar to those of pure TTF evaporated films. Upon doping, the 520 nm band in the as-deposited spectrum is slightly shifted to 570 nm, while a strong band located around 870 nm appeared. The 570 nm band is due to intramolecular transitions of DiMe-$TTF^{+\cdot}$ [2]. The absorption at 870 nm has been reported before for TTF salts and has been attributed to intermolecular charge-transfer between $TTF^{+\cdot}$ molecules within a stack [2-4]. No other bands were observed in the infrared region, suggesting that the compound was in the full charge-transfer state. Therefore, only intermolecular transitions of the type

$$\text{DiMe-TTF}^{+\cdot} + \text{DiMe-TTF}^{+\cdot} \rightarrow \text{DiMe-TTF}^{2+} + \text{DiMe-TTF}^{0}$$

are possible.

For TTF-halide salts, the composition directly and unambiguously defines the extent of oxidation of the TTF chains, and therefore the degree of charge-transfer, ρ [2]. This is because the halogen, with its large electron affinity, is always crystallographically present as X^-. However, for some iodine salts, ρ can be lowered through the formation of I_3^-, i.e.

$$2TTF^{+} + 3I^{-} \rightarrow 2TTF^{0} + I_3^{-}$$

The in-plane, dc room temperature conductivity of the undoped samples was difficult to measure reliably. For all iodine doped samples examined, the current versus voltage characteristics were linear, suggesting ohmic behaviour (Figure 7.6). An increase in

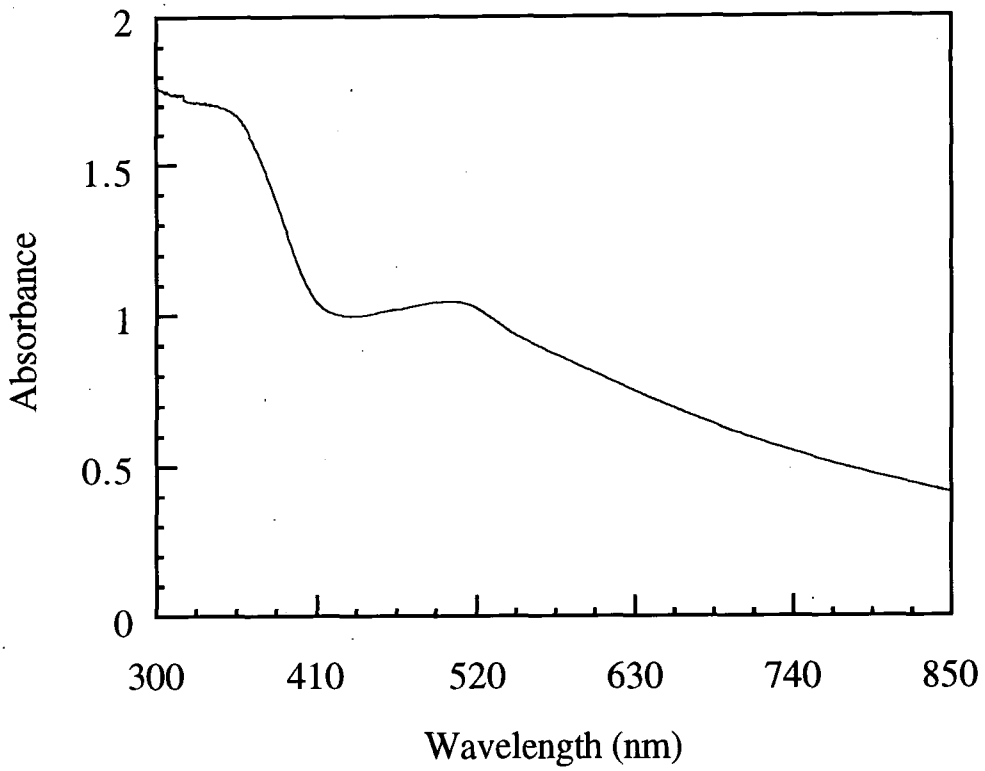

(a)

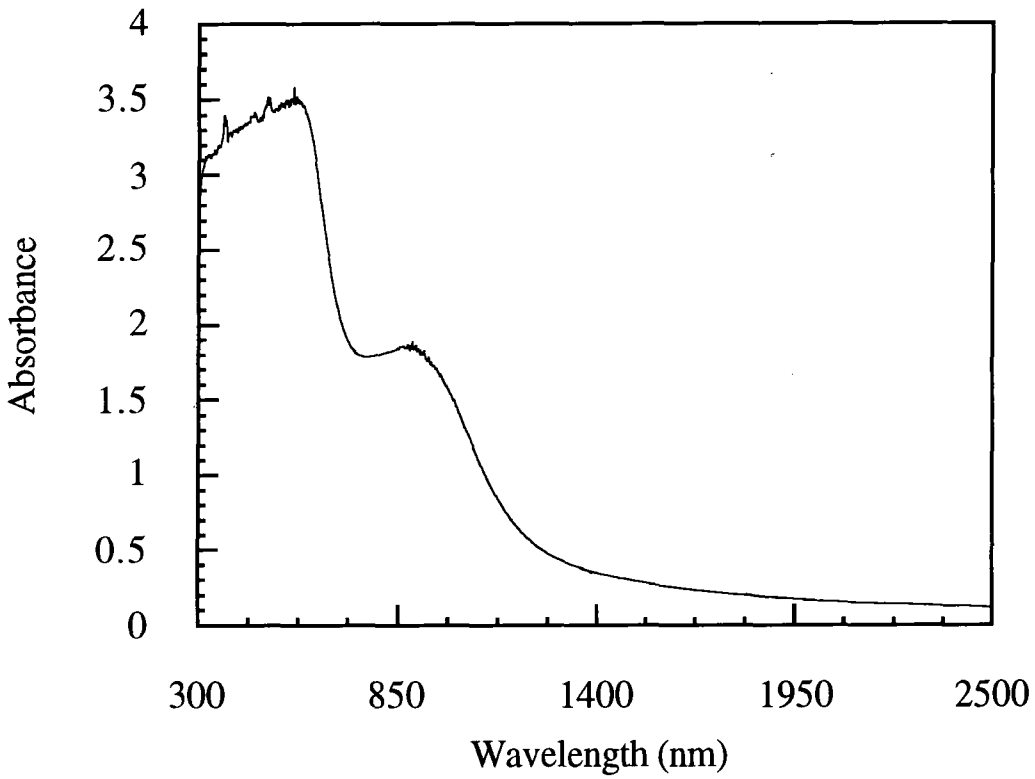

(b)

Figure 7.5: Optical spectra of a DiMe-TTF evaporated thin film deposited on a glass substrate (a) 0.4 μm thick as-deposited and (b) the same film after iodine doping, now 1 μm thick.

conductivity was observed after iodine doping. The highest value achieved was 10^{-4} S cm^{-1}. However, this decreased over a period of two hours to a final steady state of 10^{-6} S cm^{-1}. This low value of conductivity, compared to the (TTF) iodide evaporated thin films, is not inconsistent with previous results. Studies on (TTF) X_ρ where X is halide, show that these materials can be crystallised with a variety of values for ρ. If $\rho = 1$, charge-transfer is complete and, in this case, the TTF molecules are fully oxidised and the compound is an insulator, in complete agreement with the results presented here. If $\rho < 1$, charge-transfer is incomplete, hence the TTF molecules are only partially oxidised and the stack is of mixed valence type (Section 2.1.1). For example, for (TTF)Br and (TTF)$Br_{0.71-0.76}$, the difference in the room temperature conductivity is six orders of magnitude [3]. The same behaviour has also been reported in salts of TCNQ where the difference in conductivity can be as large as ten orders of magnitude [5].

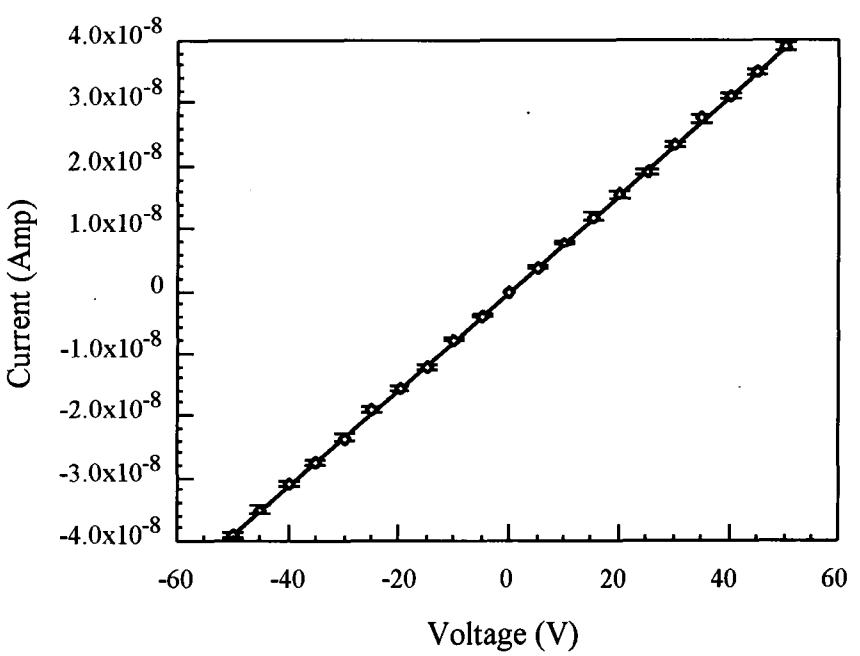

Figure 7.6: In-plane, dc room temperature current versus voltage characteristic for a 0.8 μm thick (DiMe-TTF) iodide thin film.

7.2 Trimethyl-Tetrathiafulvalene

7.2.1 Film Deposition Parameters

Trimethyltetrathiafulvalene (TriMe-TTF), with a melting point of 103-104°C, was provided by the Chemistry Department in Durham and used without further purification. Its molecular formula is shown in Figure 7.7. A small quantity (35-50 mg) was placed in a glass crucible whose temperature was raised to 55-60°C. Glass microscope slides, of dimensions 25x15 mm^2, were used as substrates. As for TTF and DiMe-TTF, T_S was set to -10°C for all the evaporations. The vacuum chamber was kept at a pressure of $2.5x10^{-5}$ mbar and the source-substrate distance was 13 cm. Deposition rates were maintained between 20 and 30 nm min^{-1} and a typical thickness of the obtained films was 0.7 μm. After exposure to iodine vapour over a period of 3-4 min, chemical doping was evident by a marked change of colour, from light yellow to black.

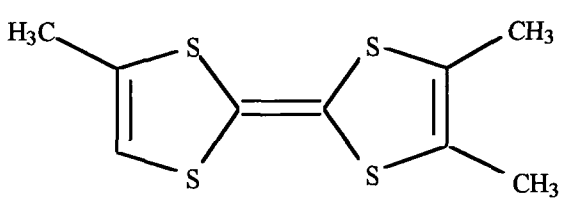

Figure 7.7: Molecular formula of TriMe-TTF

7.2.2 Film Morphology

The adherence of the material onto glass was found to be very poor in comparison to DiMe-TTF and TTF layers. The difference in film quality between DiMe-TTF and TriMe-TTF could be seen using optical microscopy where, for TriMe-TTF, uncoated substrate areas were larger and more abundant (Figure 7.8). Figure 7.9 compares electron micrographs

Figure 7.8: Transmission optical micrograph of a 1 μm thick (TriMe-TTF) iodide thin film deposited on a glass substrate.

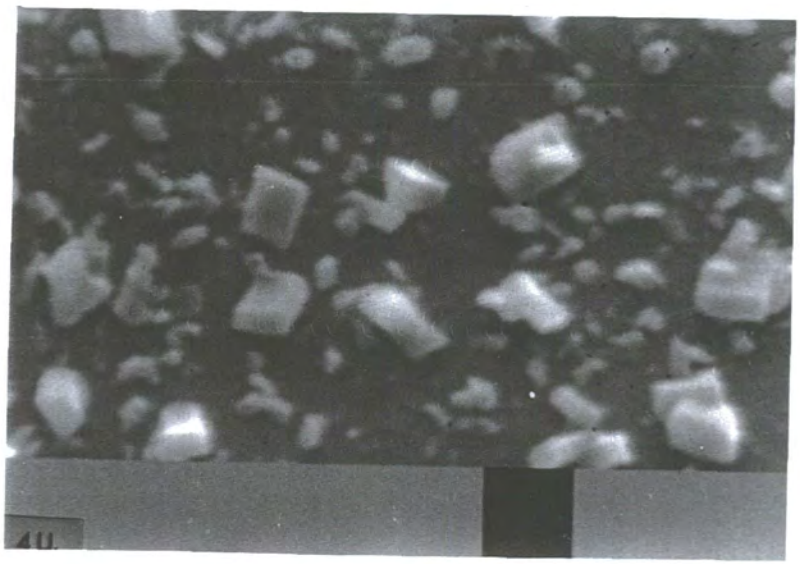

→ ←
4 μm

(a)

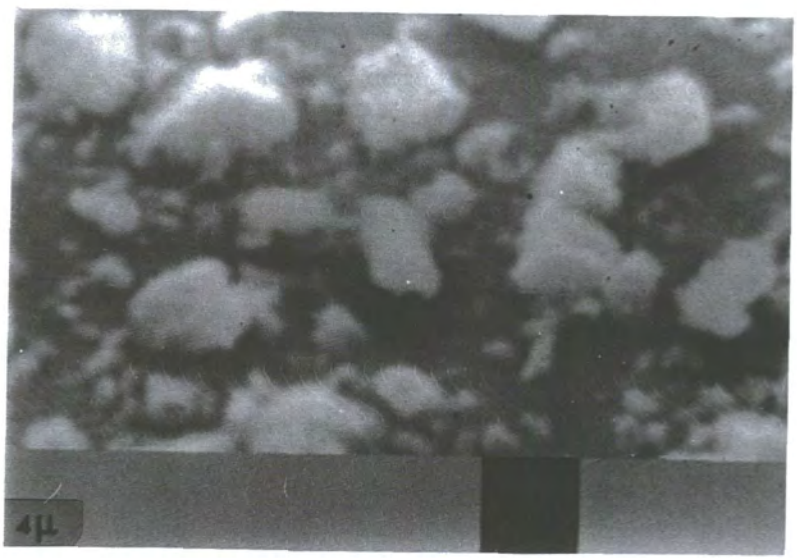

(b)

Figure 7.9: Electron micrographs of a TriMe-TTF evaporated film (a) 0.5μm thick as-deposited and (b) the same film after iodine doping, now 1 μm thick.

of an evaporated TriMe-TTF thin film, both before and after doping. Scanning electron microscopy revealed that the growth proceeded in the 3-D island growth mode (Section 3.2.1). The as-deposited film was hardly continuous, with crystalline plates scattered randomly over the substrate. Upon doping, an irreversible increase in thickness (~ 200%) was observed, as for DiMe-TTF. The films still consisted of crystalline plates, but these were now larger, accounting for the change in film thickness.

Figure 7.10 shows the results of EDAX analysis on a doped film. Again, the relative intensity of the iodine peak is high, consistent with data for (DiMe-TTF) iodide films. The strong silicon peak originates from the glass substrate.

7.2.3 Optical and Electrical Properties

The optical absorption spectra for the undoped TriMe-TTF evaporated thin films were identical to those of DiMe-TTF and pure TTF films, and also to the spectrum of this material in solution [6]. The optical spectra of the doped samples in the visible region were also the same as those of (TTF) iodide. In Figure 7.11, bands around 300 nm, 380 nm and 500 nm were present and, as noted before, were attributed to intramolecular transitions between TriMe-$TTF^{+\cdot}$ molecules. The full charge-transfer band appeared around 870 nm (as for DiMe-TTF).

The dc room temperature conductivity of the undoped samples could not be measured, suggesting insulating behaviour. After doping, an increase in conductivity was observed but, as the optical spectra suggested, full charge-transfer was taking place between the donor and acceptor molecules and electron conduction was only possible at the expense of a large Coulombic repulsion energy (between two electrons in the same molecule). Ohmic behaviour was found in all the doped samples examined. Following doping, the highest value

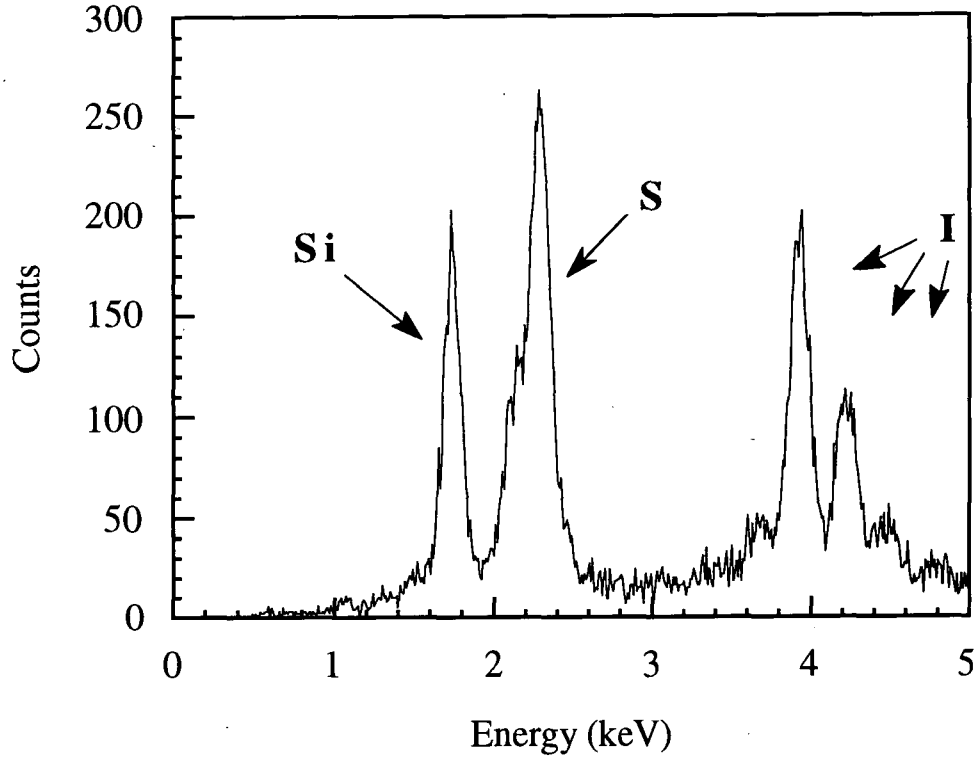

Figure 7.10: EDAX analysis for a 1 μm thick (TriMe-TTF) iodide thin film.

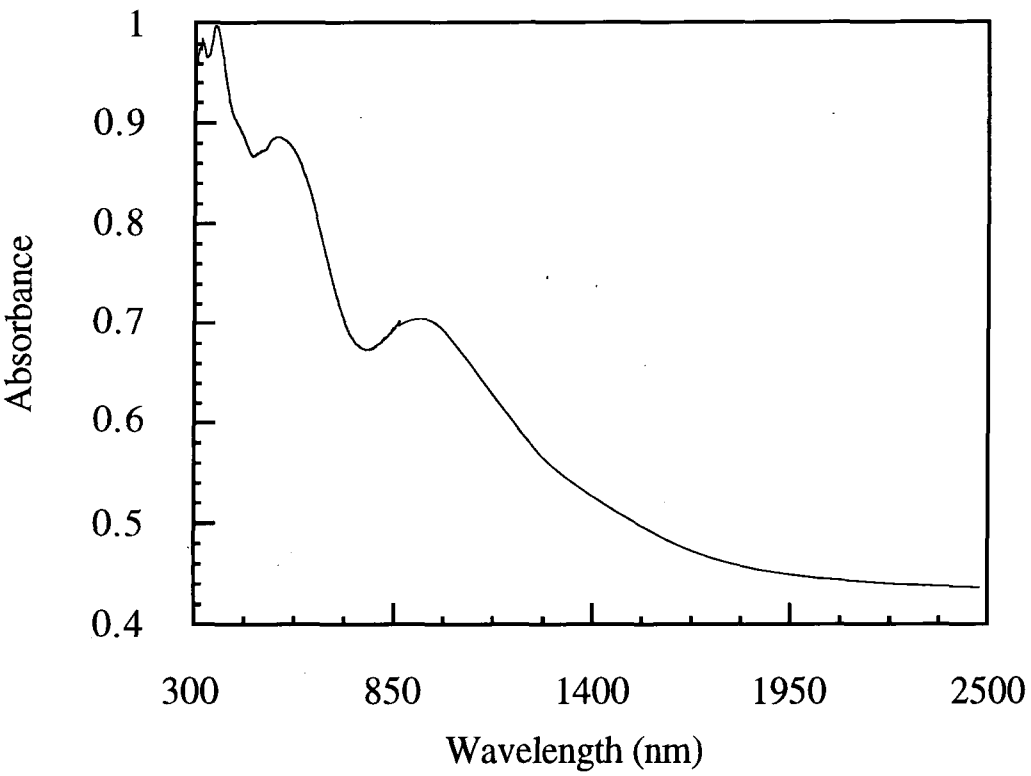

Figure 7.11: Optical spectrum of a 1 μm thick (TriMe-TTF) iodide thin film.

of the dc room temperature conductivity observed was 10^{-6} S cm^{-1}. However, this decreased over a period of 2 hours to a final steady state of 10^{-7} S cm^{-1}.

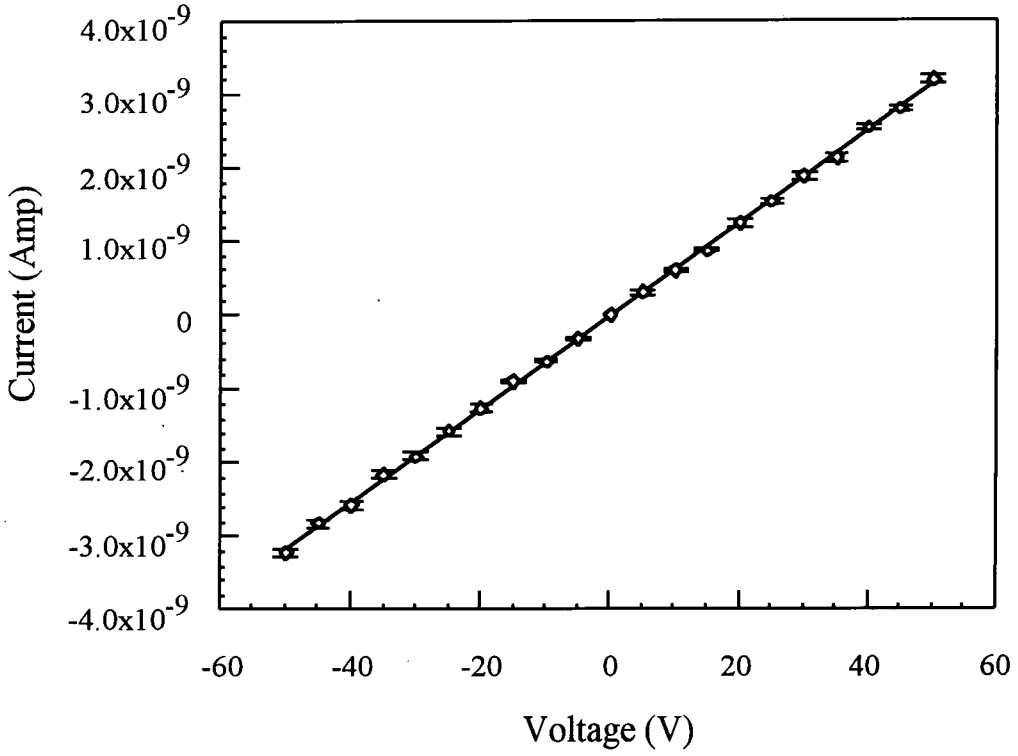

Figure 7.12: In-plane, dc room temperature current versus voltage characteristic for a 1.1 μm (TriMe-TTF) iodide thin film.

7.3 BEDT-TTF

7.3.1 Film Deposition Parameters

BEDT-TTF (ET), 98% pure and with a melting point of 244°C, was purchased from Aldrich and used without further purification. Its molecular formula is shown in Figure 7.13. A small quantity (35-50 mg) was placed in a glass crucible and the temperature raised to 110-120°C. Glass microscope slides of dimensions 25x15 mm^2 were used as substrates. It was found that ET would deposit on substrates which were kept at ambient temperature, so

T_S was set at 25°C. The temperature at which evaporation commenced was determined experimentally as 105°C. However, the deposition rate was very low and adhesion of the ET on the glass substrate was poor, in comparison with the other materials examined. The source temperature was therefore raised above 105°C and the source-substrate distance was fixed at 6 cm. Films prepared with deposition rates 60-75 nm min^{-1} and thicknesses ranging between 0.3-0.6 μm were obtained. The chamber was evacuated to $2.5x10^{-5}$ mbar during deposition. The samples were doped with iodine and were annealed in air at 60°C.

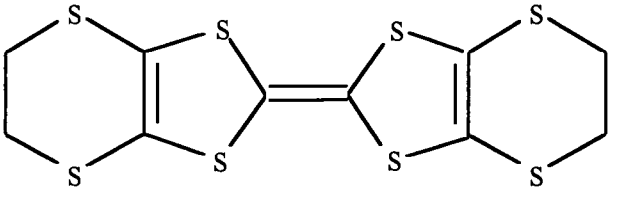

Figure 7.13: Molecular formula of BEDT-TTF.

7.3.2 Film Morphology

The structure of the ET films was polycrystalline and was similar to that of TTF. For the as-deposited films, needle-type crystals and crystalline plates were both present [Figure 7.14(a)]. Larger crystalline plates (large areas), identified by EDAX analysis, were also evident. Compared to evaporated films of other materials, reported in this chapter earlier, the general crystal size was very small and, perhaps for this reason, no significant uncoated areas were evident. After exposing the films to iodine vapour for a period of 3-4 min, the colour of the samples changed from light yellow to a pearl-like colour. The film morphology, revealed by the SEM, appeared unchanged. After annealing in air at 60°C for 35 min, the

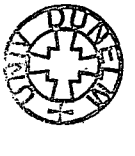

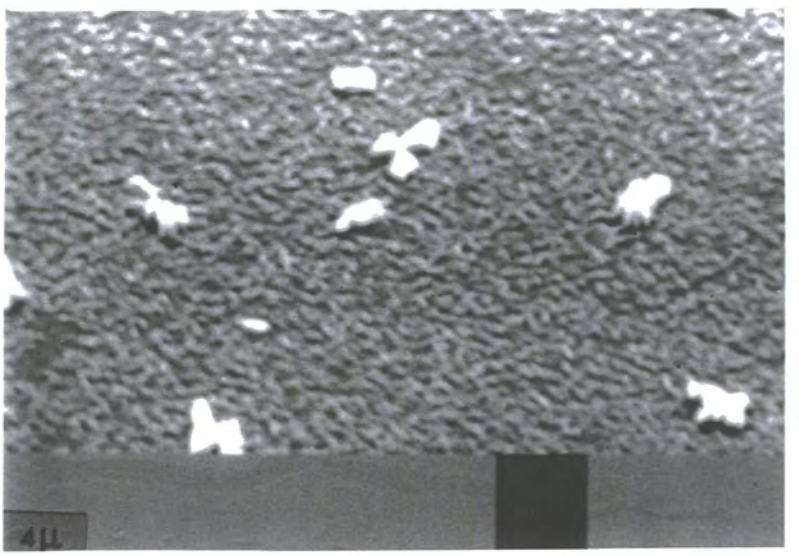

→ ←
4 μm

(a)

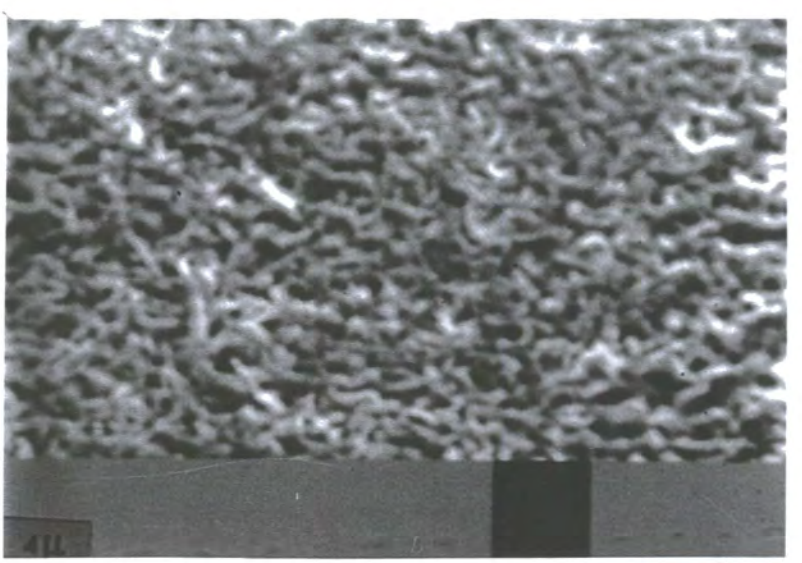

(b)

Figure 7.14: Electron micrographs of a 400 nm thick (BEDT-TTF) evaporated film, (a) as-deposited and (b) the same film after doping and annealing in 60°C for 35 min.

structure was examined again. The doped-annealed samples were also polycrystalline and consisted of both needle-type and crystalline plates. A plate-like morphology has been observed before for evaporated films of the (BEDT-TTF) iodide [7]. No difference in thickness upon doping or annealing was observed. Figure 7.14 compares electron micrographs of an as-deposited (BEDT-TTF) thin film and a doped and annealed at 60°C film of (BEDT-TTF) iodide. The results of EDAX analysis on an annealed sample can be seen in Figure 7.15. Note the low level of iodine present in the film; this will be discussed later in this chapter. The strong silicon peak originates from the glass substrate.

7.3.3 Infrared/Visible Spectroscopy

The samples were characterised using optical spectroscopy. Figure 7.16 compares optical spectra of a 500 nm thick (BEDT-TTF) thin film, as-deposited, doped and doped and annealed in air at 60°C for 35 min. The spectra of the as-deposited samples exhibited no strong absorption peaks. Broad shoulders observed at 400, 450 and 500 nm resembled those of pure TTF. In this spectral region, only intramolecular transitions of the ET molecules are anticipated. Upon doping, a 400 nm band in the optical region became evident while a very broad band around 1000 nm appeared. Goldenberg *et al.* have also observed the former band in (BEDT-TTF) iodide films prepared by the Langmuir-Blodgett technique [8]. The very broad absorption at 1000 nm extends from 800 nm to 1400 nm and consists of two main bands: at 850 nm and 1300 nm. The former is also observed for doped thin films of TTF, DiMe-TTF and TriMe-TTF and has been attributed to the full charge-transfer between the donor ET and the acceptor iodine molecules. Transitions of the sort

$$\text{BEDT-TTF}^{+\cdot} + \text{BEDT-TTF}^{+\cdot} \rightarrow \text{BEDT-TTF}^{2+} + \text{BEDT-TTF}^{0}$$

are responsible for this absorption.

The band at approximately 1300 nm is considered to be a charge-transfer band, revealing the mixed valence state of a CT salt. It is attributed to intermolecular transitions between the ion radicals of the kind

$$BEDT\text{-}TTF^{+\cdot} + BEDT\text{-}TTF^{0} \rightarrow BEDT\text{-}TTF^{0} + BEDT\text{-}TTF^{+\cdot}$$

(TTF) iodide thin films, prepared both with the single and co-evaporation technique, have exhibited a similar absorption but at higher wavelengths (1400 - 2500 nm).

After annealing the sample for 35 min at the above temperature, the band around 850 nm retains its intensity but the mixed-valence around 1300 nm has diminished. No other band is observed in the near infra-red region.

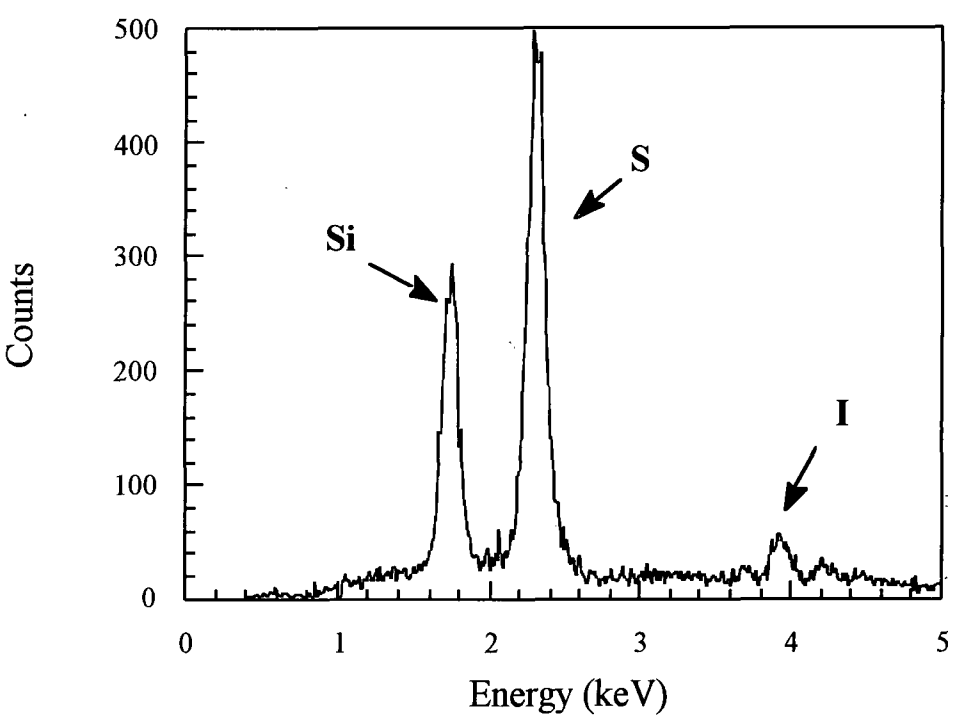

Figure 7.15: EDAX analysis on a 400 nm thick (BEDT-TTF) iodide film on a glass substrate, annealed in air at 60°C for 35 min.

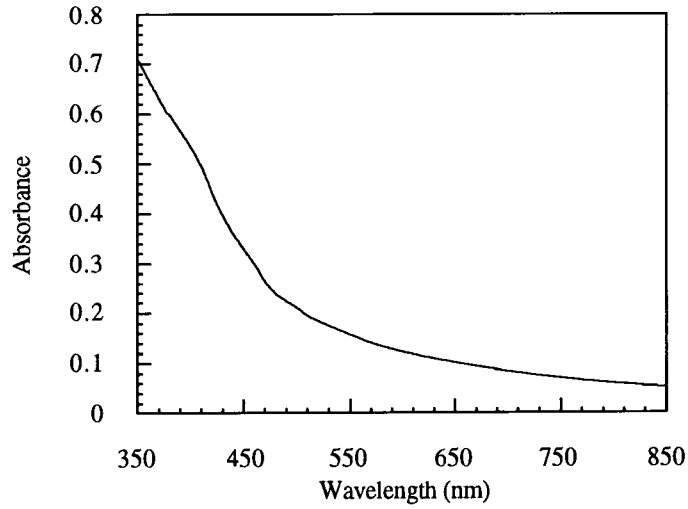

(a)

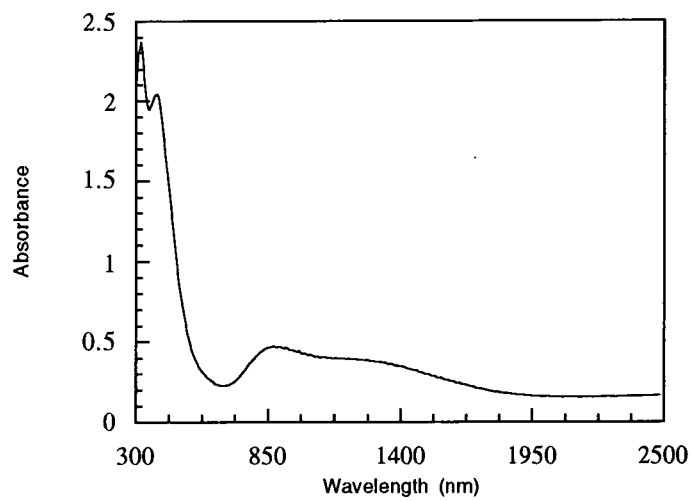

(b)

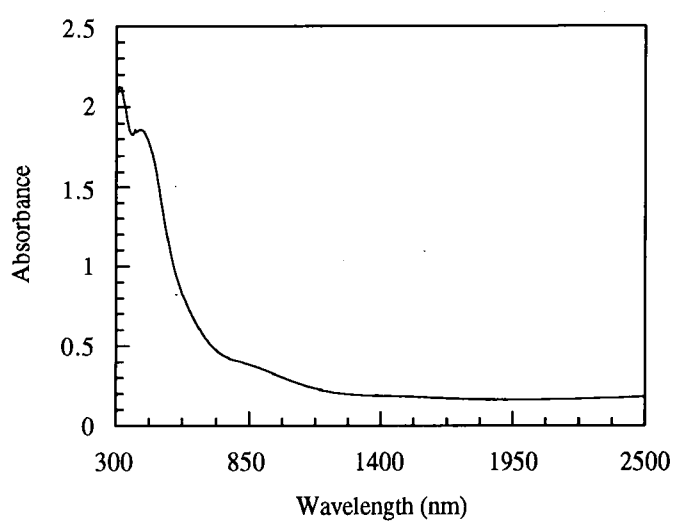

(c)

Figure 7.16: Optical spectra for a 500 nm thick (BEDT-TTF) iodide film, (a) as-deposited, (b) after doping and (c) after doping and annealing in air at 60^{o}C for 35min.

7.3.4 Electrical Properties

The as-deposited samples exhibited insulating behaviour, their conductivity was comparable to that of the glass substrate. After exposure to iodine vapour, a conductive material was formed. Ohmic behaviour was exhibited (Figure 7.17) and the dc room conductivity observed was in the range (0.5-1.1) 10^{-3} S cm^{-1}. Doped samples were annealed in air at 60°C. The change in dc room temperature conductivity with annealing time, is shown in Figure 7.18. As evident from the graph, the optimum annealing time was 35 min, giving a maximum room temperature conductivity of 1.6±0.6 S cm^{-1}. Annealing for longer times produced a reduction in the conductivity, eventually reaching the level noted in the

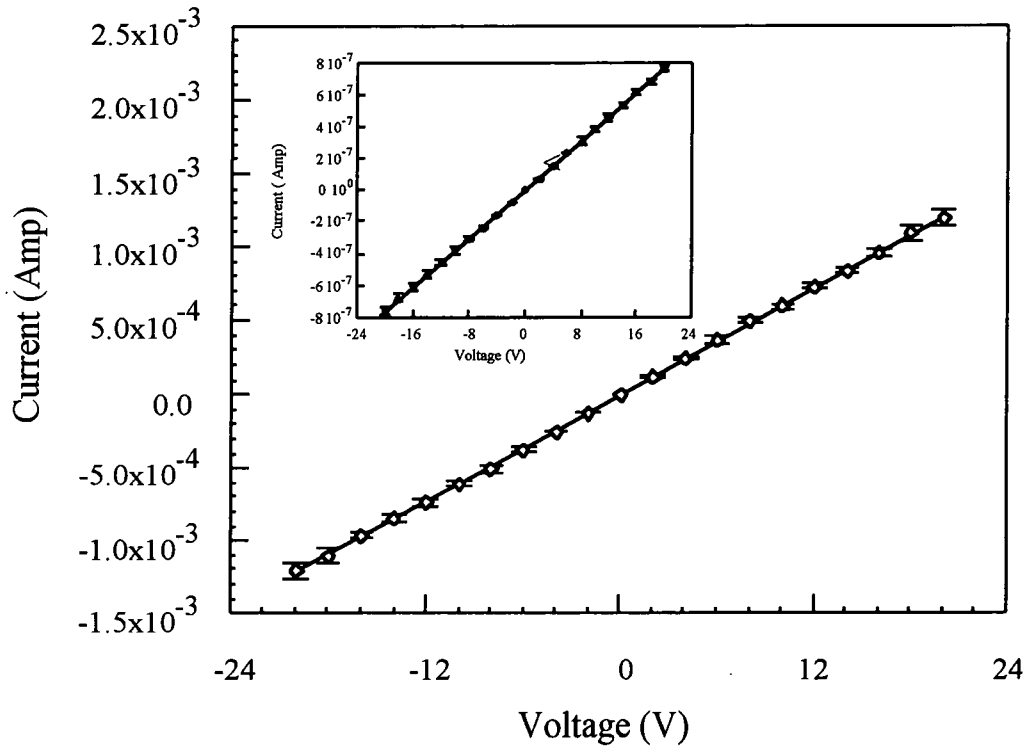

Figure 7.17: In-plane, dc room temperature current versus voltage characteristic for a 400 nm annealed (BEDT-TTF) iodide thin film. In the inset, the I-V characteristic for the same film after doping but before annealing is shown.

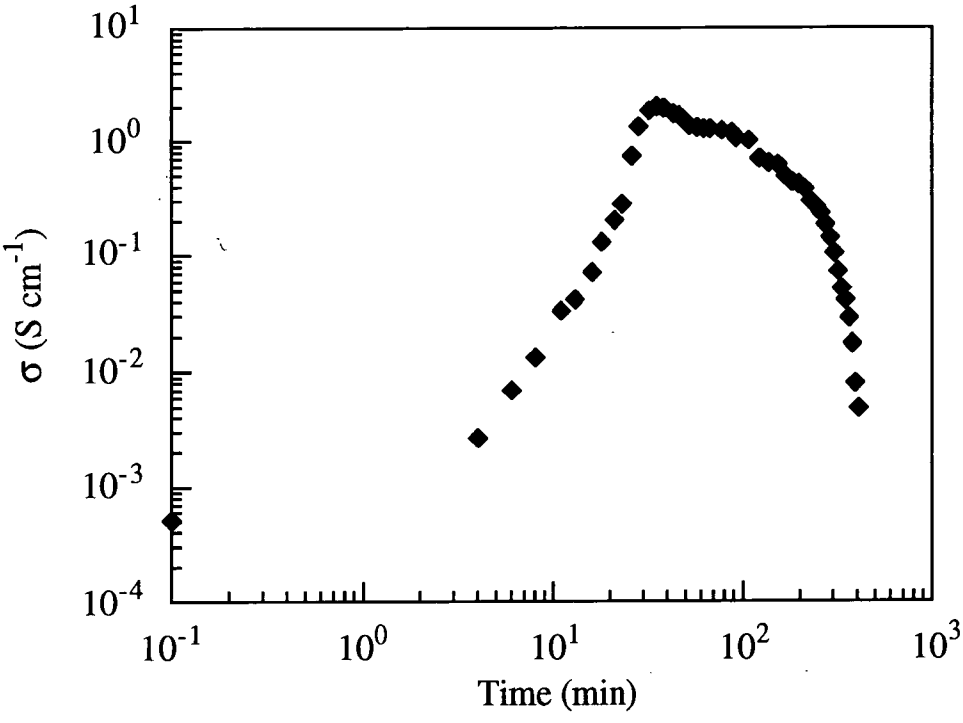

Figure 7.18: In-plane, dc conductivity at 60°C versus annealing time for a 400 nm thick (BEDT-TTF) iodine thin film.

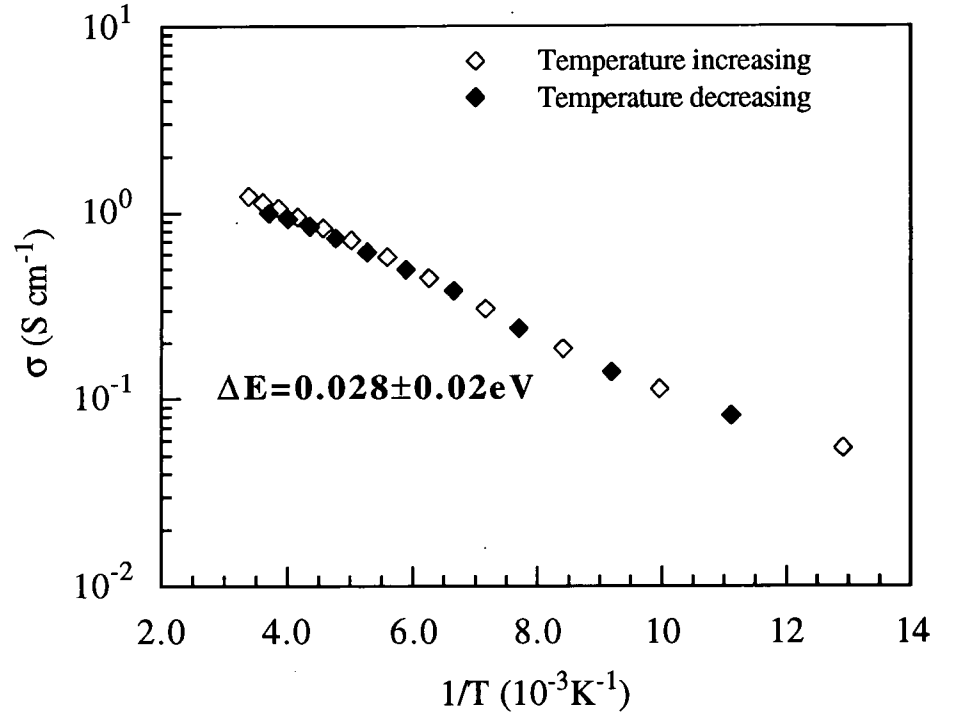

Figure 7.19: In-plane, dc conductivity versus temperature for a 400 nm thick annealed (BEDT-TTF) iodide thin film.

as-deposited films. Subsequent EDAX analysis revealed that all the iodine content had left the film. For the sake of simplicity we will refer to these films as insulating-annealed from now. If the insulating-annealed films were re-doped and also annealed at 60°C again, the electrical behaviour varied. Some of the samples became quite insulating, while others became conductive but not as highly as before. Thus, the same film, as-deposited and after becoming insulating-annealed (at both stages consisting only of BEDT-TTF molecules) behaves differently after doping and annealing in air at 60°C for 35 min. This may simply be a result of a different crystallographic form for the as-deposited and insulating-annealed films.

The temperature dependence of the dc conductivity of the annealed films was weakly semiconducting in nature, a single activation energy of 0.028±0.002 eV was measured. From the shape of the curve in Figure 7.19, the possibility of annealed films consisting of the α-phase can be excluded, as the sharp decrease in the temperature dependence of the conductivity of the α-phase (BEDT-TTF) iodide around 140°K was not observed here [9]. The dc conductivity of the annealed films was monitored for a period of 60 days and was found to be stable.

(BEDT-TTF) iodide is known to crystallise in numerous phases [10, see also Section 2.4]. Thin films of (BEDT-TTF) iodide have been produced previously by thermal evaporation but using crystals of (BEDT-TTF) iodide as the starting material [7,11-13]. Kawabata *et al.* showed that, depending on the substrate temperature, different phases- amorphous, α-, β- and α_t- (by annealing the α-phase [14])- can be obtained. In this work, the means to determine the exact phase of our evaporated films were not available. However, we can speculate by comparison the properties of our films with those of

Kawabata's. Our doped films exhibit a conductivity value of three orders of magnitude (10^{-3} S cm^{-1}) lower than that of Kawabata's α-phase (1 S cm^{-1}, obtained as-deposited). For our annealed films, the conductivity is similar to that of Kawabata's β- or α_t-phase. However, there is significant difference in the activation energy value (for our annealed films ΔE = 0.028 eV and for Kawabata's β- and α_t-phase ΔE =0.017 eV). The fact that heat treatment can result in complete evaporation of iodine has also been reported in Kawabata's films, but for temperatures above 100°C. It is possible that our films follow a similar pattern: the doped films consisting of the α-phase and the annealed layers of the α_t-phase.

On the other hand, the following explanation is also plausible: it has been found that on heating phases with large iodine content, i.e. ε and ζ, iodine is readily lost with conversion to β-ET_2I_3 [10, 15]. It has to be noted here that the α- and β- phases are those containing least iodine. If our evaporated doped samples consisted of the ε- or ζ- phase, then heat treatment might result in the above phase transition. This could also explain the low iodine level at Figure 7.15. For single crystals, longer annealing times (~4h) at temperatures higher that 60°C (100°C) are needed for this structural change.

7.4 Summary

Thin films have been prepared of three materials. (DiMe-TTF) iodide and (TriMe-TTF) iodide proved to be very poor electrical conductors with values of dc conductivity in the range of 10^{-6} S cm^{-1} to 10^{-7} S cm^{-1}. Both salts are compounds in which full charge-transfer occurs between the acceptor and donor molecules, making electron conduction difficult. This could arise from the stronger donor abilities of DiMe-TTF and TriMe-TTF [6,

Section 2.3] compared to TTF and ET. Furthermore, the quality of the thin films was found to be very poor, with no uniformity and large uncoated areas.

Conductive films of (BEDT-TTF) iodide (maximum σ = 1.6 S cm^{-1}) were obtained by doping the as-deposited samples and subjecting the latter to specific heat treatment. Their activation energy was found to be almost double of that reported for β- and α_t- (BEDT-TTF)$_2I_3$. Further work is needed to identify fully the crystallographic structure of our thin layers.

References

1. F. Wudl, A.A. Kruger, M.L. Kaplan, R.S. Hutton, 'Unsymmetrical Dimethyltetrathiafulvalene', *J. Org. Chem.*, **42** (1977) 768.
2. J.B. Torrance, B.A. Scott, B. Welber, F.B. Kaufman and P.E. Seiden, 'Optical Properties of the Radical Cation Tetrathiafulvalenium (TTF^+) in Its Mixed-Valence and Monovalence Halide Salts', *Phys. Rev. B.*, **19** (1979) 730.
3. B.A. Scott, S.J. La Placa, J.B. Torrance, B.D. Silverman and B. Welber, 'The Crystal Chemistry of Organic Metals. Composition, Structure and Stability in the Tetrathiafulvalinium-Halide systems', *J. Am. Soc.*, **99** (1977) 6631.
4. T. Sugano, K. Yakushi and H. Kuroda, 'Polarized Absorption Spectra of Single Crystals of Tetrathiafulvalenium Salts', *Bull. Chem. Soc. Jap.*, **51** (1978) 1041.
5. J.B. Torrance, 'The Difference Between Metallic and Insulating Salts of Tetracyanoquinodimethane (TCNQ): How to design an Organic Metal', *Acc. Chem. Res.*, **12** (1979) 79.
6. A.J. Moore, M.R. Bryce, A.S. Batsanov, J.C. Cole, J.A.K. Howard, 'Functionalised Trimethyltetrathiafulvalene (TriMe-TTF) Derivatives via Reactions of Trimethyltetrathiafulvalenyllithium with Electrophiles: X-ray Crystal Structures of Benzoyl-TriMe-TTF and Benzoylthio-TriMe-TTF', *Synthesis*, **6** (1995) 675.
7. K. Kawabata, T. Tanaka and M. Mizutani, 'Conducting Thin Films of α-(BEDT-TTF)$_2I_3$ by Evaporation Method', *Sol. Stat. Comm.*, **74** (1990) 83.
8. L. Goldenberg *et al.*, unpublished data.
9. E.B. Yagubskii, I.F. Shchegolev, V.N. Laukhin, R.P. Shibaeva, E.E. Kostyuchenko, A.G. Khomenko, Yu. V. Shusko and A.V. Zvarykina, 'Superconducting Transition in the Dielectric α-phase of Iodine-Doped (BEDT-TTF)$_2I_3$ Compound', *JETP Lett.*, **40** (1984) 1201.

10. E.B. Yagubskii and R.P. Shibaeva, 'Organic Conductors and Superconductors Based on Bis(ethylenedithio) Tetrathiafulvalene and its Derivatives', *J. Molec. Electr.*, **5** (1989) 25.

11. K. Kawabata, T. Tanaka and M. Mizutani, 'Superconducting Thin Films of (BEDT-TTF) iodide', *Synth. Met.*, **39** (1990) 191.

12. K. Kawabata, T. Tanaka and M. Mizutani, 'Superconducting Organic Thin Films Prepared using an Evaporation Technique', *Adv. Mater.*, **3** (1990) 157.

13. K. Kawabata, T. Tanaka and M. Mizutani, 'Thin Films of (BEDT-TTF)iodide Prepared by Evaporation Method', *Synth. Met.*, **41-43** (1991) 2097.

14. G.O Baram, L.I. Buravov, L.S. Degtyarev, M.E. Kozlov, V.N. Laukhin, E.E. Laukhina, V.G. Onishchenko, K.I. Pokhodnya, M.K. Sheinkman, R.P. Shibaeva and E.B. Yagubskii, 'Transformation of the α-phase $(BEDT\text{-}TTF)_2I_3$ to the Superconducting β Phase with T_c = 6-7 K', *JETP Lett.*, **44** (1986) 376.

15. V.A Merzhanov, E.E Kostyuchenko, V.N. Laukhin, R.M. Lobkovskaya, M.K. Makova, R.P. Shibaeva, I.F. Shchegolev and E.B. Yabuskii, 'An Increase in the Superconducting-Transition Temperature of β-$(BEDT\text{-}TTF)_2I_3$ to 6-7 K at a Normal Pressure', *JETP Lett.*, **41** (1985) 179.

CHAPTER EIGHT

THIN FILMS TRANSISTORS: RESULTS AND DISCUSSION

8.0 Introduction

In this chapter, the fabrication and characterisation of thin film transistors (TFTs) using an organic evaporated film as the active semiconducting layer are reported. TTF and BEDT-TTF evaporated layers were used. The electrical behaviour of these TFTs was examined with organic layers both in the as-deposited state and the after doping with iodine.

8.1 Thin Film Transistor Model

The most widely used field-effect transistor (FET) is the metal-insulator-semiconductor FET (MISFET) [1]. Silicon MISFET's are also known as MOSFETs, because their insulating layer is a thermally grown silicon oxide film. A schematic view of the a conventional MOSFET structure is given in Figure 8.1(a). The source and drain contacts each form a p-n junction with the silicon substrate. If a sufficient and properly polarised gate voltage V_G is applied to the gate contact, the bands at the semiconductor/insulator interface can bend to form an inversion layer (an n-type surface layer on an p-type substrate or the inverse). This layer establishes a conductive channel between the source and the drain. A conventional MOSFET is therefore a minority carrier device, i.e. a device where the current is carried by holes for an n-type semiconductor and by electrons for p-type. From capacitance-voltage measurements on organic MOS diodes, no evidence for formation of an

inversion regime has yet been reported [2-4]. Because of this, organic MOSFETs operate by the formation of an accumulation layer. The basic equations are derived below [5-7].

An ideal MOS diode is defined as follows [1]:

(i) At zero applied bias, the energy difference between the metal work function and the semiconductor work function is zero. (The work function is defined as the energy required to remove an electron from the Fermi level to a position just outside the material (vacuum level).) In other words, the energy bands are flat (flat-band condition) when there is no applied voltage.

(ii) The only charges that exist in the diode under any biasing conditions are those in the semiconductor and those with equal but opposite sign on the metal surface adjacent to the oxide.

(iii) There is no carrier transport through the oxide under any biasing conditions, i.e. the resistivity of the oxide is infinite.

A schematic view of TFT is shown in Figure 8.1(b). The x-axis is directed from the source-drain channel to the gate, and the y-axis from the source to the drain. The total charge per unit area induced by the gate voltage at a distance y from the source is given by

$$Q_s(y) = - [V_G - \psi_s(y)] C_i \qquad (8.1)$$

where $\psi_s(y)$ is the surface potential and C_i the insulator capacitance per unit area. In the case of accumulation, there is no depletion region and the total surface charge is located in the accumulation layer. We shall assume that

$$\psi_s(y) = V(y) + V_o \qquad (8.2)$$

where $V(y)$ is the bias between point y and the source (assumed to be grounded) and V_o is a constant which is explained later in this section. The channel conductance g is then given by

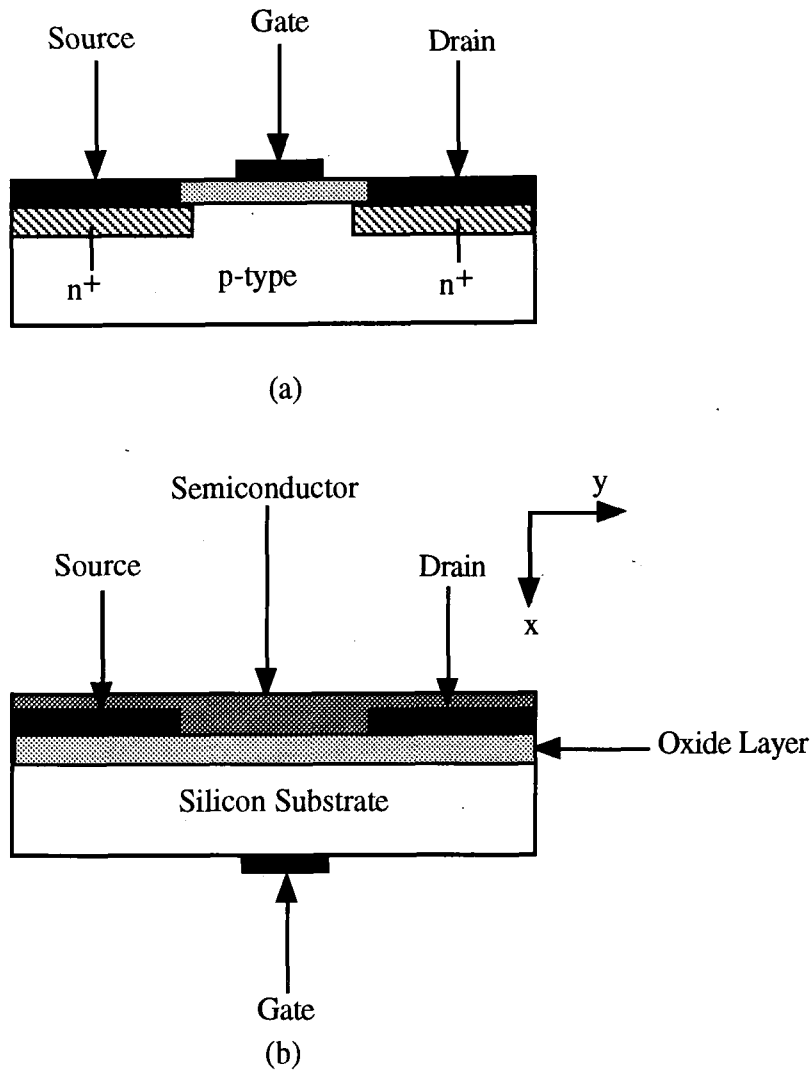

Figure 8.1: Schematic view of the structure of a) a MOSFET device and b) a thin film transistor.

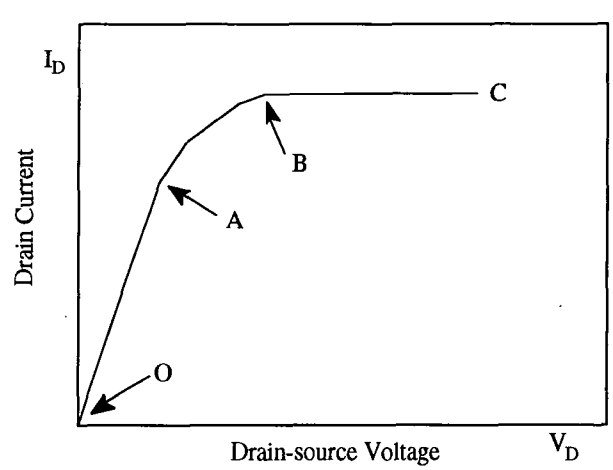

Figure 8.2: A typical drain current versus drain-source voltage curve for a TFT.

$$g = \int_0^{x_a} \sigma(x)\, dx, \tag{8.3}$$

where x_a is the thickness of the accumulation layer. If we assume a constant mobility μ in the accumulation layer, we obtain

$$g = qZ\mu \, |Q_s(y)| / L \tag{8.4}$$

q is the absolute electron charge and Z and L are the channel width and length, respectively. The resistance dR of an elemental section dy is given by

$$dR = \frac{dy}{gL} = \frac{dy}{[Z\mu Q_s(y)]} \tag{8.5}$$

and the voltage drop across this elemental section by

$$dV = I_D dR = \frac{I_D dy}{[Z\mu Q_s(y)]} \tag{8.6}$$

where I_D is the current flowing between the source and the drain. Substituting Eqs. (8.1) and (8.2) into Eq. (8.6) and integrating from the source (y and V = 0) to the drain (y = L and $V = V_D$) gives

$$I_D = (Z\mu C_i/L)\,[(V_G - V_o)V_D - V_D^2/2] \tag{8.7}$$

The region OA in Figure 8.2, where I_D varies linearly with V_D, corresponds to small values of the drain voltage ($V_D < V_G$). As V_D is increased for fixed V_G, the point will be reached where $V_D \geq V_G$. The gate electrode is then effectively positive with respect to the drain and the film begins to deplete in the vicinity of the drain, giving the portion AB of the characteristic in Figure 8.2. Saturation (BC in Figure 8.2) is reached when the drain current is pinched off. This condition corresponds to depletion of all the carriers in the vicinity of the drain which occurs when

$$V_D = V_G - V_o \tag{8.8}$$

The drain current at saturation $I_{D,sat}$ is obtained by substituting this value to Eq. 8.7

$$I_{D,sat} = (Z\mu C_i/2L)\,(V_G - V_o)^2 \qquad (8.9)$$

From the above, V_o seems to have the same role as the threshold voltage in conventional MOSFETs. However, the threshold voltage arises from the fact that, for strong inversion to occur, the gate voltage has to be large enough to make the Fermi level cross the middle of the semiconductor bandgap. In an ideal TFT, where such an requirement does not exist, one should have V_o=0. This voltage has been introduced to account for a 'pseudo threshold voltage' that is observed in organic TFTs. Several explanations might be found for this, e.g. flat-band shift due to a work-function difference between the semiconductor and the gate contact, fixed charges in the semiconductor-insulator interface. It has to be noted that V_o is strongly dependent on the preparation of the FET.

In an accumulation MOSFET, the channel is not isolated from the bulk (neutral) region by a depletion region and an ohmic current I_Ω has to be taken account in parallel with the channel current I_D. Thus, the measured source-drain current is

$$I_{tot} = I_D + I_\Omega$$

8.2 Fabrication of Thin Film Transistors

Devices were similar to those used in other investigations at Durham University. Processing was undertaken in a class 1000 microelectronics clean room. A schematic diagram and a plan view of the TFT structure is shown in Figure 8.3(a,b). Single-crystal silicon with a resistivity of 13.9 Ω cm was used as a substrate. The type of the silicon wafer did not matter as far as it does not affect the conduction mechanism. The gate insulator was provided by a layer of silicon dioxide, grown by dry oxidation. An array of interdigitated

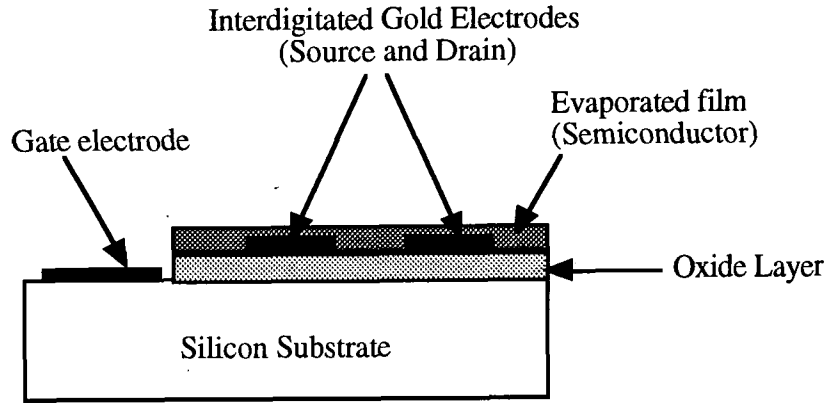

(a)

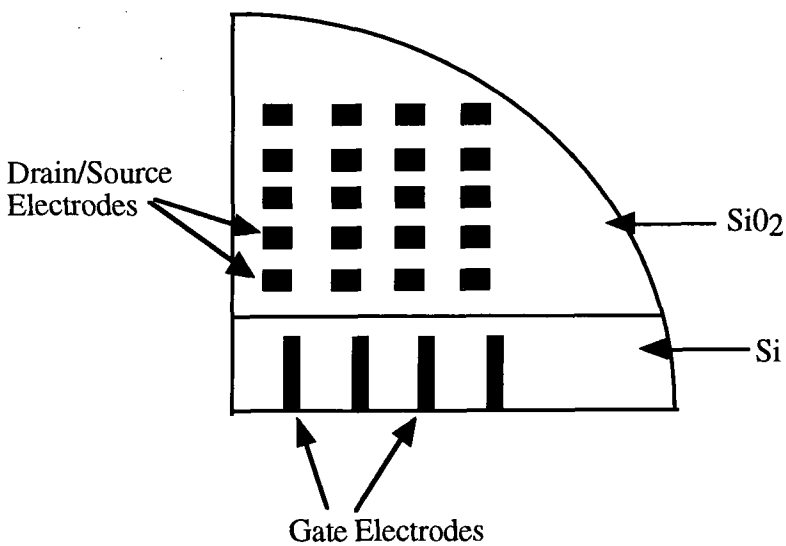

(b)

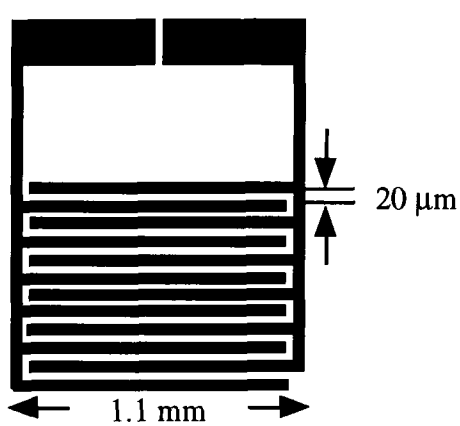

(c)

Figure 8.3: (a) Schematic diagram of the structure of the TFT devices used.

(b) Plan view of a TFT.

(c) The interdigitated drain-source electrode.

electrode patterns (Figure 8.3(c)), to act as source and drain, with a channel length of 20 μm and width of 4 cm, was etched, using a standard photolithography technique, into an evaporated layer of gold undercoated with chromium to improve adhesion to the oxide layer. The gate electrode was deposited by thermal evaporation onto the substrate after removal of the oxide layer using a solution of hydrogen fluoride. Finally, an organic film, to act as the active layer, was added.

8.3 TTF Devices

8.3.1 Evaporation of TTF

The evaporation conditions for TTF described in Section 6.1.1 were also followed here. For the TFT substrates, the gate insulator (silicon dioxide layer) was 320±20 nm thick. Film deposition rates were kept between 400 and 800 nm min^{-1} and typical film thicknesses were 1-2 μm. Doping was achieved by exposure to iodine vapour in a sealed container for 3-5 min.

8.3.2 Electrical Characterisation

The TFTs were characterised using the electrical circuit shown in Figure 8.4. To check the quality of the oxide, the measurements were first undertaken before addition of the evaporated film. Figure 8.5 shows the drain current (I_D) versus source-drain voltage (V_{DS}) for such a TFT. From currents exhibited for TFTs with an organic layer (to be presented later in this section), it is evident that the conduction via the oxide is negligible, i.e. oxide layers can be regarded as insulating. It is also essential to establish that the gate is fully insulated from the drain-source electrodes, so no current should be observed on application

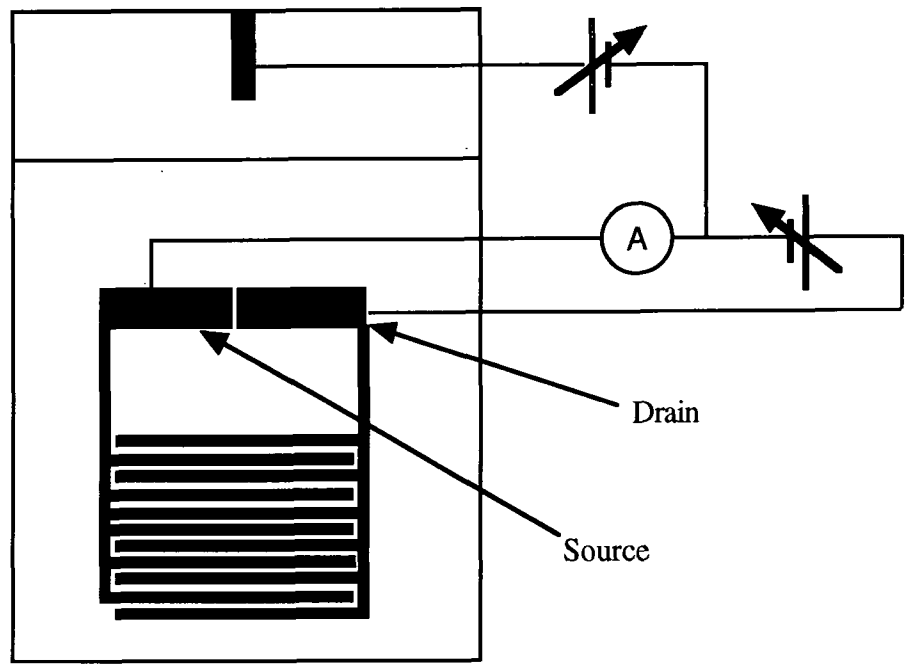

Figure 8.4: Electrical circuit used for TFT characterisation.

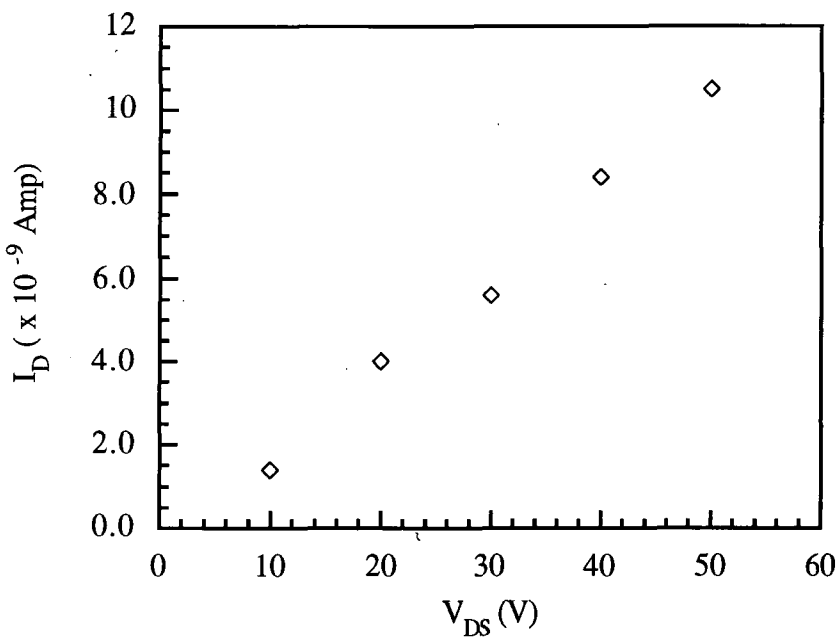

Figure 8.5: Drain current versus source voltage for a TFT for all gate voltages without the addition of the evaporated layer.

of a gate voltage for zero V_{DS}. For the TFTs used here, this latter current could not be measured ($<10^{-13}$ Amp for 40 V). After evaporation of TTF, the TFT was characterised again. Figure 8.6 (a) shows the I_D versus V_{DS} characteristic for an TFT with an 1.4 μm thick evaporated as-deposited TTF film. At low drain voltages, Ohm's law is obeyed ($I \propto V$). This linear variation is attributed to the ohmic current resulting from the bulk free-carriers. For higher drain voltages the current increases more rapidly than the voltage. This supralinear behaviour is evidence for a space-charge-limited current (SCLC) resulting from carriers injected by the metallic electrodes[8]. Such effects have been reported previously for organic TFT structures [9-11]. Varying the gate voltage (-100 V, 100 V) did not result in a change of the I_D-V_{DS} curve, i.e. no effect of the gate voltage was observed. After doping, an increase in the drain current of almost six orders of magnitude was exhibited. Figure 8.6(b) shows the I_D versus V_{DS} characteristic for an TFT with an 1.4 μm evaporated TTF film after doping. In this case, Ohm's law is obeyed for low voltages but at higher voltages (>11 V) the heat dissipated in the film is too high resulting in damage to the film, evident from a decrease in conductivity. In a semiconducting film, Joule heating will raise the temperature of the sample and, as a consequence, increase the carrier density. At constant bias, the current flow through the film will rise and it will, in turn, increase the heating effect and generate more carriers. The sample temperature will continue to rise until damage in the film ensues. The critical value of voltage for this phenomenon to happen, was found to be $V_c = 11$ V. If after reaching this point, the low voltage readings were taken again, these were found to be lower that the ones taken the first time. Figure 8.6 (b) shows two sets of readings, the second (full circles) being taken after the voltage was allowed to reach the value of the critical voltage (V_c). As for the device before doping, varying the magnitude and polarity of V_G (from

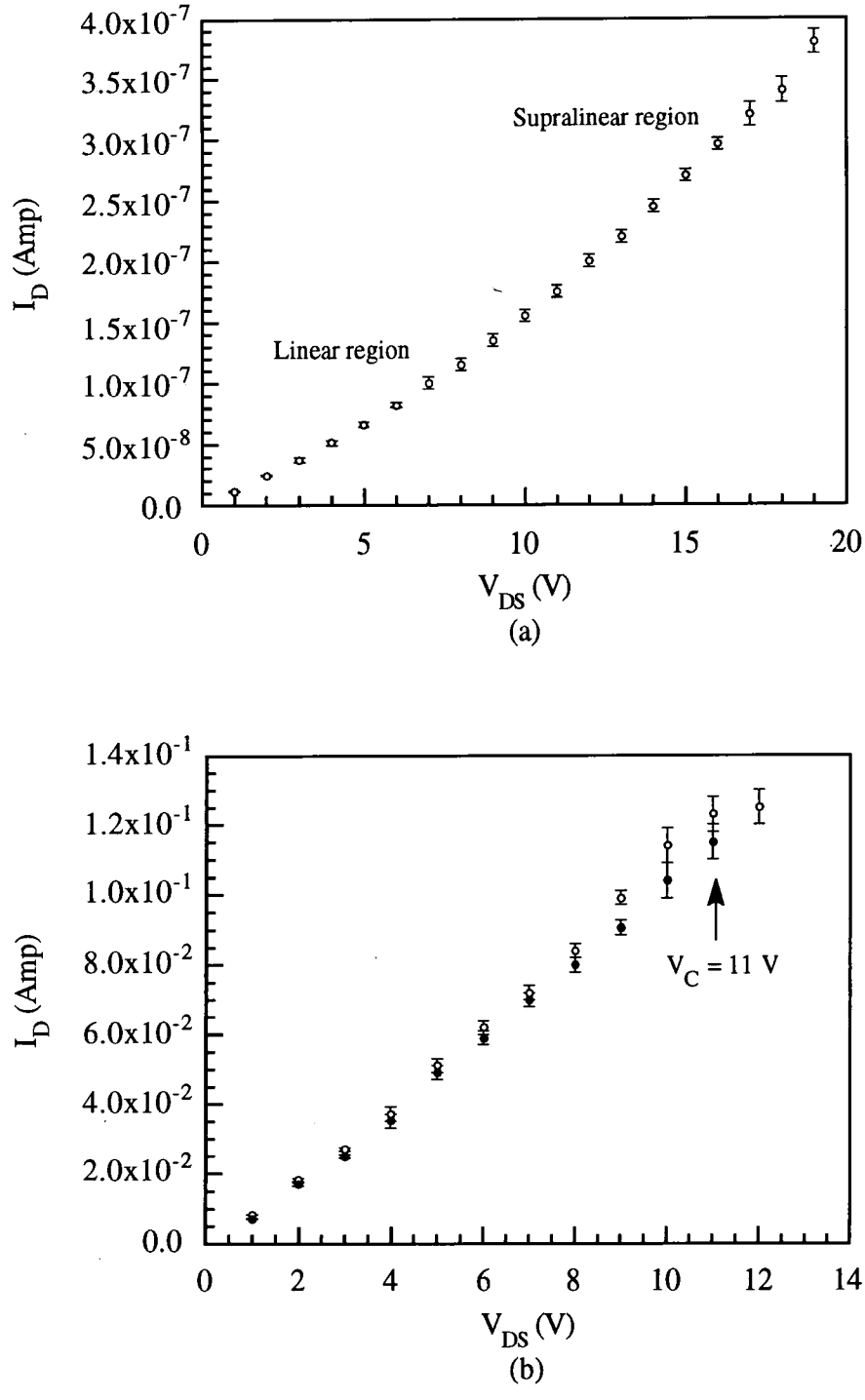

Figure 8.6: (a) Drain current I_D versus drain-source voltageV_{DS} for an as-deposited 1.4 μm thick TTF thin film transistor for V_G = 0 V. Varying the V_G (from -100 V to 100 V) did not alter the characteristic.

(b) Drain current I_D versus drain-source voltage V_{DS} for an 1.4 μm thick (TTF) iodide thin film transistor for V_G = 0 V. Varying the V_G (from -100 V to 100 V) did not alter the characteristic. The arrow indicates the value of the critical voltage for overheating to occur. The data points represented by the full circles were taken after sample overheating.

z-100 V to 100 V) did not alter the shape of the I_D versus V_{DS} curve, i.e. no field effect was observed.

The important role of the semiconductor-insulator interface in determining the characteristics of a TFT has been discussed in the literature. Different inorganic insulators in a TFT have resulted in no field-effect for SiO_2 and a field-effect for Si_3N_4 for the same organic semiconductor [11]. The difference arising from different inorganic insulators is the number of surface states at the interface which act as traps for the semiconductor carriers. To overcome the above problem, the combination of an inorganic and an organic insulator has been investigated on. Madru *et al.* [12], have reported the fabrication of an organic TFT device in which the gate insulator consisted of two layers: $Si0_2$ plus an organic insulating layer. A field effect was not observed for devices which did not include the insulating organic film. Again, it was suggested that states at the SiO_2 surface could neutralise the charges produced by the gate voltage and that an additional insulating layer of a molecular crystal was required to guarantee a field effect. Horowitz *et al.* [13], have also reported on the role of the semiconductor-insulator interface. Their study showed a carrier mobility that depended on the nature of the insulating layer (being ten times higher for a TFT with an organic insulator than for a TFT with an inorganic one, for the same organic semiconducting layer), which shows that the charge transport of the device was predominantly governed by the properties of the semiconductor-insulator interface. Although organic TFTs using SiO_2 as the gate insulator have been successfully fabricated [14,15], the use of organic insulating layers has also been explored [16]. Garnier *et al.* [17] have reported an all-organic TFT. Summarising, the choice of the insulating layer in the TFTs reported here could be the

reason for the devices not exhibiting a field effect. The use of other inorganic or organic materials or a combination of the two, acting as the gate insulator might optimise the device performance.

The values of in-plane, dc room temperature conductivity calculated from the TFT electrode pattern were found to be 10^{-7} - 10^{-8} S cm^{-1} and 10^{-3} - 10^{-2} S cm^{-1} for the undoped and doped samples, respectively. These figures are one to three orders of magnitude lower than those being reported in Chapter 6 for samples deposited on glass. There are two possible explanations for these differences: a) the different substrate, deposition rates were found to be higher for silicon than for glass for the same source temperature (800 nm min^{-1} at T_{sc}=75°C for silicon) and b) the different electrode pattern. To check these ideas, silver-paint electrodes were made on the silicon oxide on which the evaporated film was deposited. This resulted in an in-plane, dc room temperature conductivity comparable to that found for films on a glass. Therefore, the electrode pattern must be responsible for the lower value of conductivity exhibited. In Table 6.1, the deposition rate of 400 nm min^{-1} noted for T_{sc}= 75°C is the same on the glass substrate and on the gold electrodes (the latter were evaporated on the glass substrate before the addition of the organic layer, Section 4.1). Thus, on the TFT structure, in the vicinity of the electrodes, evaporation took place with different deposition rates onto the different regions of the substrate, i.e. 400 and 800 nm min^{-1} on gold and on the silicon oxide, respectively. This could have resulted in an interfacial region of high resistance. Clearly, further experiments are required to substantiate this.

8.4 BEDT-TTF Devices

8.4.1 Evaporation of BEDT-TTF

The evaporation conditions for BEDT-TTF described in Section 7.3.1 were also used here. In the TFTs used as substrates, the gate insulator (silicon dioxide layer) was 360±20 nm. ET layers prepared with deposition rates 80-95 nm min^{-1} and thicknesses ranging between 0.4 and 0.7 μm were evaporated on the TFTs. Samples were doped with iodine and were annealed in air at 60 °C for 35 min (this is the optimum annealing time as calculated in Section 7.2.3)

8.4.2 Electrical Characterisation

Again, the electrical circuit shown in Figure 8.4 was used for measurements on the TFTs. Using the same procedures as in Section 8.3.1, the quality of the oxide layer and the insulation between the gate and the drain-source electrodes were first checked. After the evaporation of the ET, the TFTs were characterised again. Figure 8.7(a) shows the I_D versus V_{DS} characteristic for a TFT with an 0.6 μm thick as-deposited evaporated ET film. Ohmic behaviour was exhibited for V_G=0 V, in agreement with the TFT theory. On varying the magnitude and polarity of the gate voltage (from -100 V to 100 V), no field effect was found. Figure 8.7(b) shows the I_D versus V_{DS} characteristic for the same device after exposure to iodine vapour and annealing in air at 60°C for 35 min. The values of current exhibited were now five orders of magnitude higher than for the as-deposited TFT. The same ohmic behaviour was exhibited for drain-source voltages up to 20 V. Overheating, as found for the TFT device, was observed for greater voltages. In Figure 8.7(b), two sets of readings are shown, the second (full circles) being taken after the value of the critical voltage

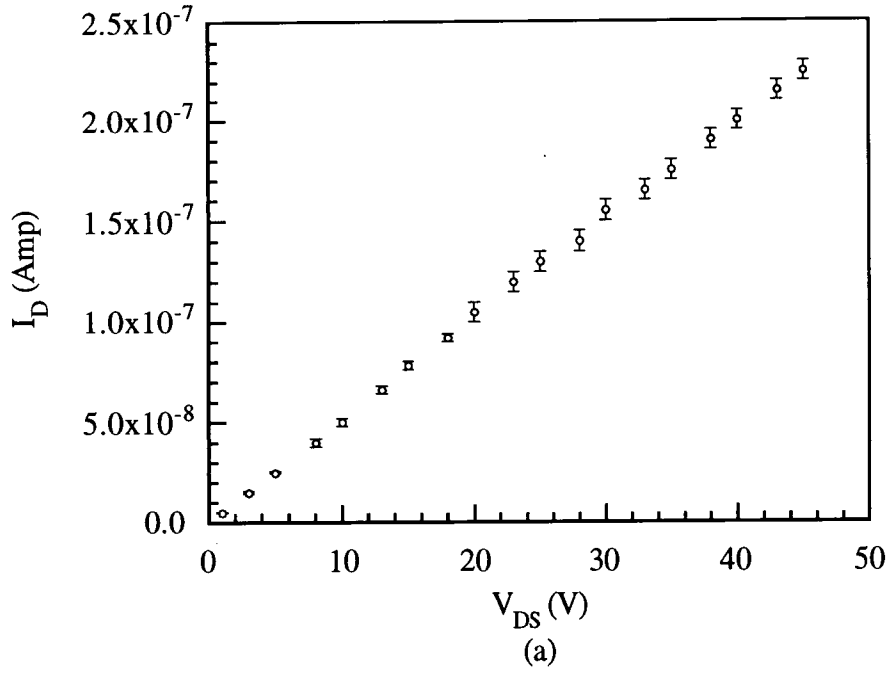

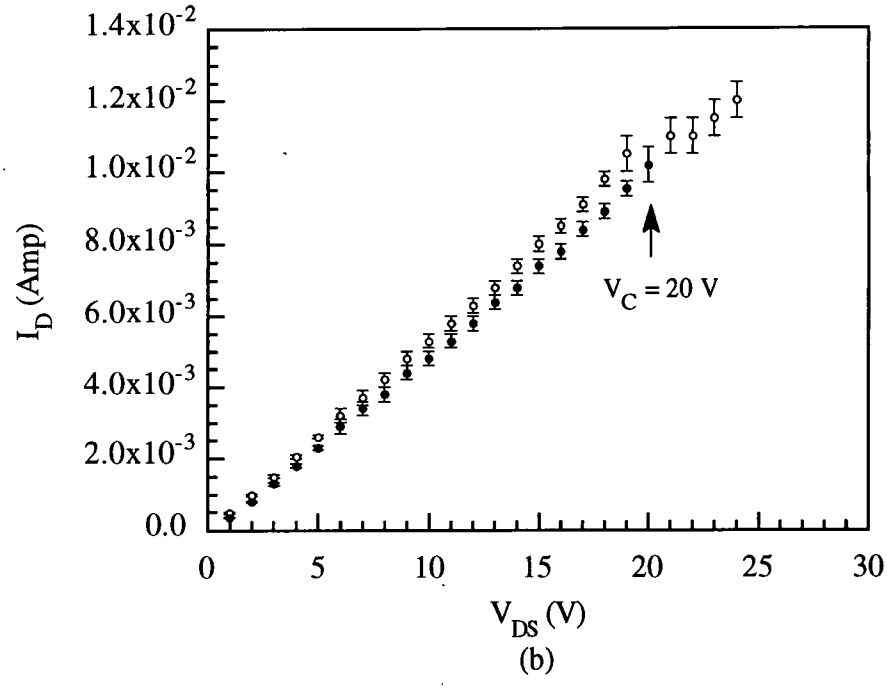

Figure 8.7: (a) Drain current I_D versus drain-source voltageV_{DS} for an as-deposited 0.6 μm thick ET thin film transistor for V_G = 0 V. Varying the V_G (from -100 V to 100 V) did not alter the characteristic.

(b) Drain current I_D versus drain-source voltage V_{DS} for an 0.6 μm thick (ET) iodide thin film transistor for V_G = 0 V. Varying the V_G (from -100 V to 100 V) did not alter the characteristic. The arrow indicates the value of the critical voltage for overheating to occur. The data points represented by the full circles were taken after sample overheating.

(V_c=20 V) had been reached. Varying the value of the gate voltage in the doped TFTs, from -100 V to 100 V had no effect on the electrical behaviour, i.e. no field effect was exhibited. We believe, that as for the TTF device, the choice of the gate insulator was responsible. Different inorganic or organic insulators might result in different electrical behaviour.

Using the electrode pattern of the TFT, a value for the in-plane, dc room temperature conductivity of 10^{-8} S cm^{-1} for the as-deposited ET films was obtained. This value could not be measured with the three point probe method (Section 7.3.3). However, this is not inconsistent with the results reported here. The resistance is given by

$$R = \frac{V}{I} = \frac{\rho l}{dt} \tag{8.10}$$

where ρ and t are the resistivity and the thickness of the film, d and l the electrode length and distance, V the applied voltage and I the current. The current is then given by

$$I = \frac{Vdt}{\rho} \frac{d}{l} \tag{8.11}$$

From the above equation is clear that the higher the ratio $\frac{d}{l}$, the higher the value of I for a fixed applied voltage. In the electrode configuration of the TFT, d=4 cm and l=20 μm which gives a much higher ratio than that in the three point probe method where $\frac{d}{l} \cong 1$. Therefore, conductivity measurements of insulating materials are favoured in an electrode configuration with a small value of d/l.

The value of the in-plane, dc room temperature conductivity exhibited by doped samples, as calculated by the TFT measurements, was 10^{-3} S cm^{-1}, lower than that reported for samples deposited on glass (Section 7.3.3). As for TTF, deposition rates were different

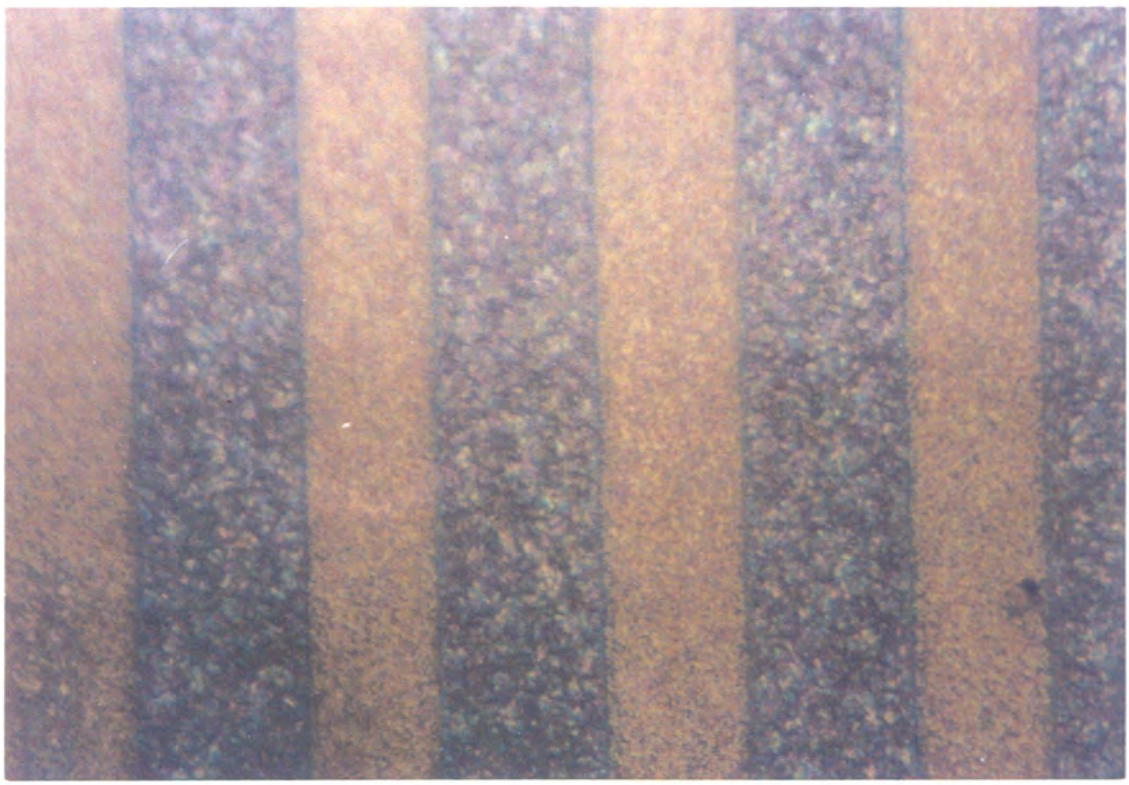

Figure 8.8: Optical micrograph of a 0.6 μm (ET) iodide thin film evaporated on a TFT, after annealing in air at 60°C for 35 min. The photograph is taken at the area of the source-drain electrodes.

onto the gold electrodes and the oxide layer. We suggest that this could result in an interfacial region of high resistance. Examining the area in the vicinity of the gold electrodes using the optical microscopy revealed no differences in structure between the films on different substrates (Figure 8.8).

8.5 Summary

TFT structures were fabricated incorporating TTF and ET as the active (semiconducting) layer. No field effect was observed for either device, either before or after the organic film had been doped with iodine vapour. We believe that the semiconductor-insulator interface played a significant role in the device operation. Further experimentation with the material used as the gate insulator is needed. Judging from other studies reported, an organic insulating layer might result in a field-effect.

References

1. S.M. Sze, 'Semiconductor Devices: Physics and Technology', *Wiley*, (1981) pp 186.
2. G. Horowitz, 'Organic Semiconductors for New Electronic Devices', *Adv. Mater.*, **2** (1990) 287.
3. J.H. Burroughes, C.A. Jones and R.H. Friend, 'New Semiconductor Device Physics in Polymer Diodes and Transistors', *Nature*, **335** (1988) 137.
4. A. Tsumura, H. Koezuka, S. Tsunoda and T. Ando, 'Chemically Prepared Poly (N-Methylpyrrole) Thin Film. Its Application to the Field-Effect Transistor', *Chem. Lett.*, (1986) 863.
5. J.C. Anderson, 'Theory of the Thin Film Transistor', *Thin Solid Films*, **38** (1976) 151.
6. G. Horowitz, X. Peng, D. Fichou and F. Garnier, 'The Oligothiophene-Based Field-Effect Transistor: How It Works and How to Improve It', *J. Appl. Phys.*, **67** (1990) 528.
7. G. Horowitz, P. Delannoy, 'An Analytical Model for Organic Based Thin-Film Transistors', *J. Appl. Phys.*, **70** (1991) 469.

8. A.M. North and G.M. Burnett, 'Transfer and Storage of Energy by Molecules', *Wiley* (1974) pp 160.

9. G. Horowitz, D. Fichou, X. Peng and P. Delannoy, 'Evidence for a Liner Low-Voltage Space-Charge Limited Current in Thin Films. Film Thickness and Temperature Dependence in Alpha-Conjugated Sexithienyl', *J. Phys. France*, **51** (1990) 1489.

10. P. Hesto, L. Aguilhon, G. Tremblay, J.P. Bourgoin, M. Vandevyver and A. Barraud, 'Field-effect Induced Modulation in Langmuir-Blodgett Films of Ethylenedithiotetrathiofulvalene Derivatives', *Thin Solid Films*, **242** (1994) 7.

11. G. Guillaud, M. Alsadoun, M. Maitrot, J. Simon and M. Bouvet, 'Field-Effect Transistors Based on Intrinsic Molecular Semiconductors', *Chem. Phys. Lett.*, **167** (1990) 503.

12. M. Madru, G. Guillaud, M. Al Sadoun, M. Maitrot, C. Clarisse, M.Le Contellec, J-J André and J. Simon, 'The First Field Effect Transistor Based on an Intrinsic Molecular Semiconductor', *Chem. Phys. Lett.*, **142** (1987) 103.

13. G. Horowitz, X.Z. Peng, D. Fichou and F. Garnier, 'Role of the Semiconductor/Insulator Interface in the Characteristic of π-Conjugated-Oligomer-Based Thin-film Transistors', *Synth. Met.*, **51** (1992) 419.

14. J. Paloheimo, P. Kuivalainen, H. Stubb, E. Vuorimaa and P. Yli-Lahti, 'Molecular Field-effect Transistors Using Conducting Polymer Langmuir-Blodgett Films', *Appl. Phys. Lett.*, **56** (1990) 1157.

15. C. Pearson, A.J. Moore, J.E. Gibson, M.R. Bryce and M.C. Petty, 'A Field Effect Transistor Based on Langmuir-Blodgett Films of an $Ni(dmit)_2$ Charge Transfer Complex', *Thin Solid Films*, **244** (1994) 932.

16. X. Peng, G. Horowitz, D. Fichou and F. Garnier, 'All-organic Thin Film Transistors Made of Alpha-sexithienyl Semiconducting and Various Polymeric Insulating Layers', *Appl. Phys. Lett.*, **57** (1990) 2013.

17. F. Garnier, G. Horowitz, X. Peng and D. Fichou, 'An All-Organic Thin Film Transistor with Very High Carrier Mobility', *Adv. Mater.*, **2** (1990) 592.

CHAPTER NINE

CONCLUSIONS AND SUGGESTIONS FOR FUTURE WORK

9.1 Conclusions

The thermal evaporation technique has been used successfully to fabricate thin films, 0.4-1.2 μm thick, of organic charge-transfer compounds. The conclusions presented here are divided into sections according to the materials used.

Tetrathiafulvalene (TTF) would not deposit on substrates held at a temperature above 0°C (T_{sc} > 0°C). However, good quality films, consisting of well-defined crystals, were prepared for T_{sc} = -10°C. Two different types of structure, plates and needles, were identified by scanning electron microscopy, suggesting 3-D island growth. The effect of the deposition rate (affected by the source temperature T_{sc}) on film structure was examined. For low deposition rates (low values of T_{sc}), mainly needles, up to 10 μm in length, were seen. In contrast, for high deposition rates (high values of T_{sc}), the films consisted solely of small-sized crystalline plates (<2μm). The latter case also resulted in more uniformly coated samples. In the optical spectra, two bands related to the charge-transfer between the donor and acceptor molecules were seen in the near infrared region; that located at 870 nm was attributed to intermolecular transitions between cation radicals while that around 1500 nm was associated with the mixed valence state. Peaks in the visible region were identified as transitions within the cation. The dc, in-plane room temperature conductivity of films doped

with iodine (σ_{max} = 8 S cm^{-1}) was two orders of magnitude lower than that for single crystals measured along the stacking axis (σ_{RT} = 100-450 S cm^{-1}). The former compared well to that reported for co-evaporated TTF-iodide films measured normal the stacking axis (~10 S cm^{-1}) [1]. However, attempts in this work to form TTF-iodide films by co-evaporating the component materials did not enhance the value of σ, which ranged from 10^{-6} to 3 S cm^{-1}. The structure of co-evaporated films was found to consist of both plates and needles and was therefore similar to that of the single-evaporated layers. The optical spectra of the two types of films also compared well. These were identical in the visible region and both exhibited the full charge transfer band at 870 nm band. The mixed-valence band around 1500 nm observed for the single-source evaporated films, ranged from 1300 nm to 2500 nm, depending on the deposition conditions, for co-evaporated films. A significant difference seen for the two types of film, was in the value of the activation energy; that for co-evaporated films (0.02 eV) being almost double that for single evaporated films (0.09 eV). An irrecoverable decrease with time was seen in the value of conductivity for both types of films. In particular, a drop of three orders of magnitude occurred in 240 days and 105 days for single and double source evaporated films, respectively.

TTF iodide films have been also prepared at Durham using LB deposition (work outside this thesis) [2]. The latter films exhibited a maximum room temperature conductivity value of 1 S cm^{-1}. This compares well with the value of σ reported in this work for evaporated layers. Both types of films were semiconducting with the same value of activation energy (0.09 eV).

Dimethyl-TTF was found to form poor quality films. As for TTF, a film would not deposit for $T_{sc} > 0$ °C. Deposition at T_{sc} = -10°C was not uniform with large uncoated

substrate areas evident. A 3-D island growth was suggested by the electron micrographs. Both types of structure, plates and needles, were seen for the as-deposited films. Upon doping, an irreversible increase in thickness (~200%) was observed. SEM analysis revealed a change in crystal orientation A difference was also observed in the structure with doped layers consisting mainly of plates. The above changes could explain the above thickness increase. In the optical spectra, only the full-charge transfer band was exhibited in the near infrared region. The in-plane, dc room temperature conductivity was low (10^{-6} S cm^{-1}). This value and the absence of any other bands in the near infrared region suggested that the compound was in the full charge-transfer state.

The results for trimethyl-TTF films were comparable to those for dimethyl-TTF. The quality of the films was very poor with plate-like crystals scattered on the substrate. An irreversible increase in thickness (~200%) was seen upon doping with iodine, as for dimethyl-TTF. Again the optical spectra and the value of the conductivity (σ_{RT} =10^{-7}S cm^{-1}) suggested that the compound was in the full charge-transfer state. There are no publications that we are aware of dealing with film films of methyl-TTFs deposited by other methods.

ET was the only material (from those studied in this work) that would deposit at substrates kept at ambient temperature. Thermal annealing was used to examine whether the well-known transformation from $\alpha \rightarrow \alpha_t$ phase [3] would be exhibited. Heating the doped films at 60°C for 35 min resulted in an increase in the value of conductivity from 10^{-3} to 1 S cm^{-1}. Annealing for longer times led, eventually, to the complete loss of iodine. In the optical spectra, a change was also seen, with the band around 1300 nm exhibited by the doped films, no longer being present in the spectra of the annealed films. The conductivity of

the annealed films was weakly thermally activated with ΔE = 0.028 eV. This value is significantly higher than that exhibited by α_t-$(ET)_2I_3$ evaporated films (0.017 eV) [4].

LB deposition has also been used to prepare ET iodide layers [5]. In general, evaporated films reported in this thesis exhibited a room conductivity value (~1 S cm^{-1}) of one order of magnitude higher that for LB films (~10^{-1} S cm^{-1}).

Attempts were made to incorporate the (TTF) iodide and (ET) iodide films into thin film transistor structures. In both cases, modulation of the source-drain current by the gate voltage was not evident. This lack of field effect has been observed before and has been attributed to neutralisation of the charge species, induced in the semiconductor by the gate voltage, by surface states at the gate insulator [6].

9.2 Suggestions for Further Work

The work reported in this thesis on single-source evaporated TTF films is fairly complete. However, a fuller understanding of the structure of the thin films could be achieved by X-ray analysis. This would allow identification of the phase of the films and comparison with results from single crystals would be easier and more precise. As evident in Section 3.3, the substrate temperature is an important factor in determining the structure of evaporated layers. In this work, the effect of the source temperature was examined thoroughly. Evaporation on different substrates, with a more organised or amorphous surface, would also be a useful factor to examine.

Results from the methyl-TTFs were quite disappointing. Single-source evaporation produced films in which full charge-transfer between the donor and acceptor molecules took

place. However, this might be avoided by regulating the degree of doping. This suggest that co-evaporation might be used for these compounds.

The ET-iodide system is very interesting. Single crystals of $(ET)_2I_3$ have exhibited ambient pressure superconductivity (see Section 2.4) The possibility of superconductivity being observed by thin films of this salt is worth examining further. Future studies on films reported in this work requires the use of X-ray analysis. The phase of the salt could then be identified. Varying the nature of the substrate and the substrate temperature could result in different phases of the iodine salt and, therefore, in improving the electrical properties. Furthermore, co-evaporation could represent an elegant way of preparing superconducting thin films.

Further experimentation is also needed for the TFT structures incorporating the thin films. The problem encountered in this work (absence of a significant field effect) has been identified and the solution has also been suggested. Alternative TFT structures should be used in which the choice of the gate insulator should be varied. If necessary, a combination of two insulators, either two inorganic or an organic/inorganic system might be used to reduce the surface state density at the semiconductor/gate insulator interface. The effect of damaging the sample by overheating could be avoided by increasing the spacing between electrodes.

As the size of microelectronics components is further reduced, it is anticipated that organic materials may become increasingly important for a wide range of electronics applications (e.g. TFTs, light emitting diodes, gas sensors) [7]. Results reported in this work show that thermal evaporation is a convenient method for fabricating organic layers. Possibly the greatest drawback is the number of parameters that can be varied in order to improve the

quality of the film (i.e. source and substrate temperature, nature of the substrate).With co-evaporation a further parameter (a second source temperature) is added. The fact that quite large thicknesses (~500 nm) are needed for a continuous evaporated film could represent an obstacle in some electronic applications. In general though, reproducible results are obtained and thermal evaporation could become a well-established method for organic thin film fabrication.

Finally, evaporation of other charge-transfer materials are possible in the new vacuum system built in this work. This system is a powerful tool that allows the researcher freedom to vary the deposition conditions to suit the needs of evaporation of individual materials and hopefully to produce high quality thin films.

References

1. M. Yudasaka, K. Hironaga, H. Yamochi, K. Nakamishi and G. Saito, 'Thin Film Formations of Charge-Transfer Complexes with Metallic Properties by Vacuum Deposition Method', *Mat. Res. Soc. Symp. Proc.*, **173** (1990) 137.
2. M.R. Bryce and M.C. Petty, 'Electrically Conductive Langmuir-Blodgett Films of Charge-Transfer Materials', *Nature*, **374** (1995) 771.
3. G.O. Baram, L.I. Buranov, L.S. Degtyarev, M.E. Kozlov, V.N. Laukhin, E.E. Laukhina, V.G. Onishchenko, K.I. Pokhodhya, M.K.Sheinkmann, R.P. Shibaeva and E.B. Yagubskii, 'Transformation of the α-Phase $(BEDT\text{-}TTF)_2I_3$ to the Superconducting β Phase with T_c = 6-7K', *JETP Lett.*, **44** (1986) 376.
4. K. Kawabata, T. Tanaka and M. Mizutani, 'Superconducting Organic Thin Films Prepared Using an Evaporation Technique', *Adv. Mater.*, **3** (1990) 157.
5. Goldenberg *et al*, unpublished data.
6. M. Madru, G. Guillaud, M. Al Sadoun, M. Maitrot, C. Clarisse, M.Le Contellec, J-J André and J. Simon, 'The First Field Effect Transistor Based on an Intrinsic Molecular Semiconductor', *Chem. Phys. Lett.*, **142** (1987) 103.
7. M.C. Petty, 'Molecular Electronics: Prospects for Instrumentation and Measurement Science', *Meas. Sci. Technol.*, (1996) 725.

PUBLICATIONS

1. M. Kilitziraki, M.C. Petty and M.R. Bryce, 'Electrical Properties of Evaporated TTF Thin Films', *Synth. Met.*, **70** (1995) 1247.

2. M. Kilitziraki, C. Pearson, A.S. Dhinsda, M.R. Bryce and M.C. Petty, 'A Comparison of Tetrathiafulvalene Thin Films Prepared by Thermal Evaporation and the Langmuir-Blodgett Technique', *Thin Solid Films*, in press.